METAL-MOUNTABLE MINIATURE FOLDED-PATCH TAG ANTENNAS FED BY COPLANAR WAVEGUIDE

MOH CAI WEI

MASTER OF ENGINEERING SCIENCE

LEE KONG CHIAN FACULTY OF ENGINEERING AND SCIENCE
UNIVERSITI TUNKU ABDUL RAHMAN
FEBRUARY 2019

METAL-MOUNTABLE MINIATURE FOLDED-PATCH TAG ANTENNAS FED BY COPLANAR WAVEGUIDE

By

MOH CAI WEI

A dissertation submitted to the Institute of Postgraduate Studies and Research,
Lee Kong Chian Faculty of Engineering and Science,
Universiti Tunku Abdul Rahman,
in partial fulfillment of the requirements for the degree of Master of Engineering Science
February 2019

ABSTRACT

METAL-MOUNTABLE MINIATURE FOLDED-PATCH TAG ANTENNAS FED BY COPLANAR WAVEGUIDE

Moh Cai Wei

In this dissertation, two projects have been conducted for studying the techniques to miniaturize the footprints of two metal-mountable UHF RFID tag antennas. To prove the validity and reliability of the proposed tags, prototypes have been made and measured. First, a folded-patch, which is centrally fed by a coplanar feedline, is proposed for designing a miniature UHF tag antenna for mounting on metal surfaces. In the design, two notches have been incorporated with an inductive stub for tuning of the tag's resonance over a larger frequency range. The proposed tag can achieve a read distance of greater than 10 m when placed on metal plate and beyond 5 m when it is placed on different dielectric slabs. In the second project, a pair of differentially fed coplanar waveguides is employed for exciting a folded-patch antenna for designing a metal-mountable UHF RFID tag. Multiple slots are incorporated into the patch for tuning the resonant frequency and optimizing the impedance matching between the chip and the antenna. Two inductive stubs are introduced at the two corners of the radiating patch to enable further frequency tuning. The read range of the proposed tag can achieve 8.9 m when tested on metal plate. The read distance is also more than 4m when attached to various dielectric materials. Both of the projects can be directly fabricated on the single surface of a single piece on

PET (polyethylene terephthalate). No vias or additional structures are needed in the designs, making the design processes simple and easy.

ACKNOWLEDGEMENTS

First of all, I would like to express my utmost thanks to my supervisor, Prof. Lim Eng Hock and co-supervisor-, Prof. Ir. Chung Boon Kuan for guiding and assisting me throughout the entire period of my research projects. Their proper guidance and support have contributed to the completion of this project.

In addition, I would like to express my gratitude to my seniors and friends specifically Bong Fwee Leong who have helped me during the research. They have provided useful information and were willing to lend me a hand whenever I encountered problems. The knowledge that I gained from them is invaluable.

Special thanks is extended to UTAR for providing the lab facilities to carry out my measurements. Also, UTAR has given me freedom to access online databases such as IEEE Xplore and Microwave and Optical Technology Letters where I could get all the important references.

Finally, I would like to express my appreciation to my family for supporting and motivating me throughout my research project.

APPROVAL SHEET

This dissertation entitled "**METAL-MOUNTABLE MINIATURE FOLDED-PATCH TAG ANTENNAS FED BY COPLANAR WAVEGUIDE**" was prepared by MOH CAI WEI and submitted as partial fulfillment of the requirement for the degree of Master of Engineering Science at Universiti Tunku Abdul Rahman.

Approved by:

_____

(Prof. Lim Eng Hock) Date:
Supervisor
Department of Electrical and Electronic Engineering
Lee Kong Chian Faculty of Engineering and Science
Universiti Tunku Abdul Rahman

_____

(Prof. Ir. Chung Boon Kuan) Date:
Co-supervisor
Department of Electrical and Electronic Engineering
Lee Kong Chian Faculty of Engineering and Science
Universiti Tunku Abdul Rahman

LEE KONG CHIAN FACULTY OF ENGINEERING AND SCIENCE

UNIVERSITI TUNKU ABDUL RAHMAN

Date:

SUBMISSION OF DISSERTATION

It is hereby certified that **MOH CAI WEI** (ID No: **16UEM06203**) has completed this dissertation entitled "**METAL-MOUNTABLE MINIATURE FOLDED-PATCH TAG ANTENNAS FED BY COPLANAR WAVEGUIDE**" under the supervision of Prof. Lim Eng Hock (Supervisor) from the Department of Electrical and Electronic Engineering, Lee Kong Chian Faculty of Engineering and Science (FES), and Prof. Ir. Chung Boon Kuan (Co-Supervisor) from the Department of Electrical and Electronic Engineering, Lee Kong Chian Faculty of Engineering and Science (FES).

I understand that University will upload softcopy of my dissertation in pdf format into UTAR Institutional Repository, which may be made accessible to UTAR community and public.

Yours truly,

_____

(MOH CAI WEI)

DECLARATION

I hereby declare that the dissertation is based on my original work except for citations and quotations which have been duly acknowledged. I also declare that it has not been previously and concurrently submitted for any other degree or award at UTAR or other institutions.

_____

(MOH CAI WEI)

Date:

TABLE OF CONTENTS

LIST OF TABLES

LIST OF FIGURES

LIST OF ABBREVIATIONS

AMC	Artificial Magnetic Conductor
EBG	Electromagnetic Bandgap
EIRP	Effective Isotropic Radiated Power
EM	Electromagnetic Wave
ERP	Effective Radiated Power
HF	High Frequency
LF	Low Frequency
PET	Polyethylene Terephthalate
PIFA	Planar Inverted F Antenna
RFID	Radio Frequency IDentification
UHF	Ultra-High Frequency

CHAPTER 1

INTRODUCTION

1.1 Background

RFID (Radio Frequency IDentification) is a wireless communication technique which was first introduced in the early 20th century. The basic working principle of the RFID is based on the technologies for RADAR and radio broadcasting. In the 20s, RADAR was first developed in the United States and it was one of the important technologies for the World War II (1939) (Dobkin, 2008). It was broadly used by the military once they knew about the significance of RADAR. At that time, the military aviation was using backscattering radios to identify friendly or foe aircrafts by modulating the backscattered RADAR signals, which were also known as IFF transponders. Later, Harry Stockman had presented a landmark paper "Communication by Means of Reflected Power" in 1948 (Stockman, 1948). In the late 1960s, Electronic Article Surveillance (EAS) (Partanen, 2015) system was developed by Checkpoint and Sensormatic. The EAS tag was a passive 1-bit tag, which was the first and most widespread commercial RFID technology that still applies today. The EAS technology is usually applied on smaller merchandise, book stores, and retail stores for preventing shoplifting and pilferage. When the products are sold, the tags are deactivated or removed. In the 1970s, the RFID technology started to receive much attention from different parties such as

governments, researchers, companies, and inventors. An important work "Short-Range Radio-Telemetry for Electronic Identification" was demonstrated by Steven Depp, Alfred Koelle, and Robert Frayman at the Los Alamos Scientific Laboratory in 1975. In the 1980s, the RFID technology was already fully implemented and developed in many countries. In the Europe and United States, the RFID technology began to be applied in transportation, animal tracking, as well as industrial and—business applications. In 1990, standardization works on various RFID systems were conducted to ensure their interoperability at different places. Then, the electronic tolling system was started to be used in the United States and the first electronic toll was opened in an open highway in Oklahoma. In 1999, the Massachusetts Institute of Technology (MIT) created the Auto-ID center which was specializing in automatic identification. The RFID was also their research area. Later, the MIT Auto-ID Center was promoting the global EPC (Electronic Product Code) standard in 2004.

All these contributions have been paving way for the RFID technology until today. It brings many advantages to our everyday lives. In recent years, the ISO (International Standard Organization) has also been involving in establishing different standards for the RFID technologies.

1.2 Overview of RFID

Recently, the RFID tagging technology has been broadly used in many sectors such as aerospace, automotive, logistics, transport, health, and management. Owing to its benefits, the application of RFID has been become an indispensable technology in our daily life. Wireless mechanism in an RFID system can be implemented using two methods - near-field and far-field. The near-field antenna produces inductive coupling to activate the tag, achieving a read distance of usually less than 50 cm. On the other hand, the far-field tag is activated by microwave radiation and the achievable read range is within a few meters. The selection of the operating frequency is very important as it is closely related to the tag's performance. Table 1.1 compares different radio frequency ranges and their properties (Understanding the Differences between LF, HF and UHF RFID Technology, 2017). The UHF-band (860-960 MHz) tagging system, with the deployment of microwave antenna, is used by most of the manufacturers because it can offer a much longer read range than their LF (120-140 KHz) and HF (13.56 MHz) counterparts, which are usually designed using inductive coupling (Ma et al., 2012). The antennas for the LF and HF RFID systems are usually designed using loop-shaped coils, where energy is transferred through inductive coupling. The two coils must be placed closely within certain ranges. When the tag comes close to the reader, the field from the reader's coil will couple to the tag's coil and a voltage will be induced in the tag. A typical inductively coupled RFID system is shown in Figure 1.1. Practically, the read ranges of LF and HF systems are shorter as inductive

coupling is near-field effect. Also, the LF and HF tag antennas usually have larger size due to long wavelength. On the other hand, the UHF RFID system uses backscattering method to transfer energy. As can be seen in Figure 1.2, the signal is transmitted from the reader to the tag and reflected back using electromagnetic wave at a specific frequency. It can achieve a longer read distance with smaller antenna size. Comparing to the LF and HF RFID tags, UHF RFID tag can achieve a farther read range.

Table 1.1: Comparison of radio frequency ranges and characteristics of different RFID systems.

	Low Frequency (LF)	**High Frequency (HF)**	**Ultra High Frequency (UHF)**
Frequency Range	120 to 140 KHz	13.65 MHz	860 to 960 MHz
Read Distance	~ 10 cm	10 cm to 1 m	~ 12 m (passive tag) ~ 100 m (active tag)
Data Transfer Rate	Low	Moderate	Fast
Radio Interference Sensitivity	Low	Moderate	High
Application	-Access control -Livestock tracking	-Ticketing -Payment -Data transfer applications	-Anti-counterfeiting -Pharmaceutical -Asset Tracking -Manufacturing

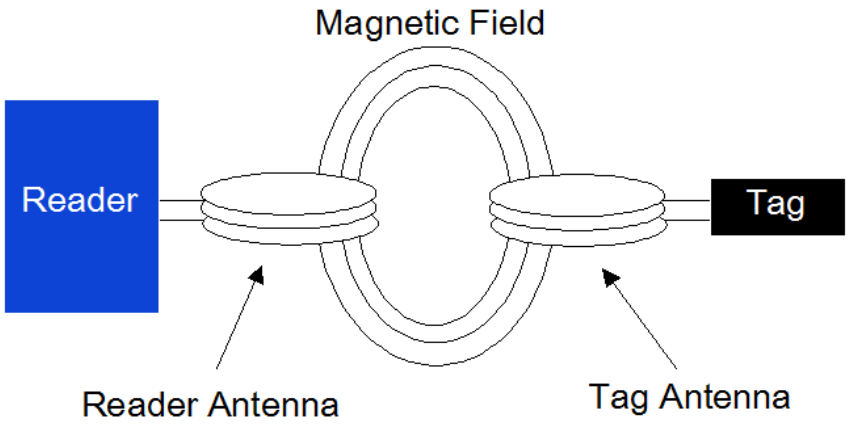

Figure 1.1: Inductive coupled RFID system.

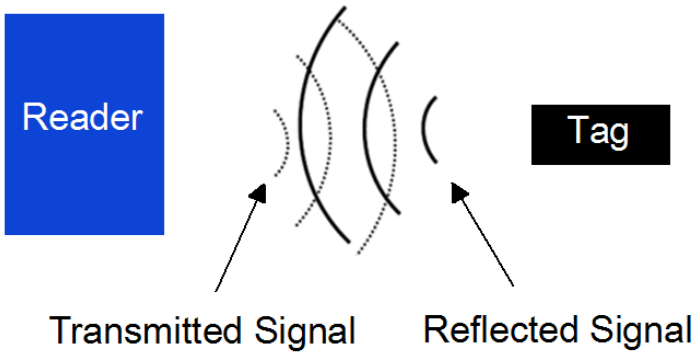

Figure 1.2: The backscattering modulation RFID system.

1.3 RFID Regulations

In the early years, there was no worldwide standard for the RFID technology. The RFID frequency bands and standards for every country can be very different. As a result, problems may arise when a tag designed for a country is unable to be read when being used in another country. To overcome these problems, the International Organization for Standardization (ISO), International Electrotechnical Commission (IEC), ASTM International, and

EPC Global have allocated the frequency bands and standards, known as the Industrial Scientific and Medical (ISM) bands and ISO 18000-6C standards, respectively, for RFID-related applications. A few factors have been included in these regulations, including the Effective Isotropic Radiated Power (EIRP) or Effective Radiated Power (ERP) occupation, bandwidth usage, frequency range as well as the channel spacing of every country. RFID systems that are designed according to these regulations will be able to interoperate all over the world. Figure 1.3 shows the worldwide regulated UHF frequency bands (Basics - RFID Regulations, 2018), where every country has its own UHF frequency bands and standards. For example, the UHF frequency band in India is set to be 865 MHz to 867 MHz with 4 W EIRP and it is assigned with 200 kHz carrier bandwidth. In the USA, the operating frequency spectrum is allocated 902 MHz - 928 MHz with a maximum transmitted power of 4W EIRP and a 500 kHz of carrier bandwidth. However, all these frequency bands and standards are subject to reallocation.

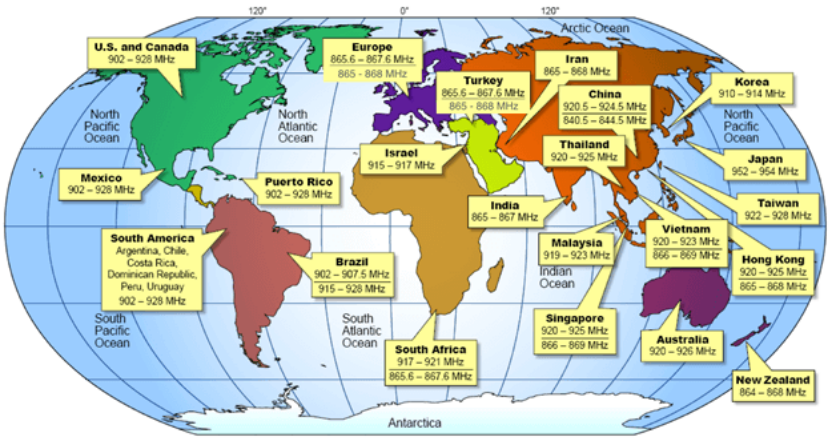

Figure 1.3: Worldwide UHF RFID frequency map (Basics - RFID Regulations, 2018).

1.4 RFID Reader and Tag

An RFID system consists of two main components – a reader and a tag. The reader is a device that reads and processes the data from the tag and it interfaces with the host computer. Tag acts as an identifier which can be used to store information electronically. An RFID tag comprises 2 parts - a microchip and an antenna. The microchip is used to store and process data. It can also be employed to modulate and demodulate the radio frequency signals. The data is stored in the chip while an antenna is used for receiving and transmitting radio waves. When a tag receives a signal sent by a reader, it will backscatter the signal together with some data back to the reader. Every tag has an individual serial number that is stored in the microchip. The reader can read hundreds of tags at a time and distinguish them by recognizing their serial numbers.

There are three types of RFID tags - passive, active and semi-active. Active and semi-active tags can be powered by their internal batteries while a passive tag needs to be activated by the reader because no battery is included, as shown in Figure 1.4. The main difference between the active and the semi-active tags is that an active tag uses its own power to send back radio waves to the reader; whereas a semi-active tag relies on the power from the reader to reply the reader. As a result, the active and semi-active tags are usually more costly and they are commonly applied on applications that require detection over a far distance. In contrast, the passive tag is cheaper and it is more suitable

for disposable applications. A passive tag antenna is usually smaller and cheaper as it does not need a battery.

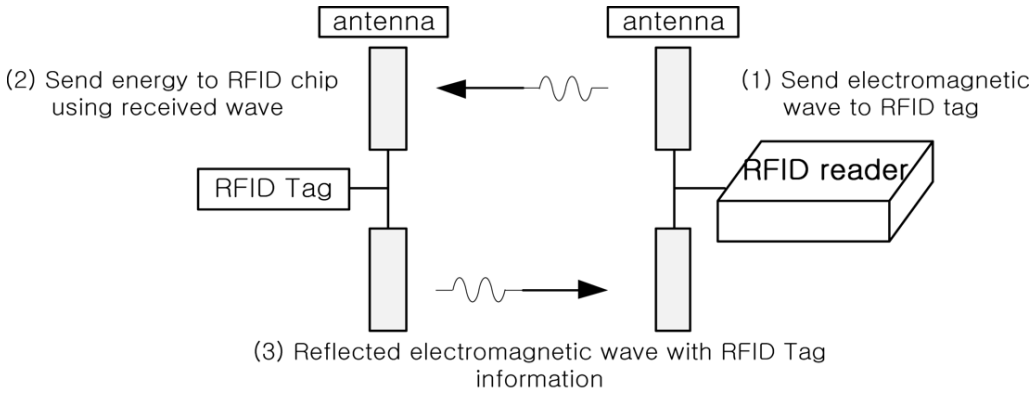

(a)

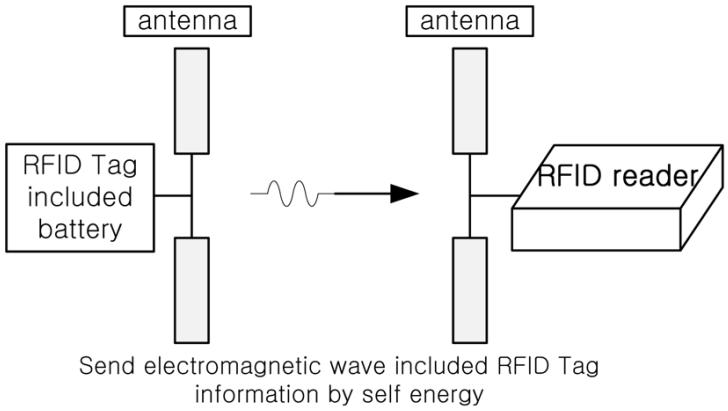

(b)

Figure 1.4: Backscattering RFID system with (a) Passive tag, (b) Active tag.

1.5 RFID Tag and Barcode

The use of RFID technology has become widespread and started to be applied on commercial products. Before this, the barcode system was a universal technology and a norm for retail products. It is cheap and can directly be simply printed on a piece of plastic or paper. However, the barcode has limited read distance and it can only be detected with direct line of sight. Since it is usually placed on the outer surface of a product, the barcode can be easily damaged by environmental pollutants such as dirt and water. It can be scratched and even become dim sometimes. Also, a barcode does not have "write" and "store" functions, making it not convenient for many practical applications. If there is mistake with the barcode printing, all the products are required to be collected back and reprinted again, which is very troublesome. On the other hand, the RFID system is more reliable and long lasting than the barcode system. The RFID tag can be detected from a greater distance and direct line of sight is not required. Although the RFID tag cannot be printed directly on the surface of a product, it can be inserted into the product and protected by an additional layer to shield it from damages. More importantly, the RFID tag has read, write and store functions, making it more convenient for information correction and storage. All the data can be easily encrypted and extra protections can be applied to the tag. In addition, hundreds of tags can be read at the same time, which can help to improve the efficiency. To sum up, we can conclude that the barcode system has less security as it can be easily reproduced or forged while the RFID system has higher security level. Also,

the RFID tag can be reused by removing all the previously written data and re-inserted with new information. This helps to reduce the production cost.

1.6 Problem Statements

Recently, the UHF RFID technology is growing rapidly due to its various advantages. However, there are still many challenges required to be solved when designing a new RFID tag. The performances of a RFID tag rely on many factors such as tag size, effects of the tagging materials, applications and so forth. Since a tag is usually attached to an object, the antenna size must be made small enough. Modern RFID tag antennas are usually required to be compact and useable in complex environments. Placing a tag antenna against metallic surface is, nevertheless, a big challenge as the image current is in the reverse direction and it can jeopardize the radiation efficiency. As a result, the read ranges of most of the commercially available metal-back tags are usually shorter than 3 meters. This has limited the automation flexibility of such tags in busy places such as department stores and container ports, where a longer read distance is expected.

Lately, the patch-type antenna structures have been studied for designing various platform insensitive UHF tags (Ukkonen et al., 2006). Patch resonator has its own ground, which can possibly isolate the radiator from the backing metal, and also a high capacitance that is useful for lowering the tag's

resonance (Chen, 2009; Ukkonen et al., 2006). The circuit size of a patch resonator can be huge as it is usually designed to operate at its half-wavelength resonance (Kuo and Liao, 2010). Metallic vias or walls can be introduced to connect one end of the patch radiator to ground, making it look like a planar inverted-F antenna in order to reduce the size of the patch (Chen and Tsao, 2010; Cho et al., 2010; Yang et al., 2011). Although the location of the vias and walls can help to tune the resonant frequency of the patch resonator, the tuning procedure can be complicated as the electrical length of the patch is very sensitive to the positions of the shorting vias. Also, extra manufacturing processes and costs are needed to fabricate these three-dimensional mechanical structures.

1.7 Research Objectives

The UHF RFID tagging technology has been more and more popular nowadays. The demands and application areas of various RFID tags grow rapidly throughout these few years. One of the important matters that has to be aware of is that the performances of a tag deteriorate when it is placed on metal surface. Also, the overall dimension of the tag antenna must be made small enough to meet all the requirements. The objective for this dissertation is to design a low profile, small size, light weight, high gain, and far read range folded-patch RFID tag antennas that are mountable on metal surface. Also, the effects of metal object on the performances of the folded-patch RFID tag

antennas are studied. Then, equivalent circuits will be derived in order to estimate the resonant frequencies of the proposed tags.

1.8 Overview

This dissertation consists of 5 chapters. The first chapter is started with introducing the backgrounds and giving a summary of the RFID technologies. The concepts and working principles of the RFID system have been explained briefly. The advantages of the RFID system over barcode and the challenges that have been faced by RFID engineers are discussed in this chapter too.

In chapter 2, five common methods that are commonly used to design metal-mountable tag antennas and a few miniaturization techniques are briefly discussed. The typical tag antenna requirements such as realized gain, impedance matching and so on are described in this section. Then, the design methodology is explained and a simple flowchart is shown to illustrate the design processes. Lastly, the measurement processes and techniques are studied in detail.

Chapter 3 focuses on a coplanar-fed folded-patch tag antenna for mounting on metal surface. The design process of the tag antenna is discussed and a simple equivalent circuit is modelled to characterize the impedance of the tag antenna. The measurement results are depicted and discussed. Parametric

studies show the useful parameters for fine- and coarse-tuning the input impedance of the tag antenna. Also, the effects of different metallic and dielectric materials are studied.

In chapter 4, a differential coplanar feedline folded-patch antenna is demonstrated for designing a metal tag antenna. The configuration of the tag is explained in detail, following by an equivalent circuit for characterizing the tag's impedance characteristics. The proposed tag is fabricated and the measurement results are illustrated. Parametric studies are analyzed and the effects of the parameters are discussed. Also, the performances of the tag on different dielectric materials and some real implementation scenarios are shown and studied.

Lastly, a conclusion is drawn in chapter 5.

CHAPTER 2

LITERATURE REVIEW AND METHODOLOGY

2.1 Introduction

The UHF RFID tagging technology is a fast growing segment. Most of the new RFID projects are using UHF systems because of their fast data processing and long read range. The UHF RFID tagging system can achieve a large read distance, which can up to 10m, and fast data processing rate that enables quicker transaction times. Also, it can function well even though it is small. This is a desirable feature as it can be attached on commercial products for tracking and manufacturing purposes. Not only this, the applications of the UHF RFID technology have also been developed into other sectors, such as retail, healthcare, life science, pharmaceutical, and anti-theft systems.

A passive UHF RFID tag can be activated by the radio wave transmitted from the reader antenna without the use of any power sources. The tag composes of a microchip and an antenna. The microchip is manufactured using semiconductor technology, which is very small in size. The footprint of the antenna is the main factor that determines the size of the tag. Few miniaturization methods have been proposed to minimize the tag size, such as applying meandered radiators, using high-permittivity substrates, and etching slots. Meandering the radiating arms can reduce the size of the antenna

efficiently. Besides, some researchers have used ceramic substrates with high dielectric constant to reduce the antenna size. Also, etching slots on the radiator patch can make the current paths electrically longer and help to miniaturize the tag size. All these miniaturization techniques will be briefly discussed in this chapter again. In spite of the aforementioned factors, the performances of a tag antenna are very sensitive to the tag size. It is usually a big challenge to keep the tag with high performance and small size at the same time.

2.2 Metal-Mountable UHF RFID Tag Antennas

As we know, most of the RFID applications are for tagging purposes. The tag antenna must be designed considering the effects of the backing object the tag is to be attached to. The resonant frequency, input impedance, radiation pattern, power transfer efficiency, and maximum read distance are easily affected by the backing objects, especially when they are metallic. The electromagnetic wave (EM) is 180° reflected from the metal surface, and it results in cancellation of the current induced in the antenna and the image current induced on the metallic surface (Zhang and Long, 2014). The maximum read distance can deteriorate and the resonant frequency can shift away from the desired frequency due to poor radiation efficiency. For example, a dipole tag antenna which works very well in free space can become very poor or malfunction when it is placed on metal surface. Therefore, it is a major challenge to design a tag antenna which can function well on various backing

materials without any severe degradation in performances, especially attaching to metallic object. In the next session, we will discuss several methods that can be used to improve the tag performances on metal surface.

2.2.1 Electromagnetic Bandgap (EBG)

Electromagnetic bandgap (EBG) structure is a metallic surface which exhibits high impedance at certain frequencies. This feature can be used to isolate the radiating elements from the ground plane. Figure 2.1 shows the design concept of a tag antenna with EBG structure. The EBG surface is inserted in between the antenna and the PEC ground plane.

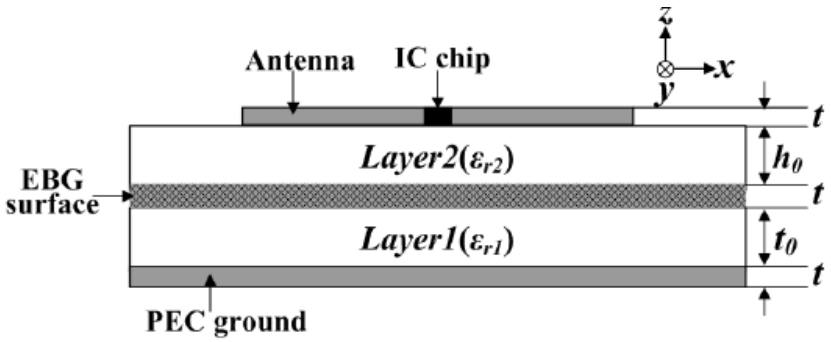

Figure 2.1: Configuration of the tag antenna with EBG structure (Sim et al., 2007).

Theoretically, the electromagnetic wave from the tag can be reflected 180° when being placed near to conductive surface. Reflection of the waves degrades the overall antenna performances including its radiation pattern and realized gain as well as resonant frequency. By applying the EBG structure, the phase of the electromagnetic waves changes continuously from -180° to 180°

at particular frequencies. As a result, the tag antenna can work well when the reflected phase is reflected near to 0° (Du, et al., 2011).

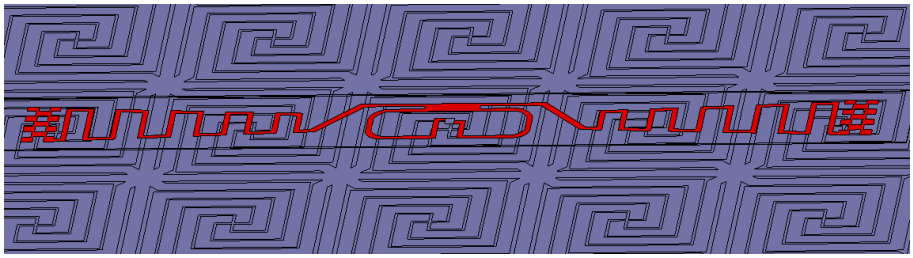

Figure 2.2: A dipole tag antenna placed on the EBG surface (Du, et al., 2011).

With reference to Figure 2.2, a dipole antenna (red colour) is placed on top of a EBG surface (grey colour). As we know, when the dipole antenna is placed directly on top of the ground plane, the power transmission coefficient of the tag is very poor and it cannot function well. In contrast, the tag antenna can work very well after the EBG structure is applied at the back of the dipole antenna, as shown in Figure 2.2. The EBG surface insulates the dipole antenna from the ground. However, the EBG surface is always large in size and the structure is usually complicated, which can increase the tag's profile and costs significantly.

2.2.2 Patch and Microstrip Antennas

Including a conducting plane at the back of a tag antenna can help to minimize the effects of the backing metal on the radiating element. Patch and microstrip antennas are applicable on metal surface as both of them also have a ground

plane to isolate their radiators. However, the patch and microstrip antennas are usually large in size because they are designed to work at their half-wavelength resonances (Kuo and Liao, 2010). In Figure 2.3, Kuo and Liao (2010) proposed a half-wavelength patch with an inductive loop for the purpose of impedance matching. The patch antenna has a dimension of 118 mm × 43 mm × 1.5 mm, and it is able to reach a maximum read range of 6 m on metal. The other microstrip patch antenna (Tashi, Hasan, and Yu, 2016), with a size of 86 mm × 58 mm × 1.6 mm, is shown in Figure 2.4. When the tag is mounted on a metallic object, its microstrip patch antenna has a maximum read distance of 1.89 m. Although both of the proposed antennas are working on metallic objects, their sizes are large and they are inconvenient to be used for mounting purposes.

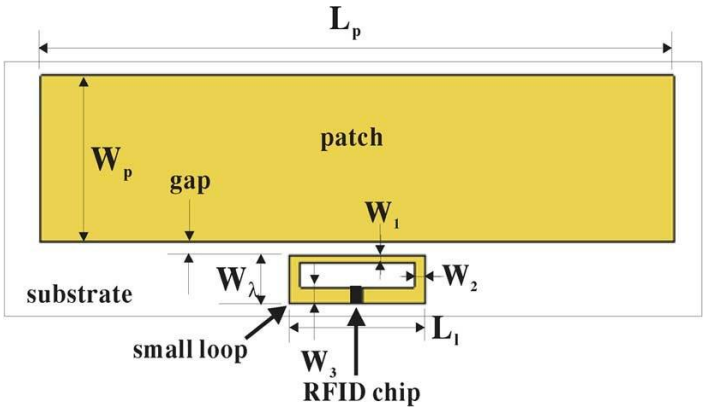

Figure 2.3: Patch antenna with an inductively couple feed (Kuo and Liao, 2010).

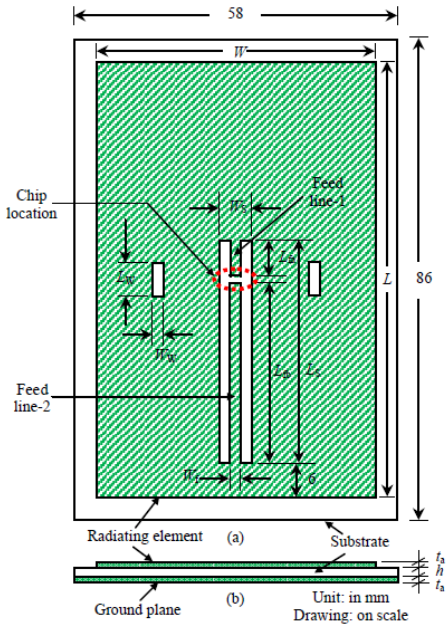

Figure 2.4: Microstrip patch antenna (Tashi, Hasan, and Yu, 2016).

2.2.3 Folded-Patch Antennas

Lately, the folded-patch antenna shown in Figure 2.5 has been proposed by Bong, Lim and Lo (2017a). As can be seen from Figure 2.5 (a) that the radiating element of the tag is connected to the ground plane through the loop-shaped stub. By controlling the width and the length of the loop-shaped stub, the inductive reactance can be easily adjusted. Also, the stub can bring down the resonant frequency essentially. The folded-patch antenna shown in Figure 2.5 (b) has a dimension of 30 mm × 30 mm × 3 mm. When being placed on a 20 cm × 20 cm metal plate, the tag can be read from a maximum read distance of 7 m with an EIRP of 4 W. With reference to Figure 2.6 (a), narrow meandered slotlines are incorporated into a folded-patch antenna with a

dimension of 26 mm × 16 mm × 1.6 mm. The dipolar patches are separated by an interdigital slot line at the centre. Then, the radiator patches are shorted to the ground through the highly inductive thin stubs, as shown in Figure 2.6 (b). Similar to the previous folded-patch antenna, both of the stubs can be adjusted to tune the resonant frequency. During measurement, it is able to be read beyond 4.5 m at the EIRP of 4 W when placed on a 20 cm × 20 cm metal plate.

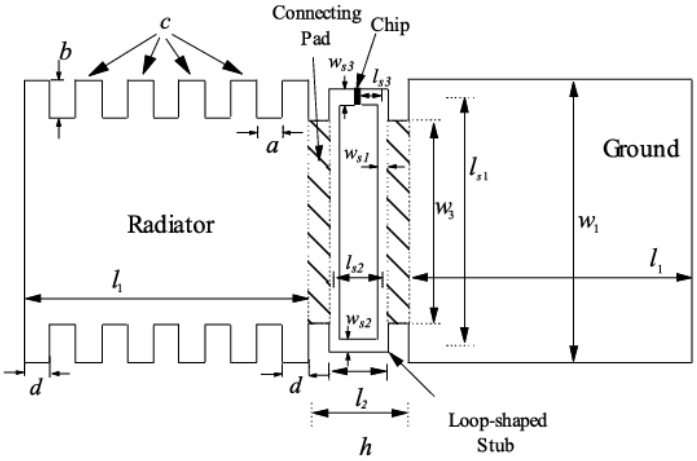

(a)

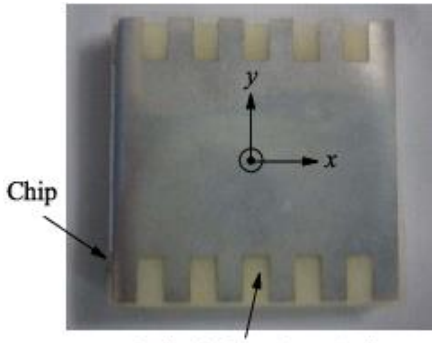

(b)

Figure 2.5: (a) Inlay of the folded-patch antenna before being folded around a substrate, (b) Prototype of the folded-patch antenna (Bong, Lim, and Lo, 2017a).

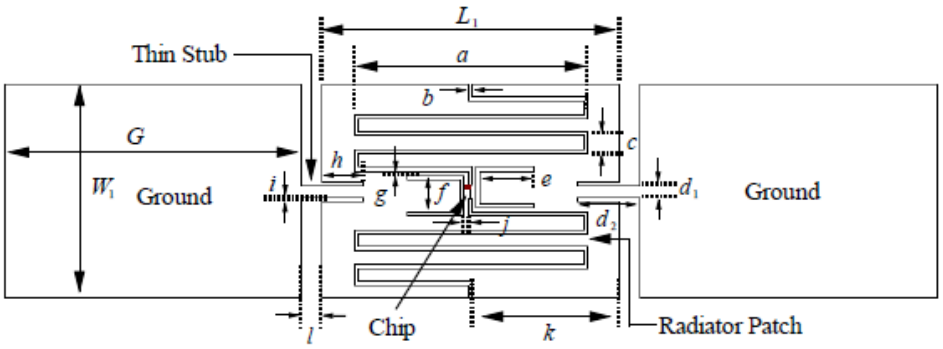

(a)

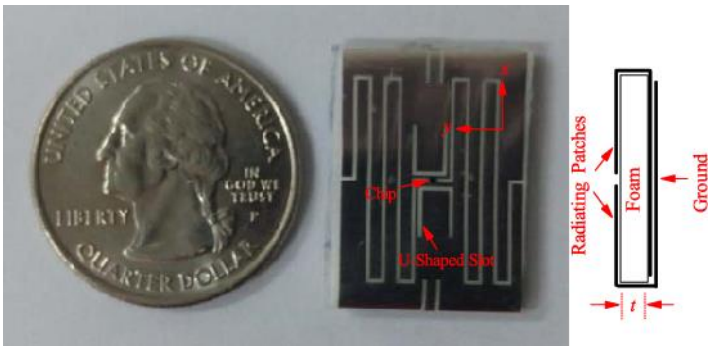

(b)

Figure 2.6: (a) Inlay of the folded-patch antenna before being folded around a substrate, (b) Prototype of the folded-patch antenna (Bong, Lim, and Lo, 2017c).

2.2.4 Planar Inverted F Antenna (PIFA)

PIFA is a quarter-wavelength antenna which is designed on the basis of inverted-F concept. The PIFA is popular as it has a low profile and omnidirectional radiation pattern. Also, it contains a ground plane at the back as isolator for the radiating elements and the backing objects. In this case, the effects of the backing metal can be significantly mitigated. Normally, a PIFA is

designed with the existence of the shorting pin in order to bring down the size of the antenna. The details will be discussed further again later.

2.2.5 Separate the radiating element from the backing metal

Figure 2.7 shows a dipole antenna where the radiating element is separated from the ground with the use of spacers (Hamani, et al., 2017).

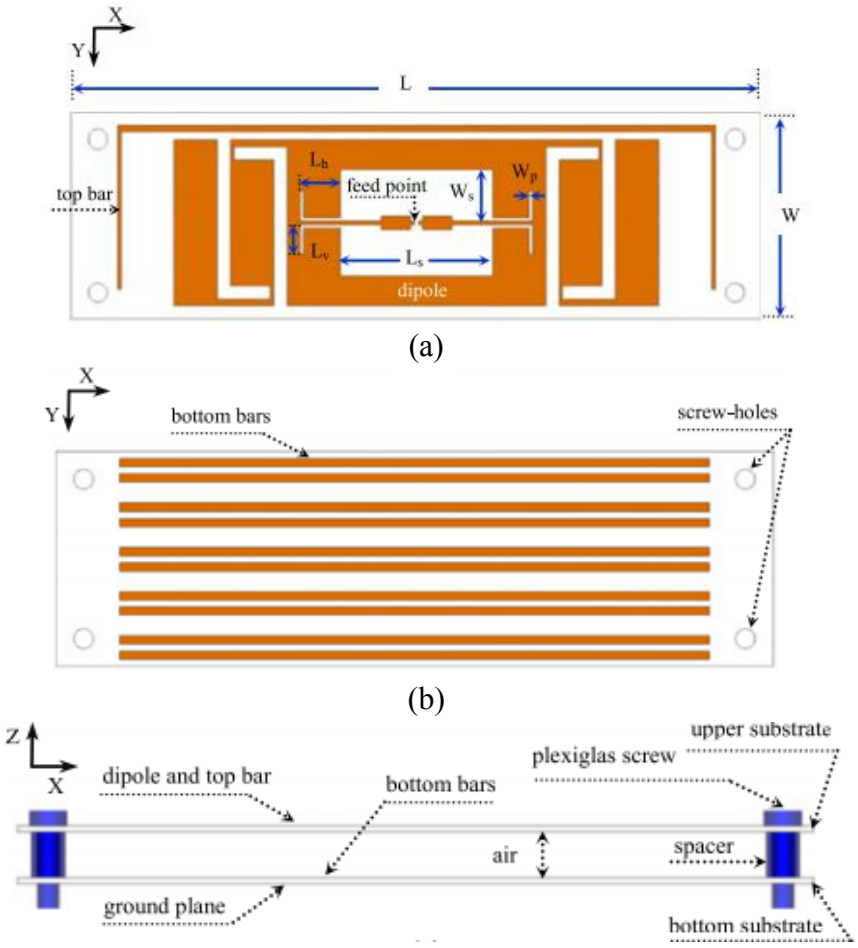

Figure 2.7: (a) Top Layer, (b) Second Layer, (c) Side view (Hamani, et al., 2017).

By doing so, the effects of the backing material on the tag performances can be lowered down, and it can produce similar performances regardless of the material of the tagging object. The maximum read distance of the proposed tag is 14.6 m at the EIRP of 4 W when placed on metal. However, it has a large size of 104 mm × 31 mm × 7.6 mm, making it not suitable for tagging purposes. Also, the fabrication process is complicated because holes are needed for inserting the spacers.

2.3 Miniaturize Techniques for UHF RFID Tag Antenna

In recent years, tag size is one of the important factors emphasized by most of the RFID engineers. The current trend in the UHF RFID technology is to design a small, cheap, and far-reading tag antenna. So, a brief discussion on the miniaturization techniques that are widely applied for designing various RFID tags will be analyzed in the next session.

2.3.1 Meandered and Laddered Feedlines

Meandered and laddered feedlines are commonly used to design RFID tag antennas for miniaturizing purposes. In Figure 2.8 (a), a meandered feedline with a T-match loop has been proposed for designing a tag antenna by Faudzi, et al. (2014). The overall tag size is 58 mm × 34 mm × 0.8 mm. By

incorporating the meander structure, the path of currents flow becomes much longer and it contributes to the additional inductance. This can help to reduce the resonant frequency of the tag antenna. However, cancellation of currents between the meandered feedline may occur if the feedlines are placed very close to each other. Therefore, another tag antenna with laddered feedlines is suggested in Figure 2.8 (b). By such, mutual coupling and current cancellation between the feedlines decrease. Consequently, the radiation efficiency can be improved with the use of the laddered feedlines. The dimension of the tag antenna in Figure 2.8 (b) is 53 mm × 28 mm × 0.8 mm. The maximum read distance when attached on a backing metal is 2.2 m for the tag antenna with laddered feedlines, while that with meandered lines is 2.0 m.

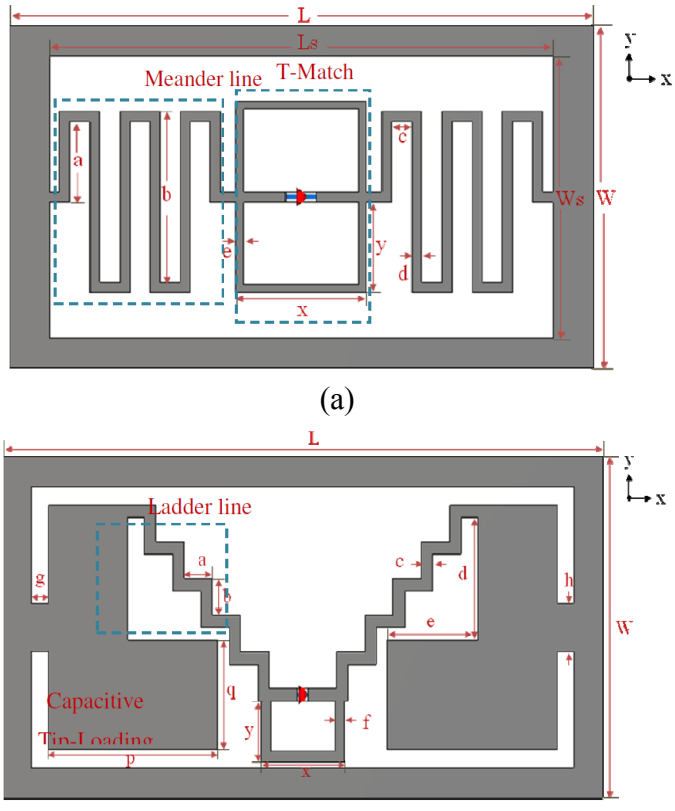

Figure 2.8: (a) Tag antenna with meandered feedlines. (b) Tag antenna with laddered feedlines. (Faudzi, et al., 2014).

2.3.2 Via or Shorting Pin

To reduce the size of the tag antenna, with reference to Figure 2.9, shorting pins are incorporated into the antenna structures. The radiating antenna on the top is a bowtie and the bottom part is a ground plane. The shorting pins are electrically connected the radiator to the ground plane to form a looped-bowtie RFID metal-mountable tag antenna. The currents at the radiator flow through the shorting pins to the conducting plane, results to a high inductive reactance. In this case, the resonant frequency and the size of the tag can be scaled down further. The overall size of tag antenna shown in Figure 2.9 is 70 mm × 24 mm × 3 mm. It can achieve a read distance of 2.8 m when mounted on a metallic sheet.

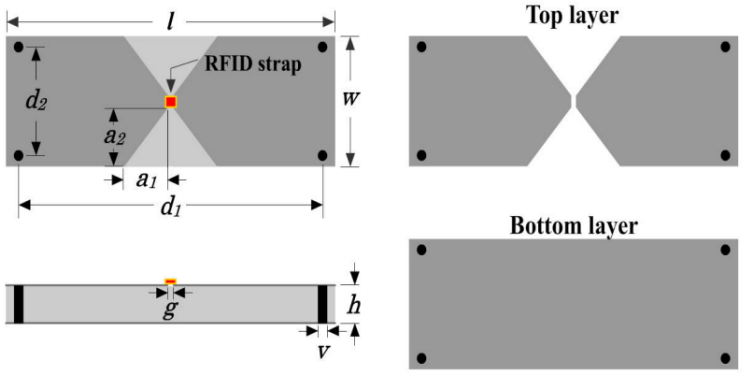

(a)

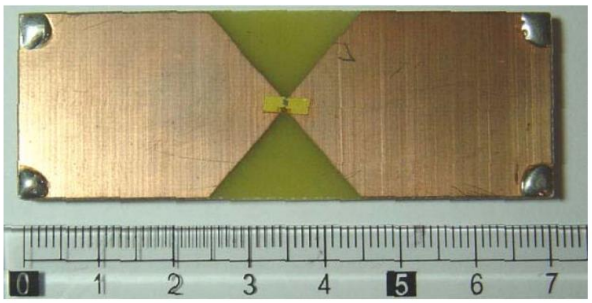

(b)

Figure 2.9: (a) Metal tag antenna with bowtie patch, (b) Prototype of the tag antenna with bowtie patch (Chen and Mittra, 2010).

In Figure 2.10, a flexible anti-metal tag antenna is designed using foam material with a dimension of 54 mm × 25 mm × 1 mm. The shorting pin is connected the radiator and the ground plane at the corner to reduce the size. When the tag antenna is placed on a 20 cm × 20 cm metallic sheet, the maximum read distances are 2.1 m and 1.8 m when being attached to a metallic cylinder.

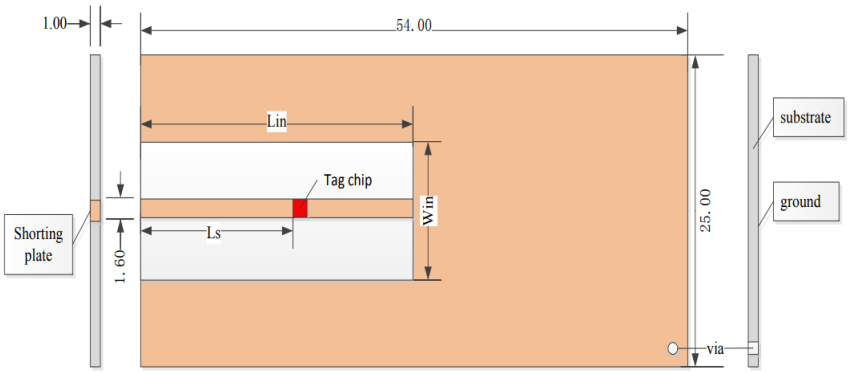

(a)

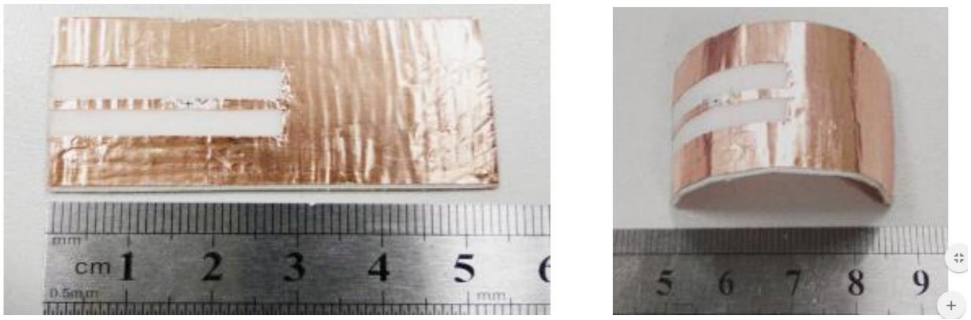

(b)

Figure 2.10: (a) Flexible anti-metal tag antenna, (b) Prototype of the flexible anti-metal tag antenna (Wu, et al., 2016).

As we mentioned before, the PIFA is a quarter-wavelength antenna due to the existence of the shorting pins. Figure 2.11 shows a PIFA tag with a dimension of 46 mm × 46 mm × 2.36 mm. There are nine shorting pins in total that are used for shorting the patch and the ground plane. The resonant

frequency and the impedance matching level can be controlled by adjusting the distances between the pins. The positions of the shorting pins can control the capacitance and inductance of the tag. The maximum read distance of the tag is 4.5 m when placed on a metallic object.

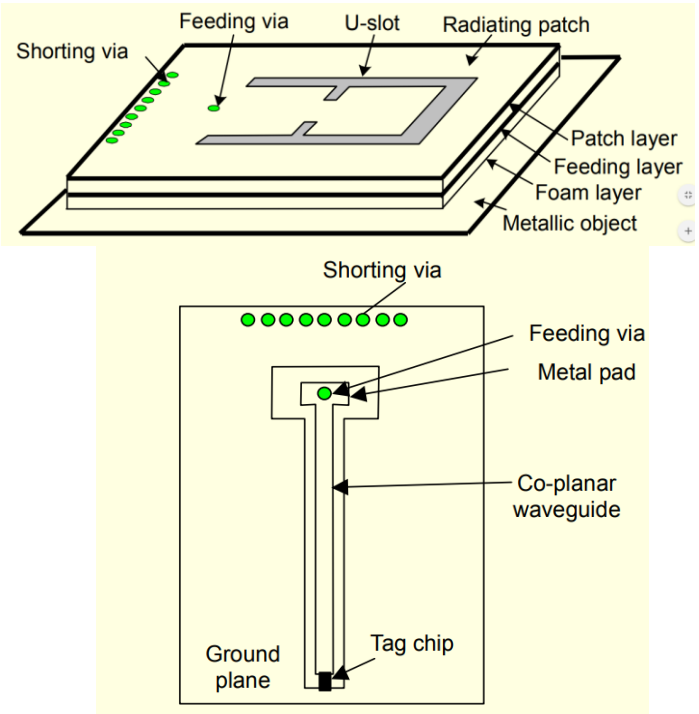

(a)

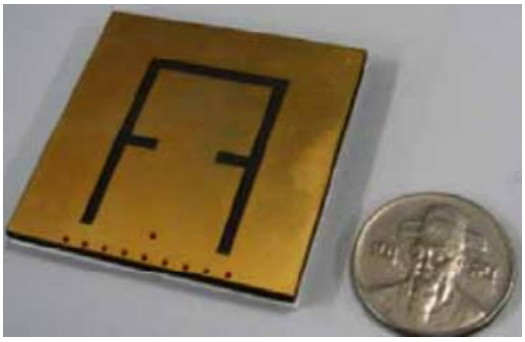

(b)

Figure 2.11: (a) Configuration of the tag antenna, (b) Prototype of the PIFA (Choi, et al., 2006).

Comparing with the EBG structure, the PIFA size is much smaller. However, the resonant frequency and input impedance are very sensitive with the positions of the shorting pins, making the tuning processes very inconvenient. Also, drilling process is needed for the addition of the shorting pin. In this case, the fabrication process has become more complicated and costly.

2.3.3 High Dielectric-Constant Substrate

High dielectric-constant substrate can be used to increase the radiation Q-factor, tag efficiency, and lower down the tag resonant frequency (Sharma and Shrivastava, 2009). In 2012, Babar, et al. presented the high-permittivity metal tag antenna shown in Figure 2.12 (a). The substrate is made of high-dielectric ceramic ($BaTiO_3$) and polydimethylsioxane (PDMS). The PDMS is a flexible, transparent, and low-loss polymer material. The permittivity of the substrate is around 12 and the loss tangent is around 0.01. The rectangular tag antenna has a dimension of 28 mm × 13 mm and it is made on a round substrate with a radius of 16 mm and thickness of 1.5 mm. As can be seen from Figure 2.12 (b), the substrate is flexible and it can be easily attached on curved surfaces. When the tag is mounted on flat metallic surface, the maximum read distance is around 3.3 m. The maximum read distance can be improved to 4.5 m when wrapping the tag on a cylindrical metal object with a radius of 15 mm. Also, the size can be minimized further by the loading effect between the radiator and the backing metal. Although the size of the tag is very small, the cost of the

substrate material is high, which is not economical for mass production.

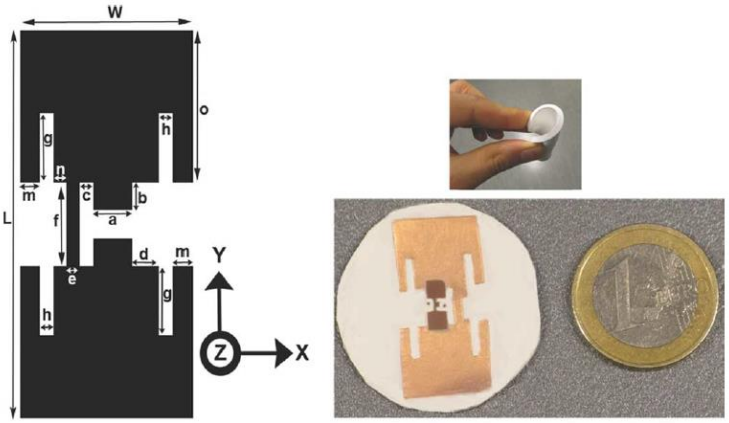

(a)

(b)

Figure 2.12: (a) Flexible high-permittivity metal tag antenna, (b) Prototype of the flexible high-permittivity metal tag antenna on metallic sheet and curved surface (Babar, et al., 2012).

2.3.4 Digital Serration

In 2017, the concept of introducing digital serrations to the edges of a folded-patch antenna was introduced by Bong, Lim and Lo (2017a) for the first time. The configuration of the serrated folded-patch antenna is shown in Figure 2.5.

Obviously, the serrated edges on the patch increase the current paths around the patch. The serrated edges introduces a higher inductance. However, the capacitance drops because the serration causes a smaller patch area. Introducing inductance can bring down the tag's resonant frequency and reduce the size of the tag antenna (Bong, Lim and Lo, 2017a).

2.3.5 Meandered Slotlines

With reference to Figure 2.6, meandered narrow slotlines are introduced for tuning down the resonant frequency of a folded-patch. Since the width of the slotline is very small, its effects on the characteristics of the patch are not significant (Bong, Lim and Lo, 2017c). With the use of meandered slotlines, the inductance of the tag antenna increases. Since the resonant frequency increases with the inductance of the tag antenna, it can be scaled down by reducing the size of the antenna.

2.4 Typical Tag Antenna Design Requirement

As an RFID engineer, the basic requirements and standards of the tag should be clarified before designing a new tag antenna. Here are some elements for the new tag design and all they play an important role in the performances of the tag.

- **Operating Frequency and Power**– Different countries allocate different RFID bands and maximum wattages allowable for the RFID applications. These frequency ranges and standards are set by a groups of international organizations and they are subject to changes. For example, China has allocated 920.5 MHz – 924.5 MHz with 2W of ERP. The United States and Canada have approved 902 MHz – 928 MHz with 4W of EIPR. Thus, a right frequency band and a proper power must first be chosen to suit the country's standards.
- **Tag Size**– The size of the tag antenna is one of the most important factors that will affect the performances of the tag. The bigger the tag size, the higher the antenna gain, resulting in a longer read distance. However, the smaller the tag size, the easier to implement the tag in most applications.
- **Usage and Application Environment**– The working environment is another important element that will affect the overall performances of the tag antenna. Before designing the tag, the usage of the tag should be known. When designing the tag, the environment especially the material of the tagged object should be considered in the simulation. Different backing materials have different dielectric constants, which will introduce different loading effects. The operating frequency and the read distance will be affected by them.
- **Material of the tag**– The characteristics of the tag's materials will affect the efficiency of the tag. If the tagged object has a curved surface, a flexible substrate should be used to design the tag.

- **Tag Orientation**– Different kinds of tag antennas have different orientations. It is very important to justify its orientation before designing a tag antenna because not all types of antennas can be detected in all angles. Normally, the high antenna gain can only be obtained in certain angles.
- **Costs-** The costs of the tag production will affect the decision of materials being used and the tag's performances as well.

2.5 Methodology

The flowchart in Figure 2.13 shows the design procedure of the proposed UHF RFID tag antenna, which will be further explained here. To design a tag with good performance and high efficiency, the tag requirements and the application environment need to be clarified. This is because the performances of a tag antenna are very sensitive to the tag size, surrounding, and even near/far objects in the adjacent. Needless to say that most of the RFID tags are usually applied for tagging purposes for identifying or tracking objects. Therefore, all these factors should be taken into consideration when designing a new tag antenna so it is able to achieve a better performance. Besides, the microchip is another important factor which affects the performances of the tag antenna. A microchip has its own sensitivities and intrinsic complex impedance. The characteristics of the microchip should be considered during the designing process as the maximum achievable read distance of the tag

antenna will be strongly affected.

The next action is to choose an appropriate structure that can generate the desired performance. In this project, the electromagnetic simulation tool (CST Microwave Studio Suite) is used to design and analyze the performances of all the tag antennas. The CST has an integrated design environment which provides access to the entire range of solver technologies. It can generate accurate and efficient solutions for electromagnetic designs.

The impedance matching, parametric studies, and optimization are all important factors to be considered when designing a tag antenna. With the use of the CST, all these parameters can be obtained and closely monitored. The characteristics of the tag can then be understood.

After all the requirements are fulfilled, the antenna prototype with optimized results is fabricated and measurement will be done in an anechoic chamber. The details of the measurement process will be discussed further in the next session.

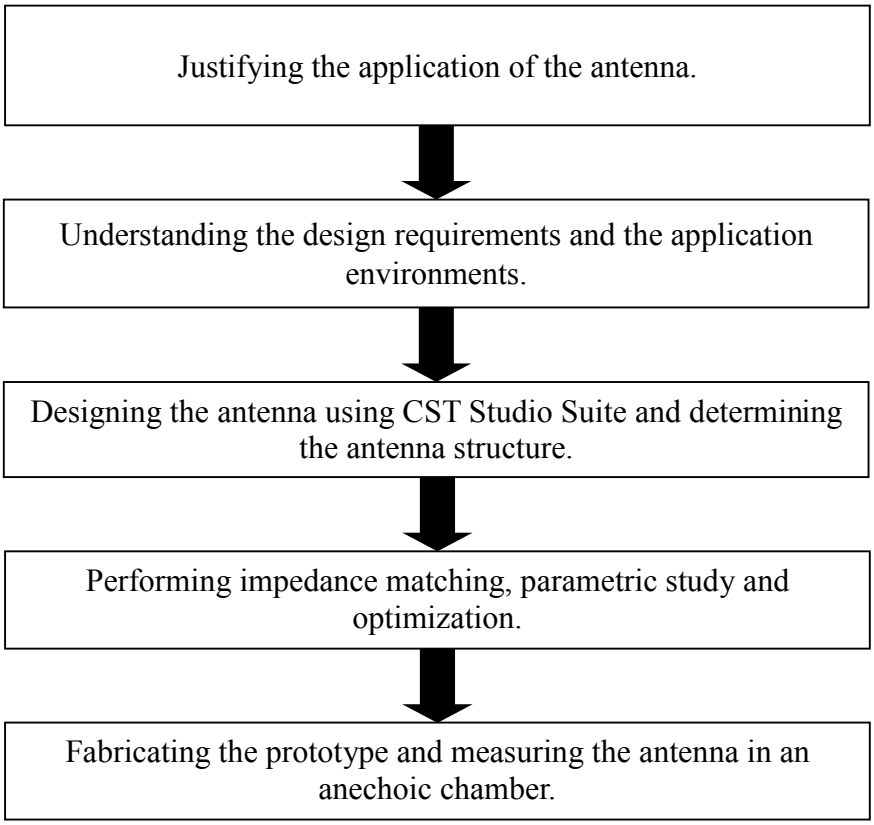

Figure 2.13: Design process of the proposed UHF RFID tag antenna.

2.6 Measurement Process

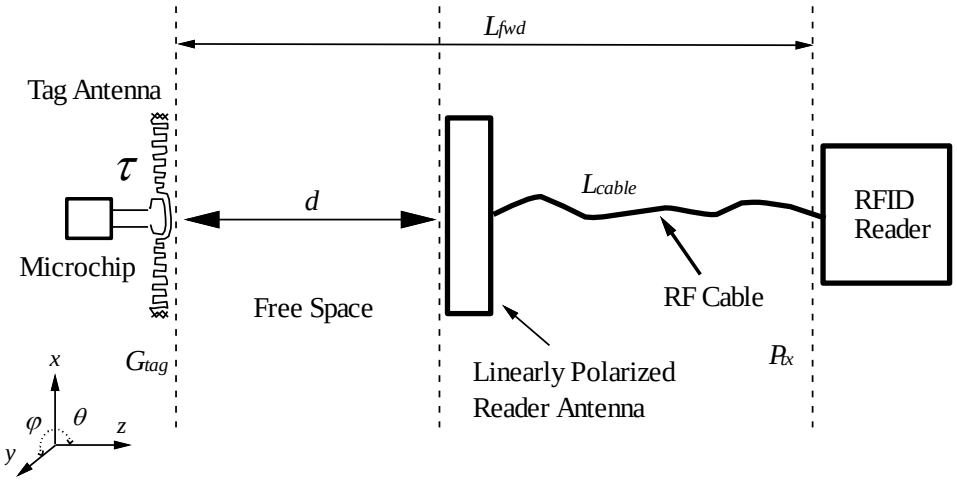

Figure 2.14: Schematic representation of the experimental setup in the anechoic chamber.

The commercial UHF RFID tagmeasurement system, Voyantic Tagformance (Tagformance, 2012), is used for measuring the read distance (D), the realized gain (G_r), and the tag sensitivity ($P_{tag.s}$) of the prototype. Before measuring the tag-under-test, the propagation path from 800 MHz to 1000 MHz is calibrated using a calibration tag, with a resolution of 1 MHz. Calibration is applied to maintain the instrument accuracy. It is one of the important processes to eliminate or minimize factors that might cause to any inaccurate measurements. The tag is attached on the middle of a Styroform with $\varepsilon_r \sim 1$ to avoid any parasitic interaction. With reference to Figure 2.14, the distance (d) between the reader and the tag remains constant in the measurement. The reader's transmission power (P_{tx}) is changed gradually during the measurement until the tag is activated. The linearly polarized transmitting reader antenna of the system has a gain (G_{tx}) of 8dBi and 4W of EIRP power is used to calculate

the maximum read distance of the tag from the reader. The tag and the reader are facing each other on a straight horizontal plane. It is important to ensure the height of the tag is exactly the same as the reader to minimize the polarization loss factor between them to $\eta_{pl} = 1$. In the setup, the reader is located at least one wavelength (λ) away from the tag in order to satisfy the far-field condition, where λ represents the wavelength at the desired operating–frequency. The reader is fixed while the tag antenna is rotated about the axis' as illustrated in Figure 2.14. The path loss L_{fwd} between the reader and the tag can be calculated as

$$L_{fwd} = G_{tx}[dBi] - |L_{cable}|[dB] - FSL[dB], \quad (2.1)$$

where G_{tx}, FSL and L_{cable} represent the gain of the reader antenna, the free space loss, and the cable loss that connects between the reader and its associated antenna, respectively. During measurement, the power of the reader is transmitted and altered gradually until a sufficient energy passes the threshold, and a backscattered power is obtained by the reader. This turn-on power is the threshold of the reader's transmitted power (P_{thr}) to activate the tag-under-test. Based on the received P_{thr}, the tag sensitivity $P_{tag.s}$ can then be expressed as

$$P_{tag.s}[dBm] = P_{thr}[dBm] - \left|L_{fwd}\right|[dB] \quad , \quad (2.2)$$

L_{fwd} will always have a negative sign (-) because it is considered as the attenuated power due to the path loss. So, the equation can be wrote as

$$P_{tag.s}[dBm] = P_{thr}[dBm] + \left|L_{fwd}\right|[dB] \quad , \quad (2.3)$$

In the threshold measurement, the microchip's sensitivity will be equal to the minimum power to activate the microchip ($P_{chip,on}$),

$$P_{chip,on}[dBm] = P_{tag.s}[dBm] + G_r[dBi] \quad , \quad (2.4)$$

where G_r indicate the realized gain of the proposed tag antenna. Reformulating the equation, where

$$G_r[dBi] = P_{chip,on}[dBm] - P_{tag.s}[dBm] \quad , \quad (2.5)$$

By converting the equation to linear scale, the proposed tag antenna gain can be formulated as follow,

$$G_r = P_{chip,on}/P_{tag.s} = P_{chip,on}/\left(P_{thr} \cdot L_{fwd}\right) \quad , \quad (2.6)$$

Then, the equivalent isotropic radiated power (P_{EIRP}) can be expressed as

$$P_{EIRP} = P_{tx} \cdot G_{tx} \quad , \quad (2.7)$$

The maximum distance for the tag to turn-on, D, (also known as read distance) can then be easily obtained using formula (2.8) (Tagformance, 2012). The calculation is derived from the Friis transmission equation (Virtanen, et al., 2010; Nikitin, Rao and Lam, 2012).

$$D = \lambda/4\pi \cdot \sqrt{P_{tx}.G_{tx}.G_r/P_{chip,on}}$$
$$= \lambda/4\pi \cdot \sqrt{P_{EIRP}/P_{tag.s}} \quad , \quad (2.8)$$

2.6.1 Input Impedance Measurement

Input impedance is an important factor when designing a tag antenna. The input impedance of the tag antenna is required to match to the chip's input impedance in order to have a better power transmission coefficient. If the input impedance is not well matched to the chip's impedance, the power delivered to the proposed tag antenna will be low and the achievable read distance is affected. Figure 2.15 shows the setup of the input impedance measurement. A differential probe is connected to a R&S ZVB8 vector analyzer to measure the input impedance of the prototype (Ng, et al., 2018). The probe is gently probed on the input port of the tag antenna. When measuring the input impedance, the tag is placed at the center of a 20 cm × 20 cm metal plate which is placed on a Styrofoam.

Figure 2.15: Experimental setup for measuring the input impedance.

CHAPTER 3

MINIATURE COPLANAR-FED FOLDED-PATCH FOR METAL-MOUNTABLE UHF RFID TAG

3.1 Introduction

The UHF RFID tagging technology has been broadly adopted by many practical applications, including electronic toll collection, asset identification, inventory management and patient monitoring (Fennani, Hamam and Dahmane, 2011). The passive UHF tag antenna is popular because of it is able to provide small footprint and long read range. Also, the passive tag can be activated by radio waves from the reader (Rao, Nikitin and Lam, 2005). In recent years, the dipole-type antennas have become popular due to their simplicity in structure. However, a dipole-type antenna is not suitable to place on the metal surface (Dobkin and Weigand, 2005). The image current, which is equal in magnitude but opposite in phase cancels out the EM field of the current on the radiator. Also in this case, the tag's resonance can deviate from the design frequency because of the fluctuation in antenna impedance. This is very undesirable as it may cause the tag to become malfunction.

To isolate the effects of the backing metal and improve the radiation efficiency, electromagnetic bandgap (EBG) and artificial magnetic conductor (AMC) structures are good ways to solve the problem (Gao and Yuen, 2011;

Park and Kim, 2014). They can exhibit high impedance at certain frequencies, which can be inserted to isolate the tag antenna from the metal surfaces. But, applying EBG and AMC are usually complicated and their inclusion can increase the tag's profile and costs significantly. The patch antenna has been employed for designing different metal-mountable UHF tags (Cho, Choo and Park, 2008), and the existence of the ground plane helps to isolate the radiator so that the effects of the backing metal can be significantly mitigated. One of the important features of patch resonator is its high capacitance that can be used for reducing the tag's resonant frequency (Chen, 2009), which is usually too high to be useful for the UHF RFID applications.

Since a patch antenna is usually designed to work at its half-wavelength resonance (Kuo and Liao, 2010), the footprint of the patch is usually very large. In recent years, new techniques have been explored for reducing the patch size. Using high-permittivity substrate is another effective way to reduce the tag's profile without affecting its performances, but the high-permittivity substrates are normally pricey (Babar, 2012). It was found that slots etched on a patch resonator can lengthen the current path and increase its electrical length so that miniaturization can be achieved (Manzari, Pettinari and Marrocco, 2012; Lin, et al., 2016). Beside, slots can provide inductive reactance for balancing the chip's input impedance, which is usually capacitive. By incorporating vias and shorting walls into the inverted-F antenna structures (Hirvonen et al., 2004; Lim and Leung, 2012), miniaturization can be easily done. However, the tuning mechanism for such antenna is very tedious as its

resonant frequency is very sensitive to the locations of the vias and shorting walls, which are more costly to fabricate as well.

In this project, a folded-patch antenna is proposed for designing a miniature UHF tag that can be mounted on metal surface. Inspired by the inverted-F structures, which are difficult to be tuned because of the existence of the metallic vias, a new antenna based on the folded-patch configuration is proposed. To make the fabrication process simple, the proposed antenna is designed only on one surface of a flexible PET polyethylene terephthalate substrate. The flexible substrate can be folded and two inductive stubs are incorporated tactfully so that they form the shorting stubs on the vertical walls after the folding process. It will be shown later that the input impedance of the tag antenna can be adjusted effectively by changing the dimensions of the stubs. Also for the first time, the coplanar waveguide is explored for feeding a tag antenna and the chip is embedded into the feedline so that it does not require additional space. Notches are extended from one of the stubs for increasing its tuning range. The proposed antenna structure is very simple and compact, and it is able to reach a far read distance of beyond 10m. Most importantly, it can be easily made by folding a single piece of flexible substrate and it does not require the use of any via holes, making the fabrication process much easier. It will be shown later that the achievable read distance of the proposed tag antenna is much superior than those contemporary miniature metal tags with antenna size of less than 50mm. Worth-mentioning is that the proposed tag is designed using foam material with $\varepsilon_r \sim 1$, and it does not require the use of high-permittivity substrate to scale down the antenna size.

This chapter is arranged as follows. In section 3.2, the configuration of the tag antenna is discussed. An equivalent circuit is proposed here for investigating the impedance characteristics. Then, the tag sensitivity, realized gain, radiation patterns, and read distances are analyzed in section 3.3. Finally, the proposed tag antenna is tested in several implementation scenarios. The tag performs very well on metal with very little fluctuation in the resonant frequency, which is a very desirable feature for tag design.

3.2 Equivalent Circuit Model and Tag Configuration

Figure 3.1 (a) shows the inlay of the proposed antenna before folding. A thin layer of aluminum with a thickness of 9 μm is deposited on a flexible PET substrate (50 μm). The proposed antenna is made by a radiating patch with two ground layers on the left and right sides. The patch is fed by a coplanar feedline and it is connected to the bottom ground layer through two inductive stubs, one of which is etched with notches for increasing the frequency tuning range. Table 3.1 is the design parameters of the proposed tag antenna. The parameters are useful in frequency and impedance tunings. The inlay shows in Figure 3.1 (a) is wrapped symmetrically around a rectangular polyethylene foam (with ε_r = 1.03, tanδ = 0.0001) and the two ground layers are overlapped together at the back, as shown in Figure 3.1 (b). The overall size of the antenna structure is $b \times a$ (40mm × 25mm) and the thickness (t) of the polyethylene foam is 3mm. With

reference to the figure, a microchip is placed in between the feedline with a distance of l_4 = 18.5 mm from the edge. The CST Microwave Studio is used in all the simulations.

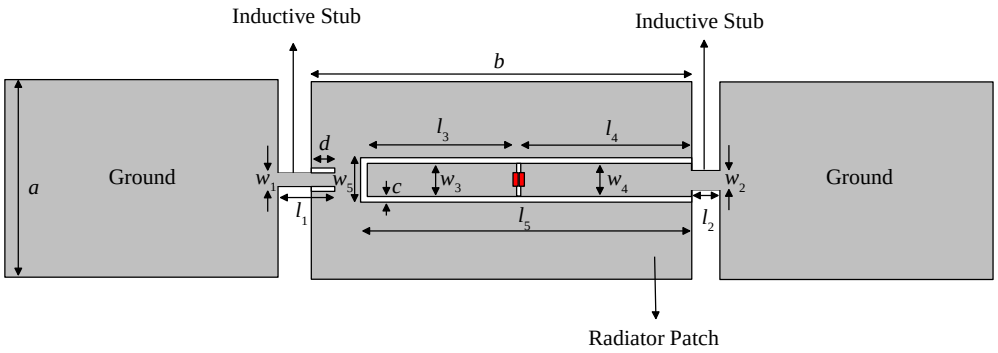

(a)

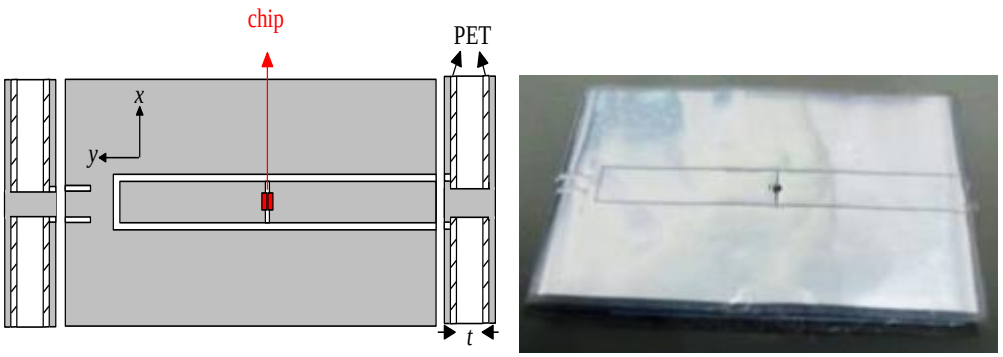

(b)

Figure 3.1: (a) Inlay of the proposed tag antenna. (b) Topdown view of the completed tag antenna.

Table 3.1: Optimized parameters of the proposed tag antenna.

Parameter	(mm)	Parameter	(mm)
a	25	b	40
c	0.2	d	2.55
l_1	5.83	w_1	1.3
l_2	3.28	w_2	2
l_3	17	w_3	4
l_4	18.5	w_4	4
l_5	36	w_5	4.4
t	3		

An equivalent circuit model is derived for the proposed tag antenna, as shown in Figure 3.2. Lumped element R_a, L_a and C_a connected in parallel represents the patch resonator. R_{si} and L_{si} are the resistances and inductances of the feedine and the inductive stubs. C_{g1} is the capacitance of the narrow gap that accommodates the chip and C_{g2} is the capacitance of the slot in between the patch and the feedline. The resistance, inductance, and capacitances R_a, L_a, C_{g1} and C_{g2} are curve-fitted using the macromodel method in (Kim and Yeo, 2010; Lim and Leung, 2012). C_a is the capacitance between the radiator patch and the ground plane, which can be calculated as

$$C_a = \varepsilon A_T / t \quad , \quad (3.1)$$

where $A_T = a \times b$ is the effective surface area of the radiator, and ε and t are the permittivity and thickness of the polyethylene foam. The resistance of the rectangular conductor can be calculated using the AC resistance equation

below (Alan Payne, 2016),

$$R_{si} = 2[(\rho l_i)/(w_i t_s)][K_C/(1 - e^{-x})] \ , \qquad (3.2)$$

where $x = 2(1 + t_s/w_i)\,\delta/t_s$, l_i is the length of the rectangular conductor, w_i is the width of the rectangular inductor and the inductance is in meter. The values δ=2.74×10^{-6} m, ρ=2.65×10^{-8} Ωm, K_c=1.77, and t_s=0.000009 m represent the skin depth, current crowding factor, and thickness of aluminum, respectively. The inductance of a rectangular conductor (Greenhouse, 1974) can be calculated as

$$L_{si} = 0.002 l_i\{\ln[2l_i/(w_i + t_s)] + 0.50049 + [(w_i + t_s)/3l_i]\} \ , \quad (3.3)$$

where l_i, w_i, and t_s are in centimeters. When the stub becomes longer and narrower, its resistance and inductance values increase proportionally. Based on the dimensions of the feedlines and the shorting stubs, the corresponding resistances and inductances of all the line segments are shown in the Table 3.2.

Table 3.2: Resistances and inductances of all the line segments corresponding to the dimensions of the feedlines and the shorting stubs.

Dimension	Resistance and Inductance
w_1, l_1	R_{s1}=0.1 Ω, L_{s1}=3.22 nH
w_2, l_2	R_{s2}=0.04 Ω, L_{s2}=1.24 nH
w_3, l_3	R_{s3}=0.1 Ω, L_{s3}=9.24 nH
w_4, l_4	R_{s4}=0.1 Ω, L_{s4}=10.34 nH

By knowing all the components, the input impedance can be derived as

$$Z_{in} = \frac{R_a+\Delta R_T+j(\Delta-R_a^2\alpha)}{\Delta-\omega C_{g1}(\beta\Delta-R_a^2\alpha)+j\omega C_{g1}(R_a+\Delta R_T)} \quad , \tag{3.4}$$

where$\Delta = 1 + R_a^2\alpha^2$, $\alpha = \omega C_a - \frac{1}{\omega L_a}$, and $\beta = \omega L_T - \frac{1}{\omega C_{g2}}$.

The parameters R_T and L_T are the total resistance and inductance in series, and they can be written as

$$R_T = R_{S1} + R_{S2} + R_{S3} + R_{S4} \quad , \tag{3.5}$$

$$L_T = L_{S1} + L_{S2} + L_{S3} + L_{S4} \quad , \tag{3.6}$$

The resonant frequency of the tag antenna can be determined from the reactive components of the equivalent circuit. It can be seen that the reactance of the antenna is X_{in} = Im$\{Z_{in}\}$with the use of equation (3.4), and it must be designed close to the chip reactance. The values of X_{in} can be easily tuned by adjusting the geometrical parameters of the tag antenna. In our case, the reactance X_{in} is calculated to be 153 Ω at 925 MHz, which is slightly higher than the simulated reactance. It should be mentioned that the equivalent circuit can only be used for approximating the reactance as it does not include the coupling effects between the components.

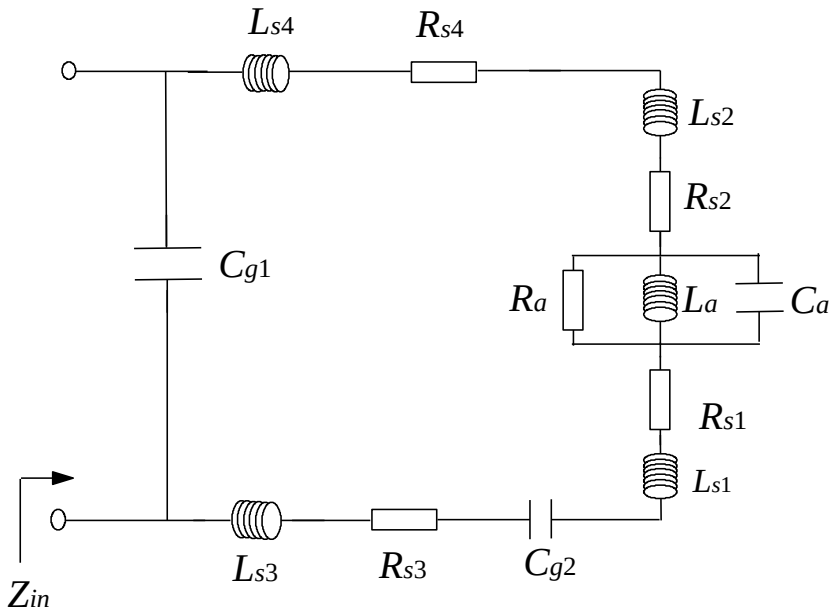

Figure 3.2: Equivalent circuit of the tag antenna.

Table 3.3: The values of the components in the equivalent circuit.

Component	Value	Component	Value
R_a	3.0 kΩ	L_{s1}	3.22 nH
L_a	7.25 nH	L_{s2}	1.24 nH
C_a	2.87 pF	L_{s3}	9.24 nH
R_{s1}	0.1 Ω	L_{s4}	10.34 nH
R_{s2}	0.04 Ω	C_{g1}	0.67 pF
R_{s3}	0.1 Ω	C_{g2}	0.93 pF
R_{s4}	0.1 Ω		

MONZA R5 (IPJ-W1610, 2016) is chosen as the microchip of the proposed tag antenna. From the datasheet, it has been provided that the reading and writing sensitivities of MONZA R5 are -17.8 dBm and -13.75 dBm, respectively. Also, the microchip has an input impedance (Z_c) of (14.25 –

j159.53) Ω at 925 MHz. Figure 3.3 shows the simulated, measured, and modelled (calculated using equation (3.4-3.6)) input impedances of the proposed tag antenna. Good matching is noticed between the simulated and modelled curves, showing that the equivalent circuit is reasonable. The simulated input impedance of the antenna is (16.55 + j152.6) Ω at 925 MHz, which is nearly in conjugate match with that of the chip.

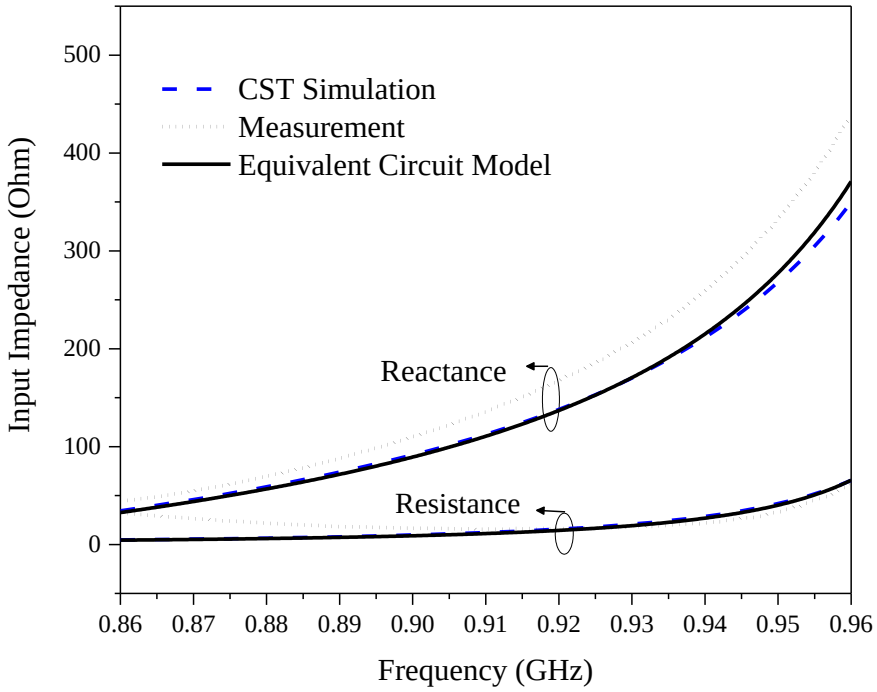

Figure 3.3: Simulated, modelled, and measured input impedances of the proposed tag antenna.

Next, the effect of the design parameters on the resistance, reactance, power transmission coefficient (τ), directivity, and radiation efficiency are studied. Power transmission coefficient (τ) is part of the power that is sent to the microchip in practical, which can be used to evaluate the performance of the proposed tag antenna (Rao, Nikitin and Lam, 2005). The formula used to

calculate τ is derived as

$$\tau = (4R_aR_c)/(|Z_a + Z_c|^2)\ ,\ 0 \leq \tau \leq 1 \qquad , \qquad (3.7)$$

where $Z_a = R_a + jX_a$and $Z_c = R_c + jX_c$ are the impedances of the antenna and the chip, respectively. Firstly, the gap distance between the feedline and the patch is studied. With reference to Figure 3.4 (a), the resistance and reactance increase when the gap distance becomes narrower due to the increase of the inductance. A larger frequency reduction from 925MHz to 1.0 GHZ is resulted when *c* is increased from 0.2 mm to 0.6 mm, which implies that this parameter can be used to coarse-tune the tag's resonant frequency efficiently, as can be seen in Figure 3.4 (b). Also observed is that the power transmission coefficient (τ) are able to remain above 80% for all cases. It can be seen from Figure 3.4 (c) that the directivity decreases when the gap distance is decreased. The radiation efficiency remains in range of 0.24 – 0.20 when the gap is changed from 0.2 mm to 0.6 m, which is reasonable as the tag antenna is electrically small.

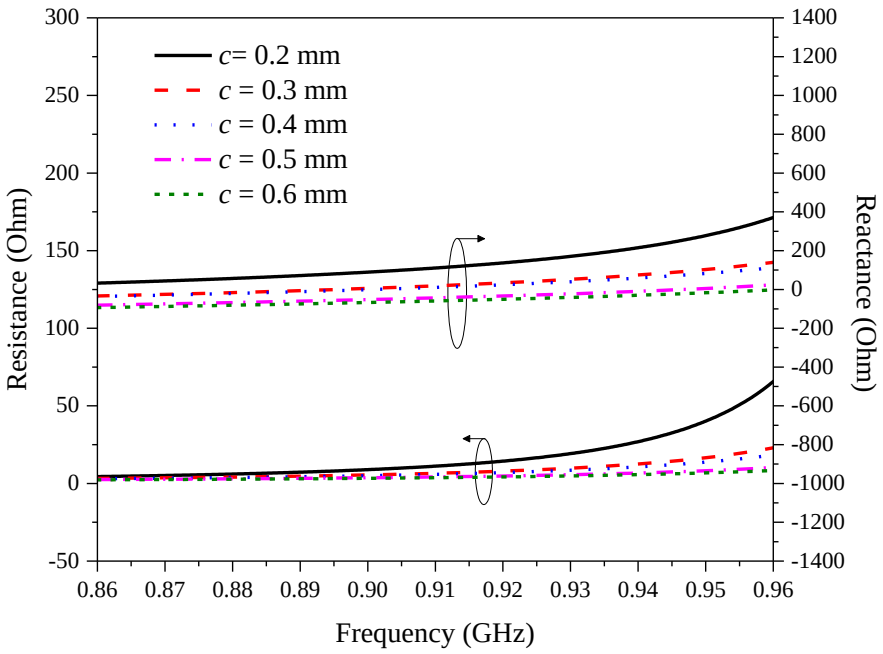
c= 0.2 mm
c = 0.3 mm
c = 0.4 mm
c = 0.5 mm
c = 0.6 mm
Resistance (Ohm)
Reactance (Ohm)
Frequency (GHz)

(a)

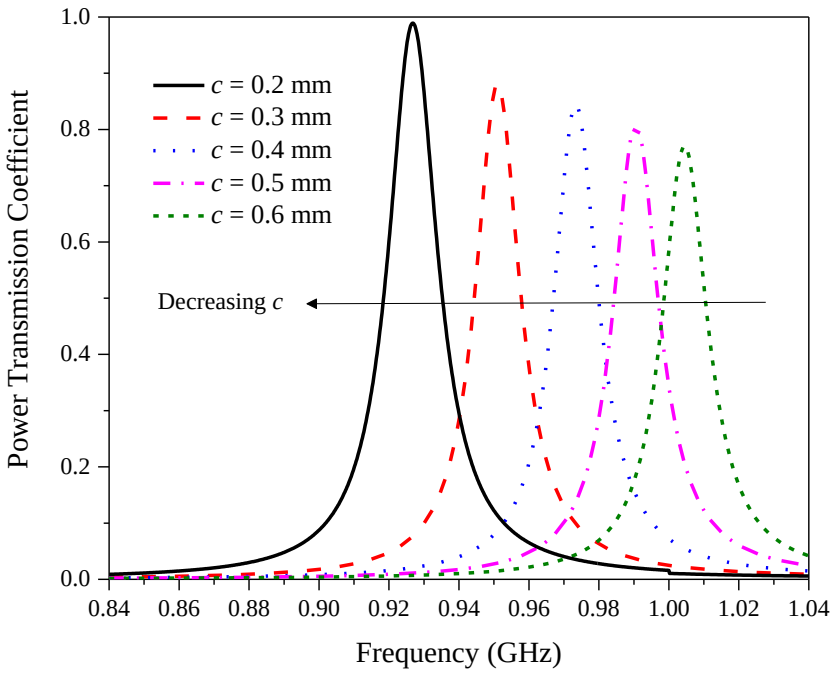
c = 0.2 mm
c = 0.3 mm
c = 0.4 mm
c = 0.5 mm
c = 0.6 mm
Decreasing c
Power Transmission Coefficient
Frequency (GHz)

(b)

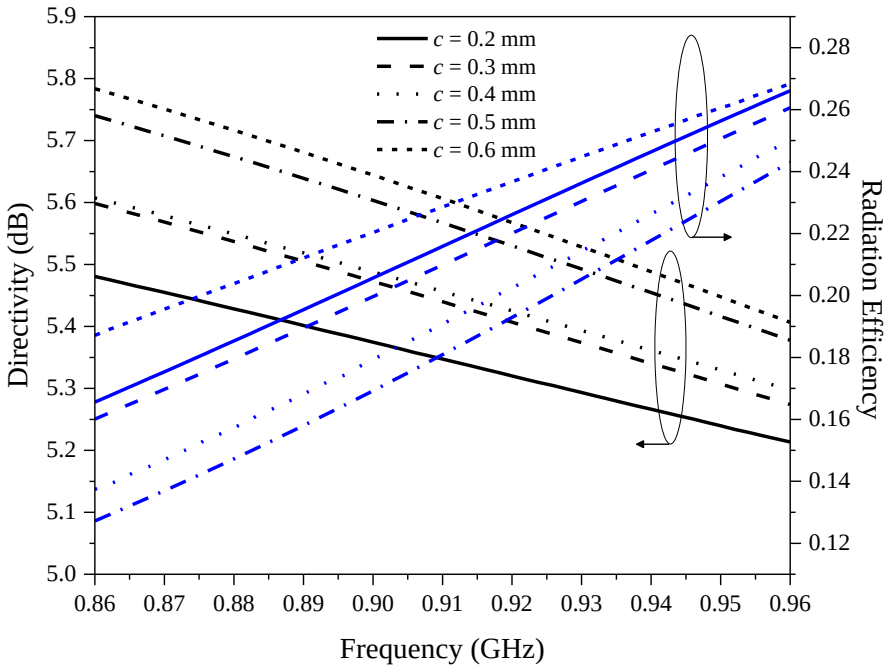

(c)

Figure 3.4: Effects of feedline length *c* on the (a) resistance and reactance, (b) power transmission coefficient and (c) directivity and radiation efficiency.

Then, Figure 3.5 depicts the effects of the inductive stub. By reducing the stub width, the resistance and reactance can be greatly adjusted as the stub becomes more resistive and inductive with decreasing width, as shown in Figure 3.5 (a). It can also be seen from Figure 3.5 (b) that becoming more inductive also causes the tag's resonant frequency to decrease, which is a reasonable trend for a parallel *RLC* resonator. Since the tag antenna is designed to be nearly in conjugate match with the chip impedance, the power transmission coefficient (τ) is found to be greater than 95 % for all w_1 values in Figure 3.5 (b). The resonant frequency reduces from 966.4 MHz to 914.6 MHz

when varying w_1, which can be applied to coarse-tune the tag's resonant frequency. It is observed in Figure 3.5 (c) that the antenna directivity decreases when the width w_1 is reduced, and the radiation efficiency falls within the range of 0.23 – 0.25 at 925 MHz. Variation in the stub width w_2 has very little effect on the resistance, but it can affect the reactance slightly. Similar trend is observed for w_1 and the results are omitted here.

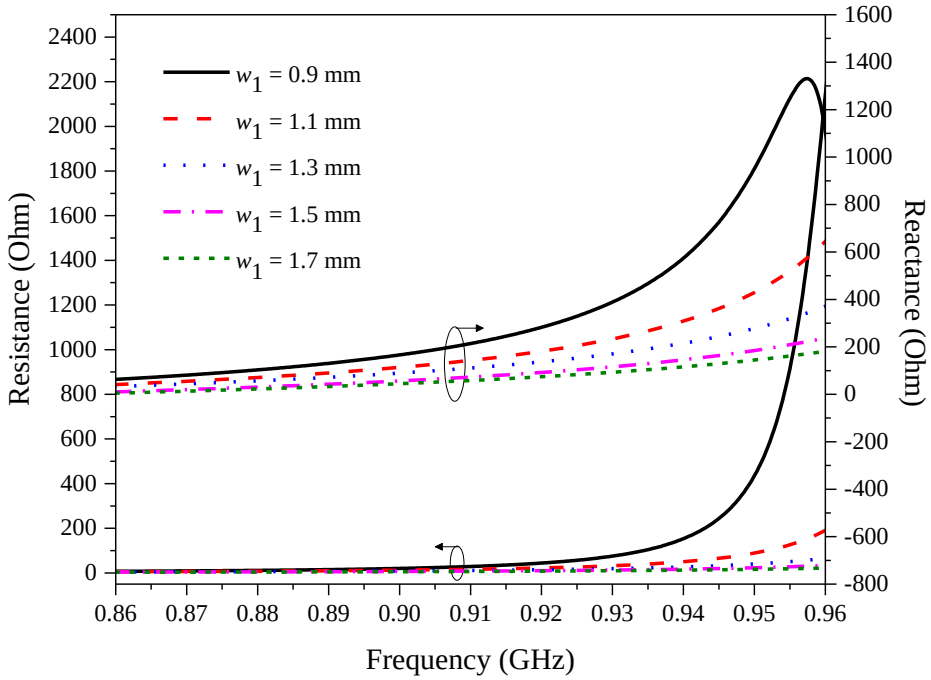

(a)

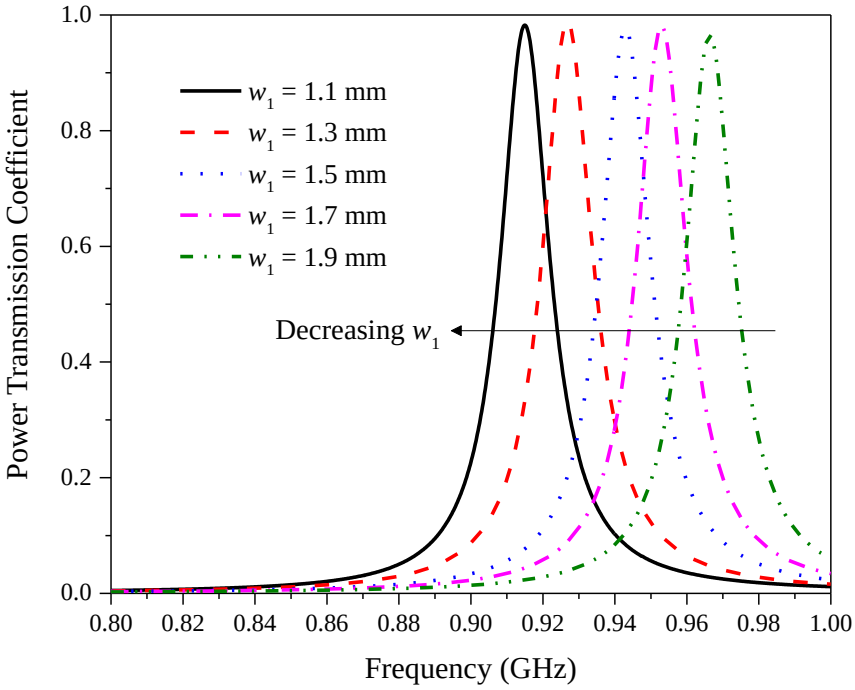

(b)

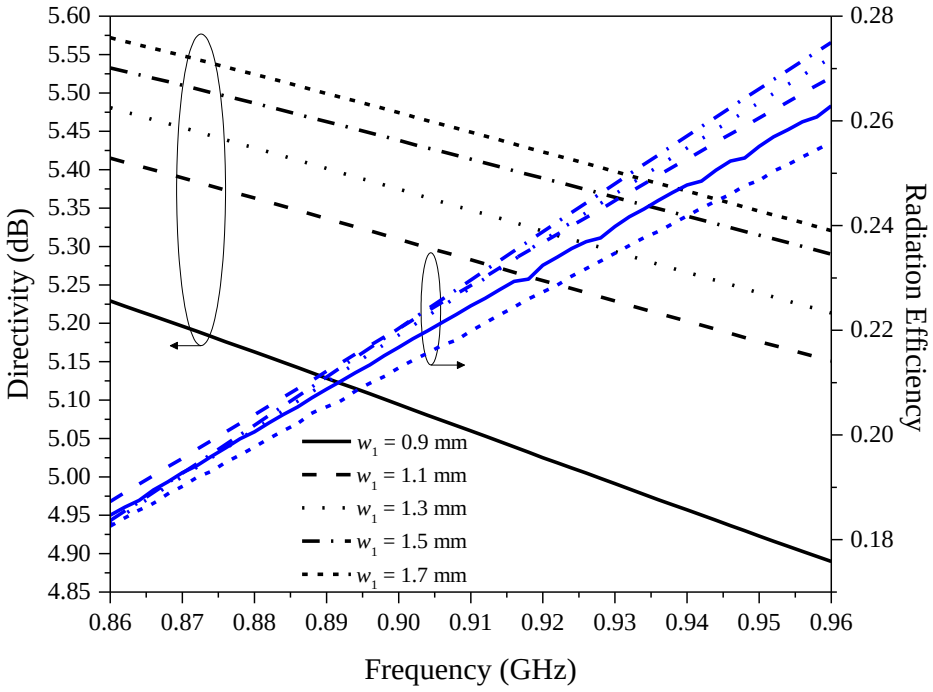

(c)

Figure 3.5: Effects of stub width w_1 on the (a) resistance and reactance, (b) power transmission coefficient and (c) directivity and radiation efficiency.

It is well know that longer stub is usually more inductive. With reference to Figure 3.6 (a), it is observed that the resistance and reactance increase when the stub length (l_1) is increased, which is expected. By incorporating the notches, the tuning range of the stub length is extended. It can be seen from Figure 3.6 (b) that longer stub introduces more inductance, enabling the tag's resonant frequency to be scaled down further. Again, the power transmission coefficient is good for all cases. Relatively smaller change in the resonant frequency with varying l_1 means that it can be used for fine-tuning. Also observed is that decreasing l_1 causes the directivity to increase, but it does not affect the radiation efficiency much, as shown in Figure 3.6 (c).

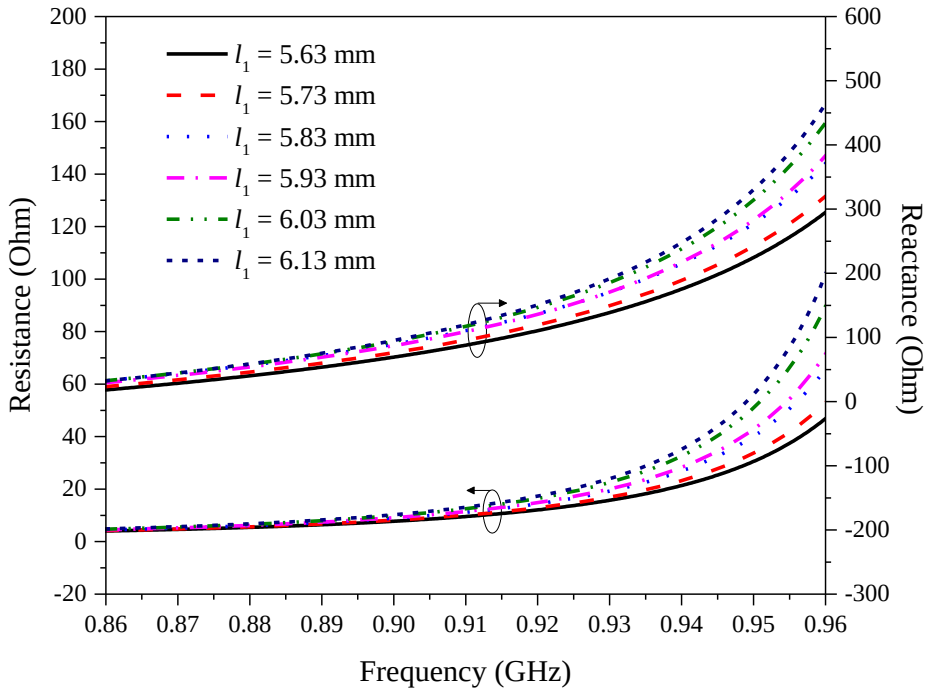

(a)

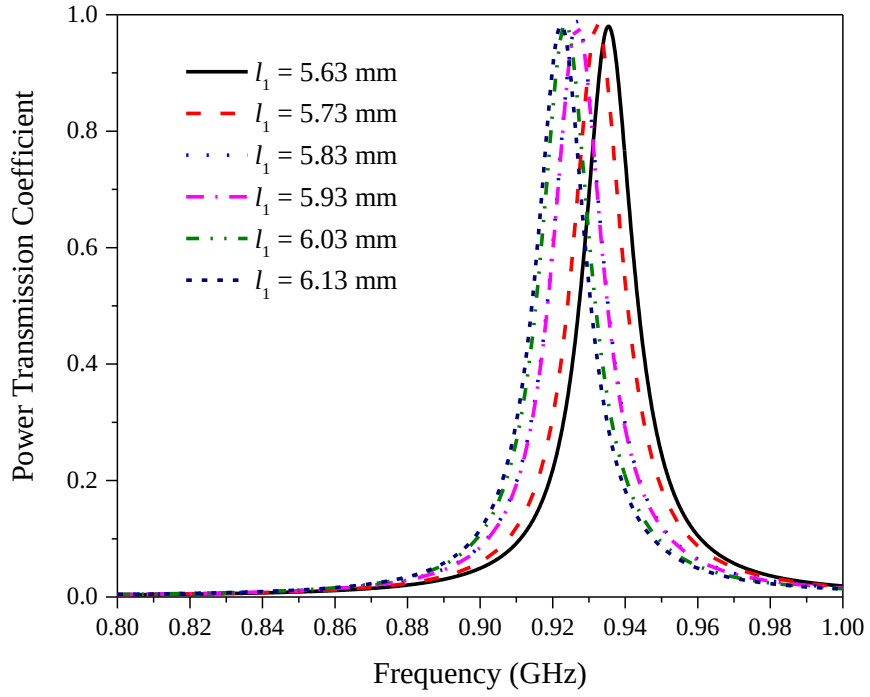

(b)

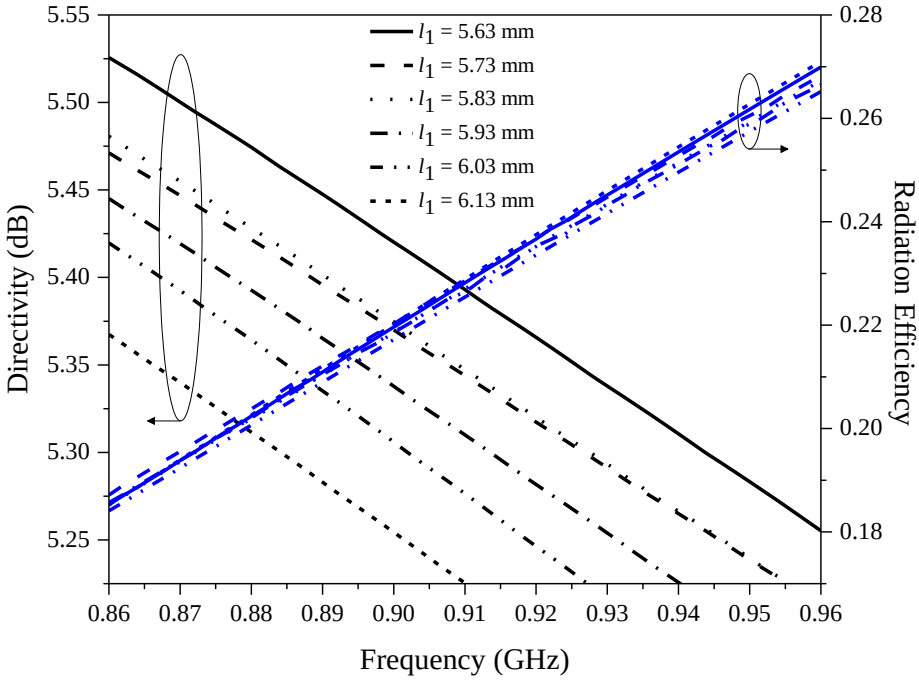

(c)

Figure 3.6: Effects of stub length l_1 on the on the (a) resistance and reactance, (b) power transmission coefficient and (c) directivity and radiation efficiency.

The feeding position of the chip is studied next by varying l_4, with the results shown in Figure 3.7. In this case, the total length (l_5) of the coplanar feedline is kept unchanged. It is found that increasing l_4 increases the resistance and reactance, where the antenna becomes more inductive, as can be seen in Figure 3.7 (a). Also seen in Figure 3.7 (b) is that increasing l_4 causes the resonant frequency of the tag antenna to decrease. The directivity varies in the range of 5.25 -5.35 dB at 925 MHz, as shown in Figure 3.7 (c), and the radiation efficiency changes from 0.23 to 0.25 when l_4 is changed.

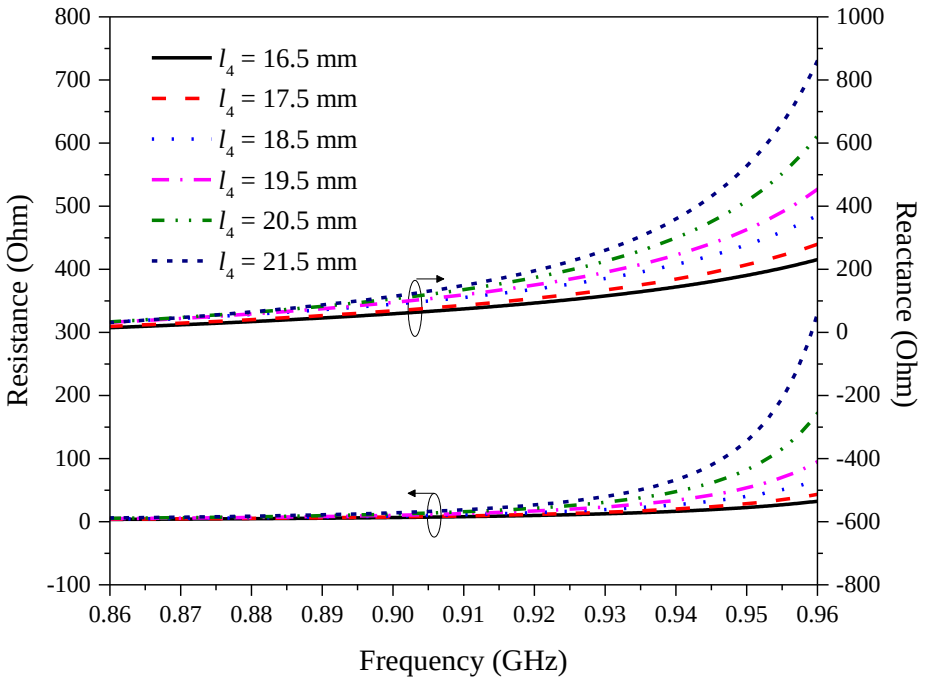

(a)

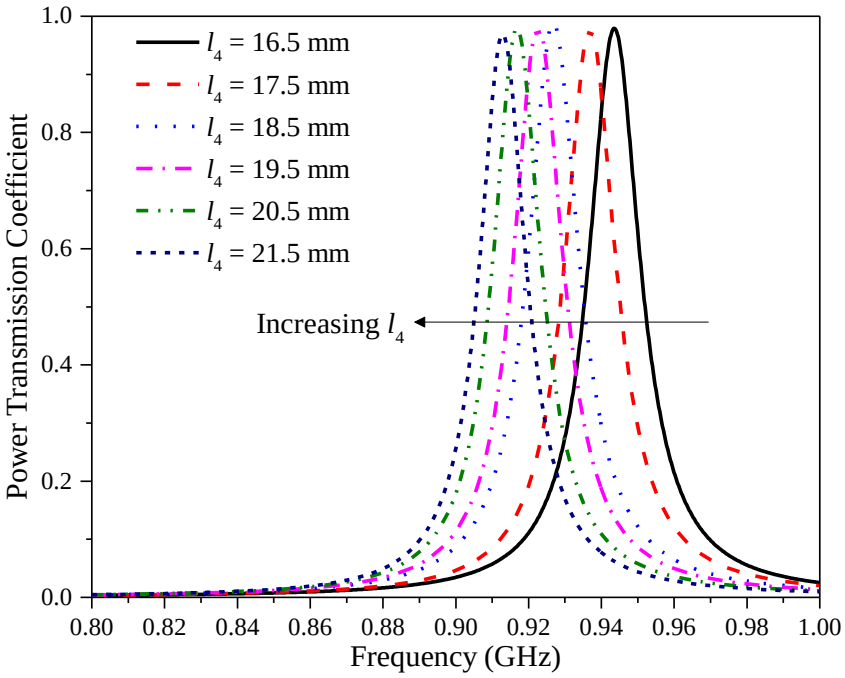

(b)

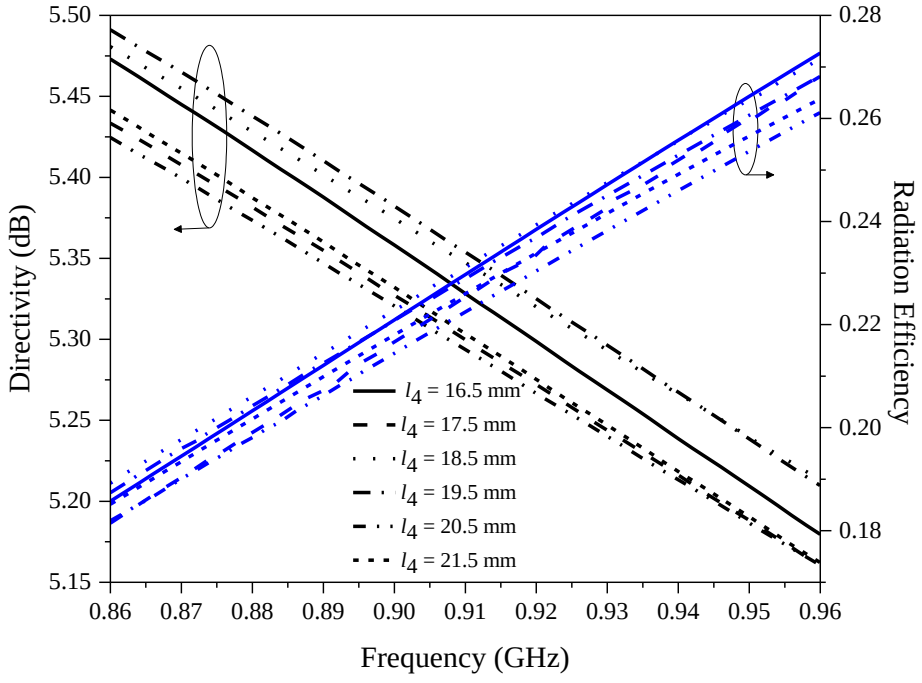

(c)

Figure 3.7: Effects of chip location l_4 on the (a) resistance and reactance, (b) power transmission coefficient and (c) directivity and radiation efficiency.

In Figure 3.8, the effects of the feedline length (l_5) are further explored with the chip position remains unchanged. Again, with reference to Figure 3.8 (a), it can be seen that longer feedline has higher resistance and reactance values. When the length of the feedline becomes longer, the reactance also increases due to the increase of the inductance. Variation in l_5 does not affect the power transmission coefficient and radiation efficiency much, as shown in Figures 3.8 (b) and (c). Collectively, the chip location and the feedline length are shown to be effective for fine-tuning the frequency of the tag's resonance.

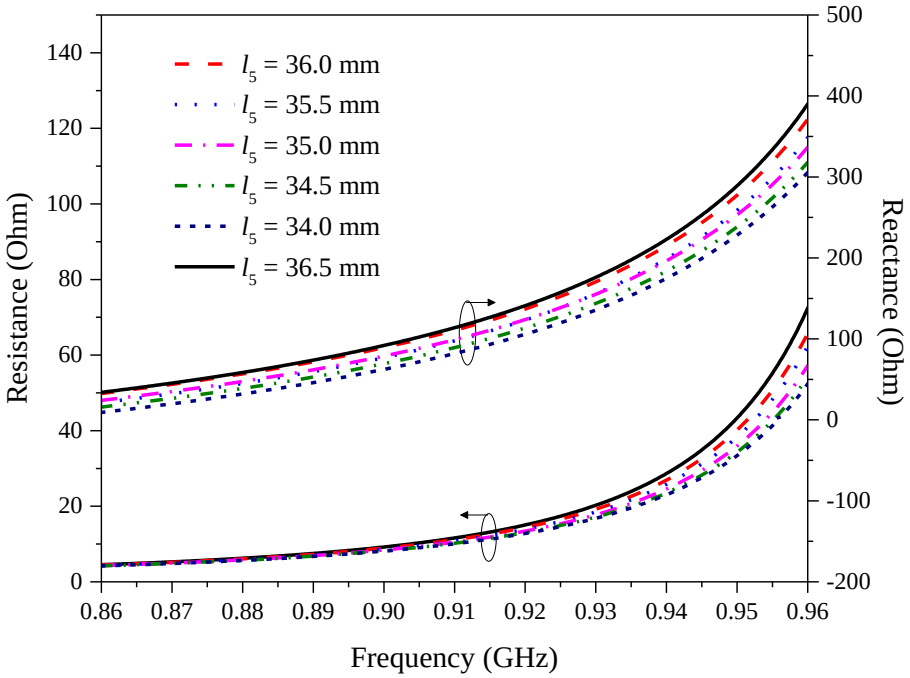

(a)

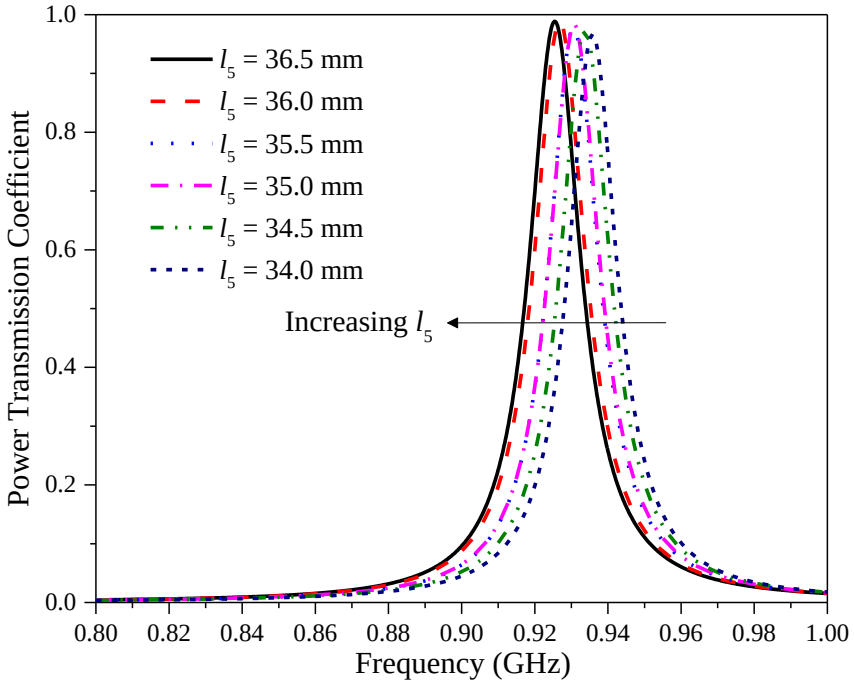

(b)

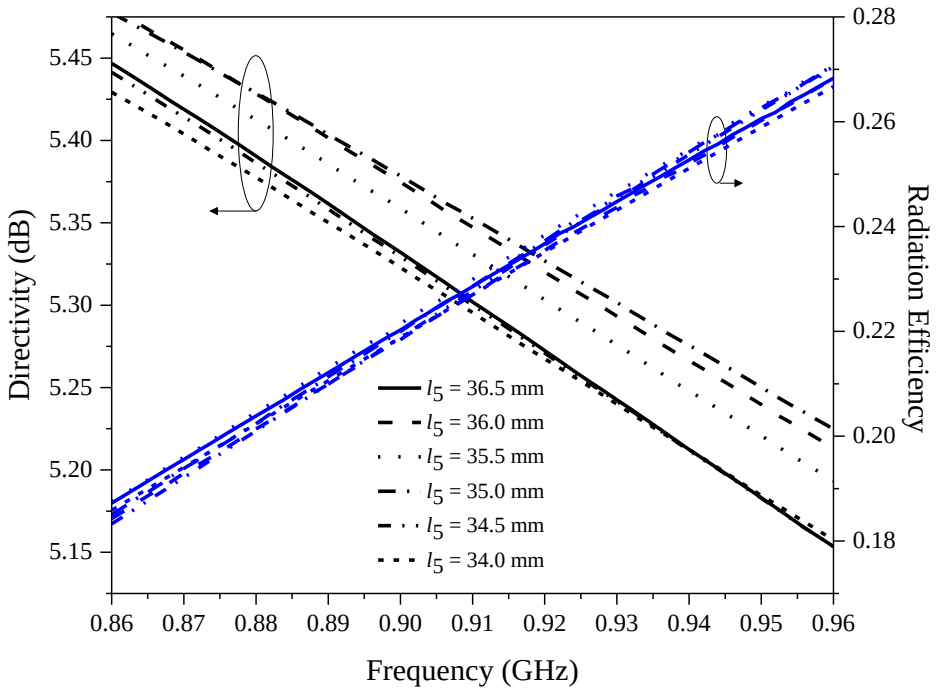

(c)

Figure 3.8: Effects of feedline length l_5 on the (a) resistance and reactance, (b) power transmission coefficient and (c) directivity and radiation efficiency.

The tuning sensitivity of every design parameters are calculated and shown in Table 3.4. By referring to the same table, we can start with changing c and w_1 when designing the tag antenna. This is because changing the two parameters are more efficient to re-scale the resonant frequency into the UHF band of interest as it causes the frequency to move faster. Particularly, the tuning sensitivity of changing c can achieve 187.5 MHz/mm, which is able to shift the frequency in a wide range. After being moved near to the UHF frequency band, the parameters l_4 and l_5 are then adjusted to fine-tune the tag's resonant frequency to make the passband fall exactly inside a certain range.

Table 3.4: Tuning sensitivity of the design parameters.

Design Parameter	Tuning Sensitivity, MHz/mm
c	187.5
w_1	67
l_1	26
l_4	6.16
l_5	4.16

3.3 Results and Discussion

The read performances of the proposed tag antenna were measured using the Voyantic Tagformance measurement system inside an anechoic chamber. Figure 3.9 (a) shows the experimental setup and the tag is placed at the center of a piece of 20 cm × 20 cm copper plate. The copper plate is supported by a Styroform with relative permittivity value of ~1. As can be seen in Figure 3.9

(b), the tag is located right under the reader when measuring the orientation of the tag antenna. During measurement, a fixed distance is set between the position of the reader and the tag antenna. The tag antenna is rotated at its own y-axis to generate the read pattern in *xz*-plane. Meanwhile, the tag antenna is rotated about its *x*-axis to generate the read pattern in *yz*-plane. Obviously, the meanings of these two planes are the same to those for the conventional spherical coordinate system. The *xy*-plane is obtained by rotating the tag antenna about its own *z*-axis. However, the *xy*-plane is not the same as the conventional spherical coordinate system for this measurement. The tag's polarization characteristic shows in the *xy*-plane is in its boresight direction ($\theta = 0^{o}$).

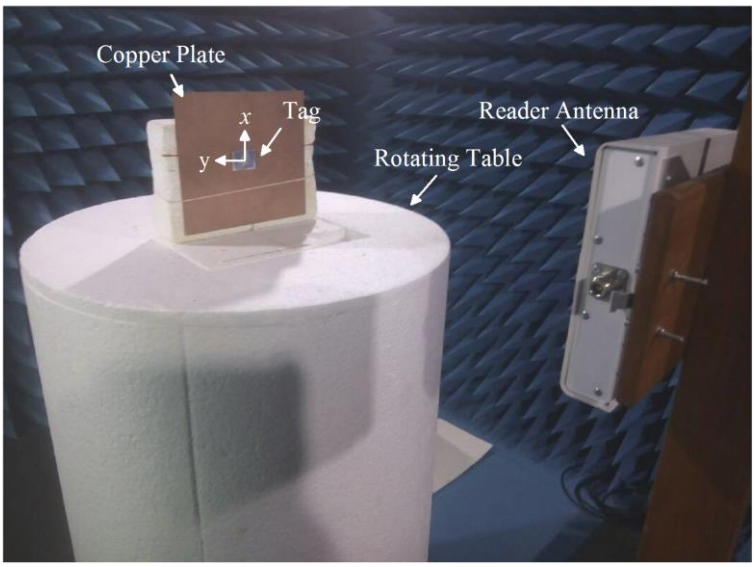

(a)

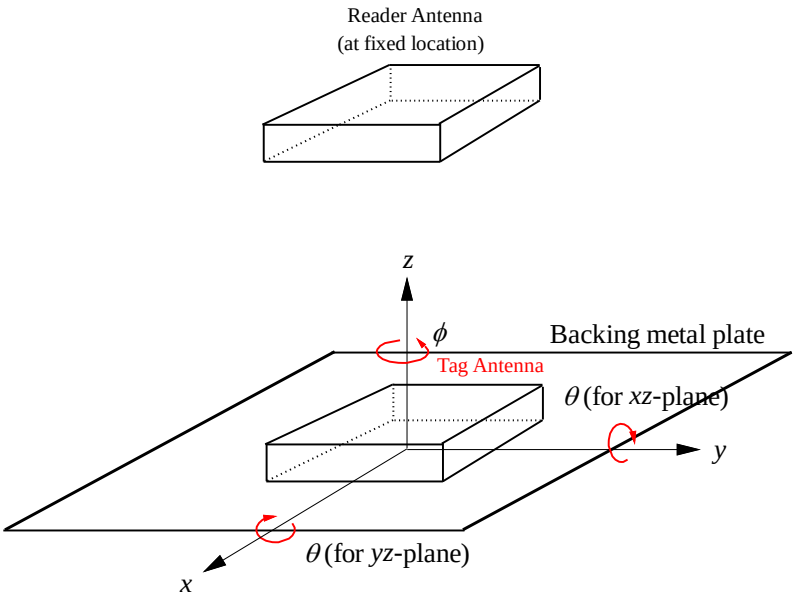

(b)

Figure 3.9: (a) Photograph, (b) plane definition of the experimental setup in the anechoic chamber.

Next, the measured tag sensitivity ($P_{tag.s}$), simulated, and measured realized gains (G_r) are shown in Figure 3.10. The proposed tag antenna is placed at the middle of a metal plate (20 cm × 20 cm) for both the simulation and measurement. With reference to the same figure, the maximum simulated realized gain is -0.9 dBi at 915 MHz, while the maximum measured realized gain is found to be -2.231 dBi at 925 MHz. The measured realized gain is 2 dBi lower than the simulation results. Also, a 10 MHz deviation is observed between the measured and simulated operating frequencies In this case, the discrepancy between the measurement and simulation is not unusual as active devices such as a microchip tend to have larger tolerances which are not able to be avoided during the fabrication process. As can be seen from the same figure, the tag sensitivity is measured to be -17 dBm at 915 MHz. With the high

realized gain and good sensitivity, good read range performance is achievable in this tag.

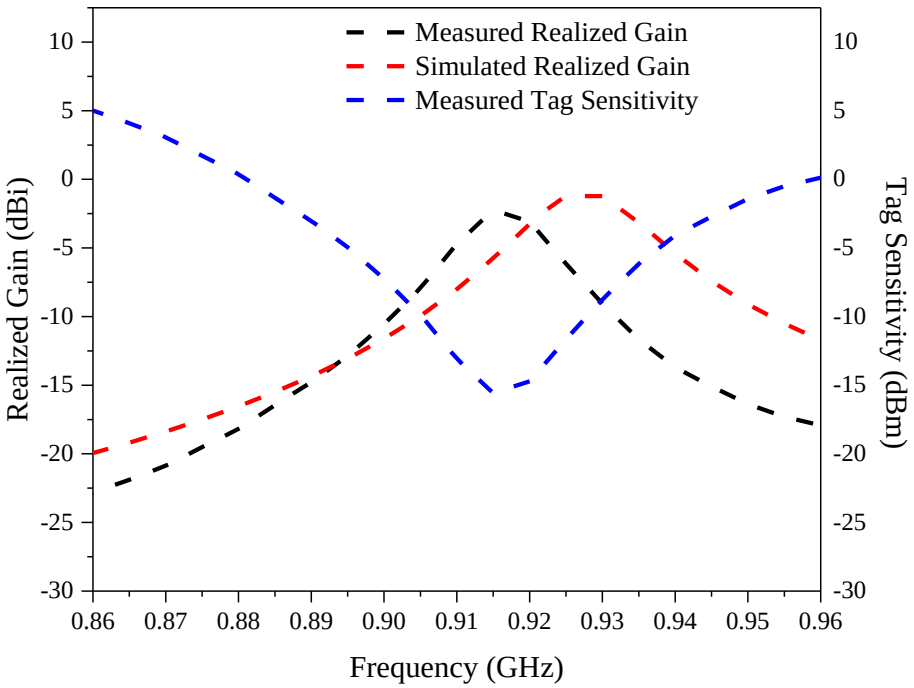

Figure 3.10: Measured and simulated realized gains and measured tag sensitivity when the tag antenna is placed on a copper plate of 20 cm × 20 cm.

Figure 3.11 (a) shows the surface current density simulated at the resonant frequency when the tag antenna is placed on a 20 cm × 20 cm metal plate. It can be seen from the figure that the coplanar feedline has excited the radiator patch by inducing currents through a gap (c = 0.2 mm). With reference to the same figure, currents flow from the patch returning to the ground through the inductive stub. High current density around the stub (Figure 3.11 (b)) implies that it is indeed highly inductive and can be used for tuning purpose. Figure 3.12 depicts the read distances for the *xz*-, *yz*-, and *xy*-planes. As can be seen in Figure 3.12 (a), the maximum read distance of the tag

antenna in the *xz*-plane is measured to be 10.7 m at θ =30°. Also, the read distance in the range of (-90° ≤ θ ≤ 90°) of the entire upper hemisphere is larger than 5 m in this plane. It can be observed in the same figure that the read distance in the *yz*-plane goes beyond 5 m in the angular range of (-60° ≤ θ ≤ 50°). In the range of (θ ≤ -90°) and (θ ≥ 90°), the read performances are much shorter as the tag is placed on a metal plate and the fields in the reverse direction is truncated. With reference to the *xy*-plane in Figure 3.12 (b), the tag antenna reads greater than 5 m in the angular ranges of (300° – 60°) and (120° – 240°). It has achieved the farthest read distances in the directions of ϕ = 0° and 180°.

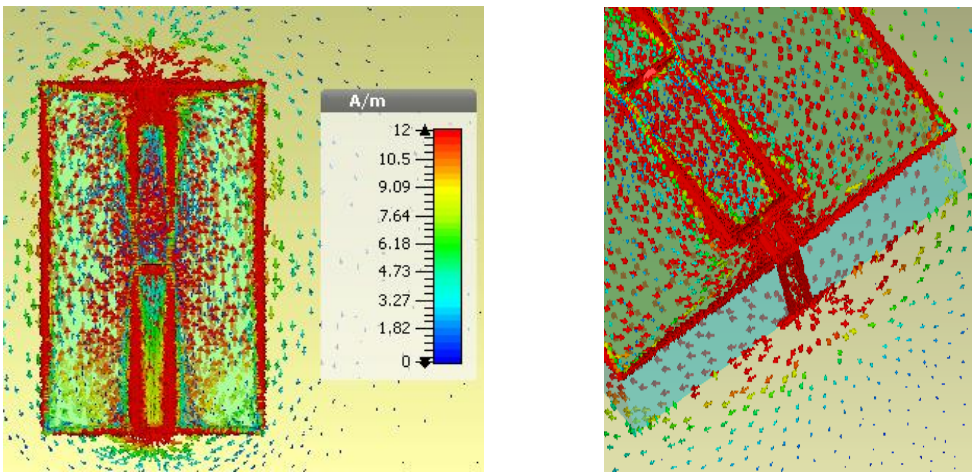

(a) (b)

Figure 3.11: Surface current distributions at the resonant frequency: (a) From the front (b) at the inductive stub of the proposed tag antenna.

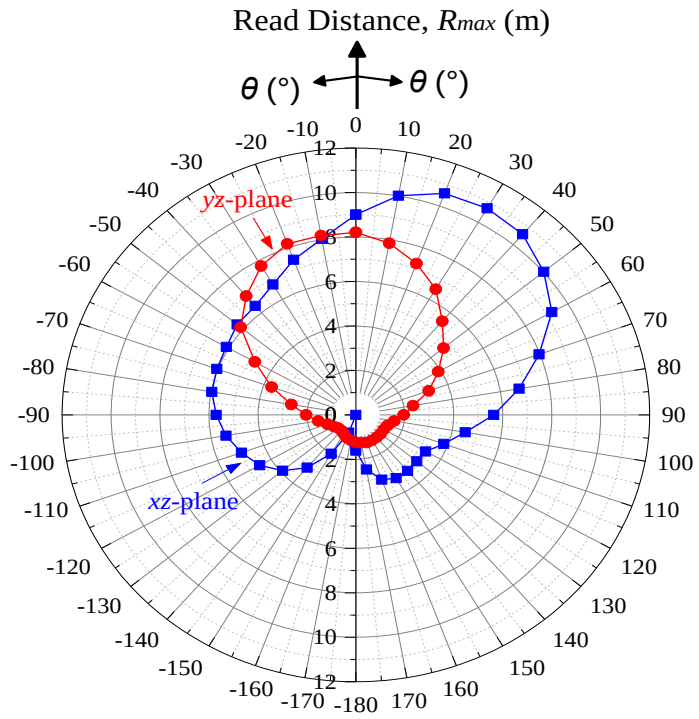

(a)

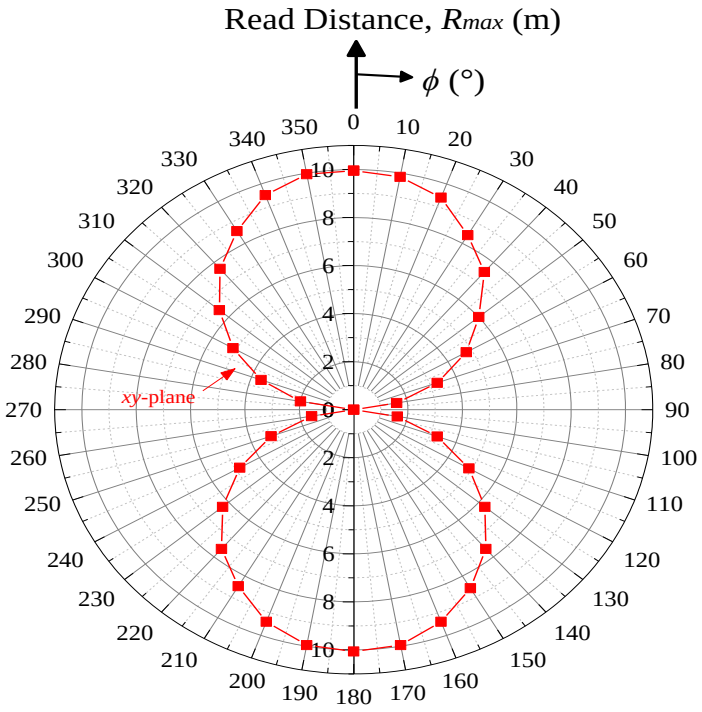

(b)

Figure 3.12: Measured read distances in the (a) *xz*- and *yz*- planes (b) *xy*-plane.

The proposed tag antenna is then mounted on the copper plates with different sizes (L cm × W cm) and the read distance of the proposed tag antenna is measured in the boresight ($\theta = 0^{o}$) direction. From Figure 3.13 (a), it can be seen that all the read distances are achieved beyond 9m when the plate length (L) is varied from 24 cm to 8 cm. This means that the performances of the tag are not much affected by the plate length (L). Meanwhile, when W is reduced from 24 cm to 8 cm, the read distance decreases to ~ 7 m, as shown in Figure 3.13 (b). It is important to mention also that the tag's resonant frequency has kept almost constant for both cases. These prove that the tag is not sensitive to the size of the backing metal object and this is a very desirable feature. The effects of the plate size on the directivity and radiation efficiency are simulated and studied. As we know, increasing plate size causes the ground plane to increase since the ground of the tag antenna is electrically connected to the copper plate, this makes the antenna characteristics converge to that for the infinitely large ground plane. As can be seen in to Figure 3.14, the directivity of the tag antenna increases when it is stuck to a larger metal plate. The radiation efficiency is found to be in the range of 0.24 – 0.27 at 925 MHz as the plate size is varied.

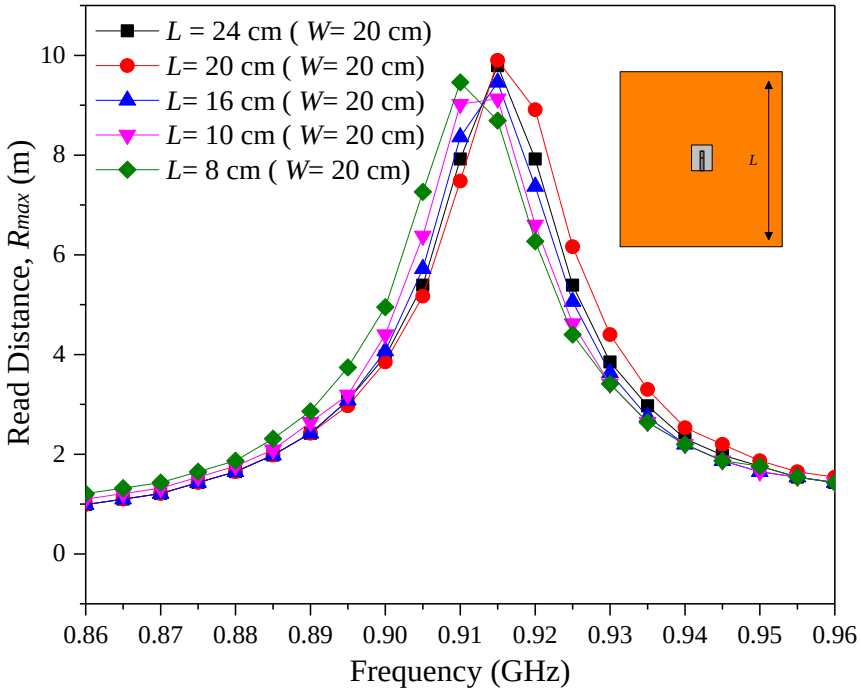

(a)

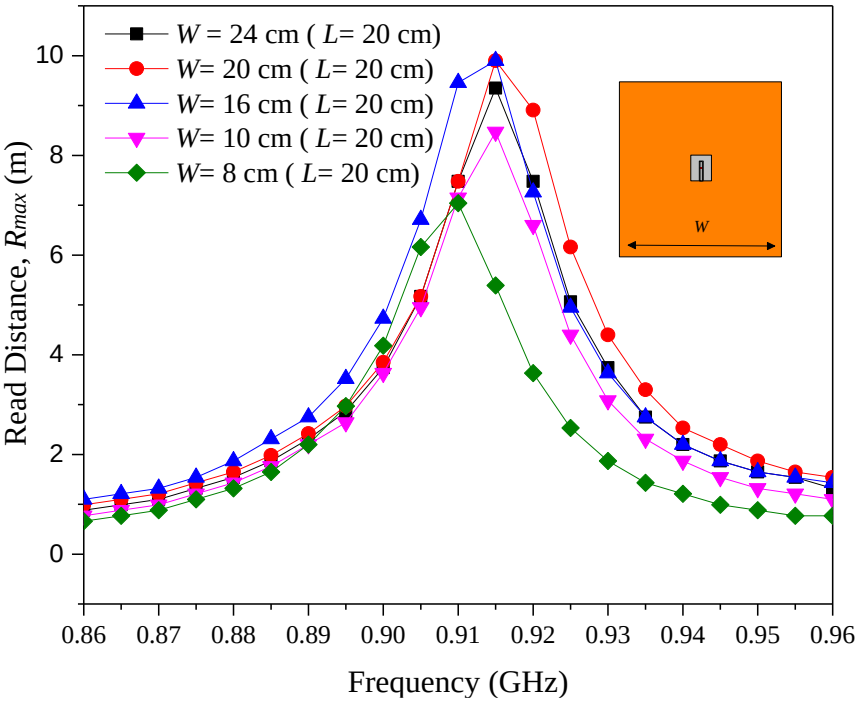

(b)

Figure 3.13: Measured read distances in the boresight (θ = 0°) for different plate sizes when changing (a) *L*, (b) *W*.

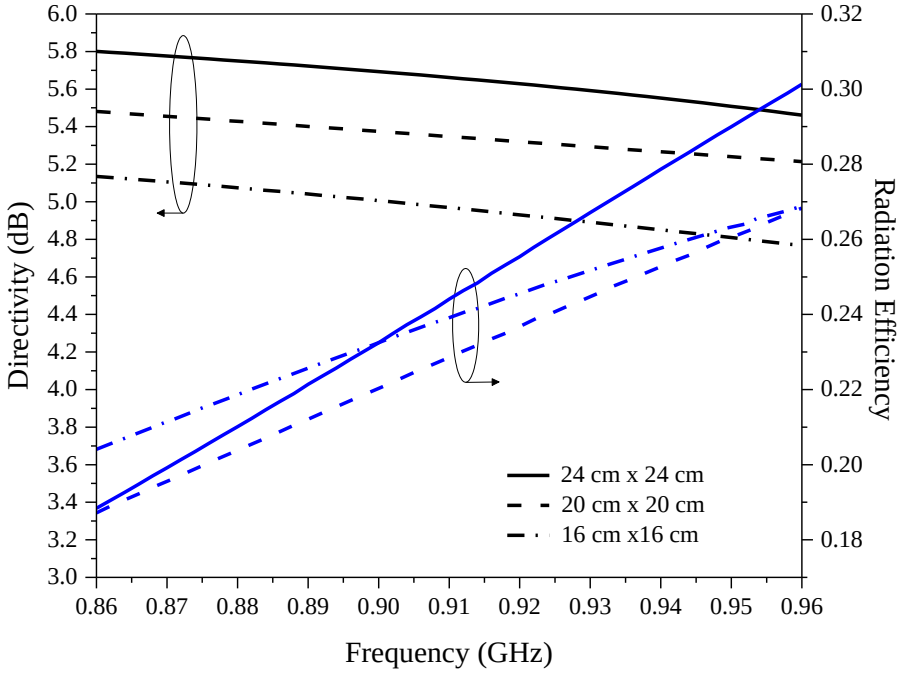

Figure 3.14: Simulated directivity and radiation efficiency of the tag antenna.

Although the tag antenna is designed for metal surfaces, it is also very interesting to study its performances for non-metal objects. The proposed antenna is tested on the dielectric slabs with the size of 24 cm × 12 cm × 1 cm in the boresight direction (θ = 0°), as shown in Figure 3.15 (a). The dielectric slabs given by the NXP Semiconductors (AN1629, 2008) have dielectric constant (ε_r) from 2.2 to 5.8. When the dielectric constant of the slab is raised from 1 to 5.8, the tag's resonance has drifted from 918 MHz to 895 MHz, as shown in Figure 3.15 (b). This is reasonable as the tag's impedance deviates when it is placed on dielectrics. In all cases, the maximum read distance is maintained above 5 m, remaining almost constant. Besides, the read distance of the proposed tag antenna are examined for a few actual implementation scenarios, as shown in Figure 3.16 (a), and the measurement results are plotted

in Figure 3.16 (b). The metal objects are randomly taken from the shelves of a department store and their metal components are unknown. It can be seen from Figure 3.16 (b) that the tag can be detect from a far distance when it is placed on the Vico (6) and Jacob (4) containers while the baked bean (1) container has the shortest read distance. It is observed that the read range has something to do with the surface area of the container. Vico and Jacob containers are found to have relatively larger surface areas than the baked bean container.

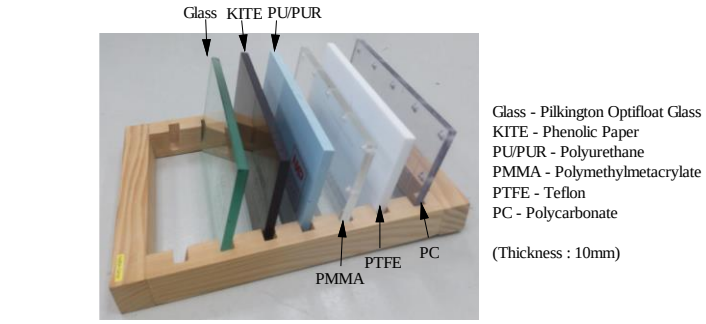

(a)

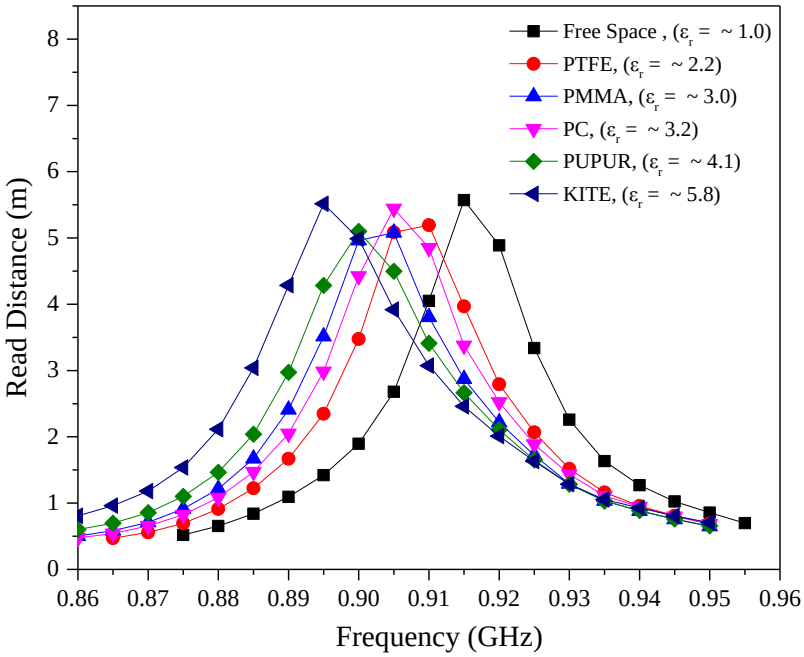

(b)

Figure 3.15: (a) The NXP reference materials. (b) Read distances in the boresight (θ = 0°) when the proposed tag antenna is tested using the NXP reference materials.

(a)

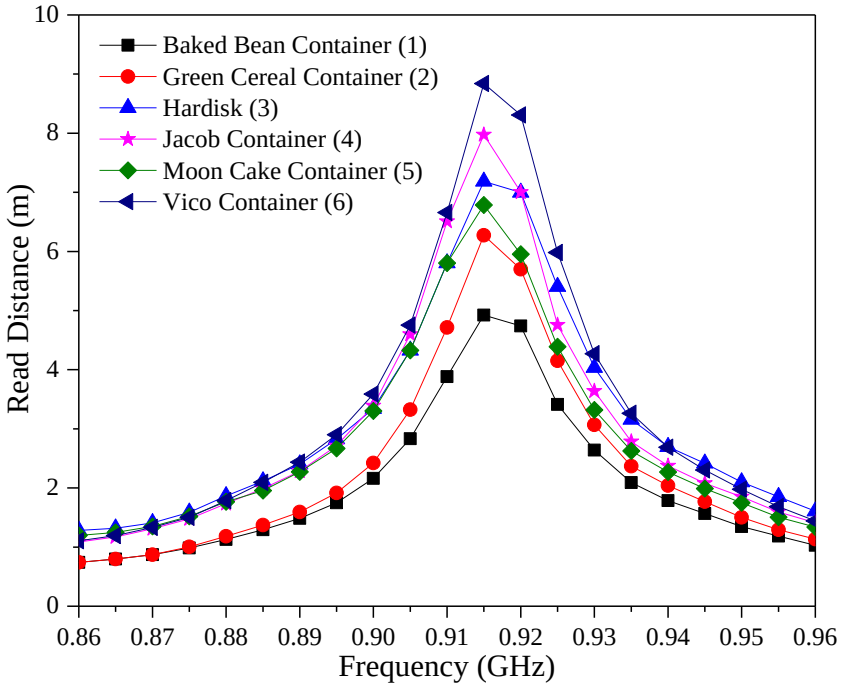

(b)

Figure 3.16: (a) Metallic objects. (b) Read distances in the boresight (θ = 0º) when the tag antenna is placed on different metallic objects.

Table 3.5: Comparing the performances of the miniature UHF metal-mountable tag antennas.

	Power	Flexibility	Tag Dimension (mm)	Backing Plate Size (cm)	Max. Read Distance (m)
This work	4W (EIRP)	Yes	40 × 25 × 3	20 × 20	10.7 (on metal) 5 (on dielectrics)
(Lin, et al., 2016)	4W (EIRP)	No (FR4 substrate)	120 × 60 × 0.4	15 × 30	10 (on metal)
(Zhang and Long, 2014)	4W (EIRP)	No (FR4 substrate + PTFE)	26 × 14 × 2.4	20 × 20	5.5 (on metal)
(Kim, Choi and Choi, 2008)	-	No (Ceramic)	34mm (diameter) × 5	Diameter 40cm	5 (on metal)
(Bong, Lim and Lo, 2017a)	4W (EIRP)	Yes	30 × 30 × 3.0	20 × 20	7 (on metal) 3.5 (on dielectrics)
(Hamani et al., 2017)	4W (EIRP)	No (FR4 substrate)	104 × 31 × 7.6	30 × 25	14.6 (on metal)
(Li, Zhu and Yu, 2017)	4W (EIRP)	No (FR4 substrate)	55 × 41.5	20 × 20	6.1 (on metal) 14.1 (on dielectrics)

Table 3.5 compares the proposed tag antenna with other miniature metal tag antennas which have a footprint of lesser than 50 mm. Vias are one of the effective methods that can be used to minimize the size of the tag antenna. Although being slightly smaller than ours, the inverted-F antennas in (Lin, et al., 2016; Zhang and Long, 2014; Kim, Choi and Choi, 2008) require the use of multiple via holes or multiple layers of substrates, which involve additional processes in the fabrication. In contrast, our proposed tag antenna is designed

with a single-layer PET without the use of any via, which makes the fabrication process much easier. The PIFA metal tag in (Kwon and Lee, 2005) employs a shorting wall to connect the radiator to the ground. However, the maximum read distance for the tag antenna is only 4 m on metal. Moreover, the tag size is much larger than our proposed tag antenna (> 50mm), and folding the inlay in such a way can be difficult to implement in mass production. In (Kim, Choi, and Choi, 2008), the author made use of ceramic material as the substrate of the tag antenna. Ceramic materials have high-permittivity which can help to scale down the antenna size efficiently. However, ceramic materials is costly to implement in practical applications. In contrast, our proposed tag antenna only employs the commercially available low-cost foam material with $\varepsilon_r \sim 1$, and high-permittivity substrate is not needed for bringing down its footprint. In addition, we have proposed a couple of metal tag antennas in (Bong, Lim and Lo. 2017a; 2017b) and particularly in (Bong, Lim and Lo, 2017a), a folded-patch is incorporated with serration for tuning its resonant frequency. Although introducing serration can help to adjust the tag's resonance, it causes the Q-factor to decrease and the read distance to reduce. Notably, our new design here is simple and is much easier to implement as no serrations are used for tuning. A different folded dipole structure with a smaller footprint has been proposed in (Bong, Lim and Lo, 2017b). When the tag is incorporated with a backing ground plane, it is able to be used on metal surface. However, the achievable read range is only 1.8 m on metal, which is much lesser than our proposed metal tag antenna. The tag antenna proposed by Hamani, et al. (2017) has a far read distance of 14.6 m. However, the tag is large in size (104 mm × 31 mm ×

7.6 mm), and it is not a miniature tag. Also, tag antenna with multiple layers requires additional fabrication processes and costs. The tag antenna in (Li, Zhu and Yu, 2017) is designed on single-layer and incorporated with a shorted meandered line. The design is compact and it is able to reach a read distance of 6.1 m on metal. However, the substrate being used is rigid and it is not physically flexible.

3.4 Conclusion

A folded-patch resonator has been proposed for designing a metal-mountable UHF tag that can be read beyond 10 m. The patch is centrally fed by a coplanar waveguide. A simple equivalent circuit has also been developed for characterizing the impedance of the tag antenna. By adjusting the width and length of the inductive stub, the tag's resonant frequency can be easily adjusted over a larger frequency range because of the introduction of the notches. When the size of the backing metal is varied, it is observed that the resonant frequency of the proposed tag antenna does not fluctuate much, which is an important feature that is much desired in the practical applications. Our proposed tag antenna is simple in structure when compared with some contemporary miniature metal tags, and it is able to achieve the farthest read distance. The proposed tag antenna can be read beyond 10m when mounted on metal surfaces and more than 5 m when placed on dielectrics slabs with dielectric constant from 1.0 to 5.8.

CHAPTER 4

MINIATURE FOLDED-PATCH WITH DIFFERENTIAL COPLANAR FEEDLINE FOR METAL-MOUNTABLE UHF RFID TAG

4.1 Introduction

Lately, the UHF RFID tagging technology has become very famous due to its many advantages. It is able to overcome many limitations that are faced by the traditional bar-code systems. Firstly, the RFID tagging system has a much larger read range than the barcode system. Barcode needs to be read within the line-of-sight while an RFID tag can be read without requiring line-of-sight even it is dirty or soiled. Also, the RFID tag contains a microchip. The chip is embedded with read/write functions and it is able to carry a much larger volume of data. In recent years, the RFID tagging technology has been widely employed by various automatic identification, transportation, logistics, infrastructure management and protection, transportation payments, animal and human identification, and others. In many practical applications, the tag is simply placed on the object surface or inserted into an object which is made from different materials. The tags can be designed to be placed on glass, textile materials, dielectrics, near-body applications, and paper materials (Phatarachaisakul, Pumpoung, and Phongcharoenpanich, 2015; Shao, 2015; Hamraoui, et al., 2017; Shao, Burkholder and Volakis, 2014; Santiago et al., 2013) for achieving good performances. However, a tag's read performances

can deteriorate when it is placed on metal surface. This is because the image current, which has equal amplitude and opposite phase, cancels out the current on the radiator, causing the radiation performances to jeopardize. Coupling between the backing metal and the tag can also affect and degrade the performances of the tag. The resonant frequency, impedance matching, and read distance of a tag can change significantly when it is attached to a metal surface (Dobkin and Weigand, 2005). It is always challenging to design a UHF metal-mountable tag antenna with far read range and compact size and this issue has attracted much attention from many researchers.

Several methods have been introduced to reduce the interferences of the backing metal. Firstly, the Electromagnetic Bandgap (EBG) and Artificial Magnetic Conductor (AMC) have been inserted to isolate the tag antennas from their backing metals (Ding, et al., 2014; Gao and Yuen, 2011). The EBG and AMC can help to improve radiation efficiency and antenna gain. They exhibit high surface impedance in certain frequency bands, resulting in in-phase reflection coefficient for the source and the reflected wave. But, the tag antennas with EBG and AMC are not suitable for designing low-profile and miniature tag antennas because they are usually large in size, complex, and costly. Next, the planar inverted-F antenna (PIFA) has been broadly used for designing the metal-mountable tags as they can achieve good read ranges on metal. However, PIFA are usually large in size and they require the use of multiple vias or shorting walls for achieving miniaturization (Chen and Tsao, 2010). Although the size of the tag can be reduced efficiently by such

mechanism, the tag's radiation characteristics are usually very sensitive to the positions of the vias and shorting walls. The tuning processes can be complicated and not suitable for further optimization. By inserting an air layer to separate the radiating element from the backing metal surface, the tag's performances can usually be improved, with the price of increasing the antenna profile. The parasitic elements were employed for reducing the effects of the backing metal and broadening the impedance bandwidth in (Lai, Li, and Tentzeris, 2010; Hamani et al., 2017). However, drilling process is required to insert spacers to separate the radiating element from the parasitic elements, making the fabrication processes harder.

In this chapter, a folded-patch antenna that is fed by a pair of differential coplanar waveguides is proposed for designing a UHF tag antenna for metal surface. Multiple slots are etched around the edges of the patch for adjusting the operating frequency effectively. The proposed tag antenna can be easily made on a single layer flexible PET (polyethylene terephthalate) substrate and it can be fabricated by simple folding. Two inductive stubs are tactfully added to the corners of the patch, and they become the shorting stubs after the inlay is folded. No via is required and it makes the fabrication process much simpler than the PIFA.

This chapter is prepared as follows. Section 4.2 discusses the configuration of the proposed tag antenna. An equivalent circuit is modelled to

analyze the impedance characteristics. Parametric studies are performed in Section 4.3. Finally, the proposed tag antenna is measured for some practical implementation scenarios and the results are shown in Section 4.4.

4.2 Equivalent Circuit Model and Tag Configuration

Figure 4.1 (a) and Table 4.1 show the configuration and design parameters of the proposed tag antenna. The tag antenna is made by depositing a single layer of 9μm copper layer on a piece of 50 μm flexible PET. Then, it is fabricated by folding a piece of inlay (Figure 4.1 (b)) symmetrically around a rectangular polyethylene foam with ε_r = 1.03 and tan δ = 0.0001 (Emerson & Cuming Microwave Products, 2011) as the structural support of the tag. The tag antenna has a footprint of $w \times h$ (25 mm × 30 mm) and a substrate thickness (t) of 3 mm. With reference to Figure 4.1 (b), the inlay consists of a radiator patch at the center and two flaps of ground planes on the left and right. Two inductive stubs with width k_0 = 0.4 mm and length $l_0 \approx t$ = 3.175 mm are connected the central patch to the ground planes. The patch is excited by a pair of coplanar lines placed diagonally, with a microchip bonded at the center of the feedlines. As can be seen in the figure, there are four open thin slots (Slot 1-4) with the same slot width (g_1 = 1 mm) but different slot lengths (Slot 1 = Slot 3, Slot 2 = Slot 4) extended from the four edges of the patch. Also, an additional slot (Slot 5) with width g = 0.2 mm is etched across the diagonal line of the patch

orthogonal to the coplanar feedline. Varying the lengths and widths of the slots will cause the impedance to change, tuning down the operating frequency to the UHF range. The software used to conduct the simulations is CST Microwave Studio and tag antenna is stuck to the center of a metal plate with the size of 20 cm × 20 cm in all the simulations. In this project, MONZA R6 (IPJ-W1700, 2016) is embedded for exciting the proposed tag antenna. The read and write sensitivities of the chip are -20 dBm and -16.7 dBm respectively. The input impedance of the chip is $(11.8 - j118.5)\ \Omega$ at 923.7 MHz.

Table 4.1: **Parameters of the proposed tag antenna.**

Parameter	(mm)	Parameter	(mm)
h	30	w	25
l_0 (t)	3.175	g	0.2
l_1	36.1	g_1	1
l_2	12.5	k_0	0.4
l_3	10.6	k_1	0.9

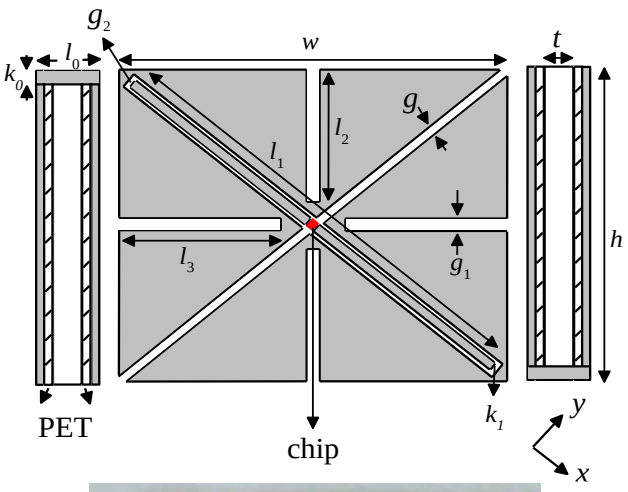

(a)

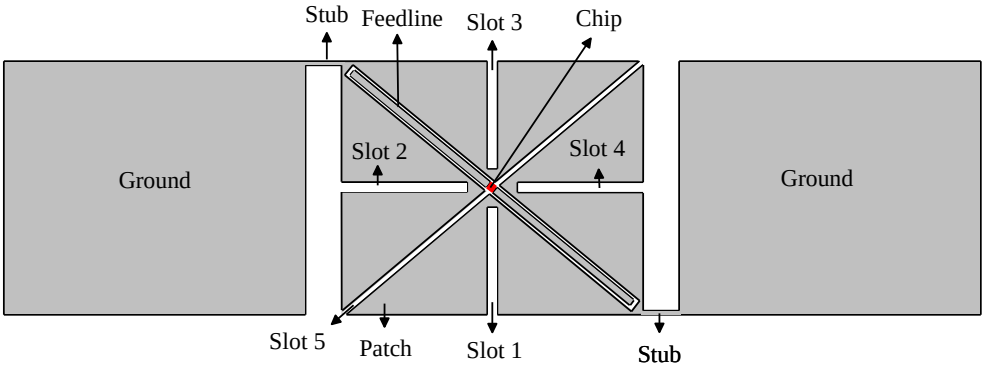

(b)

Figure 4.1: (a) Completed tag antenna. (b) Inlay.

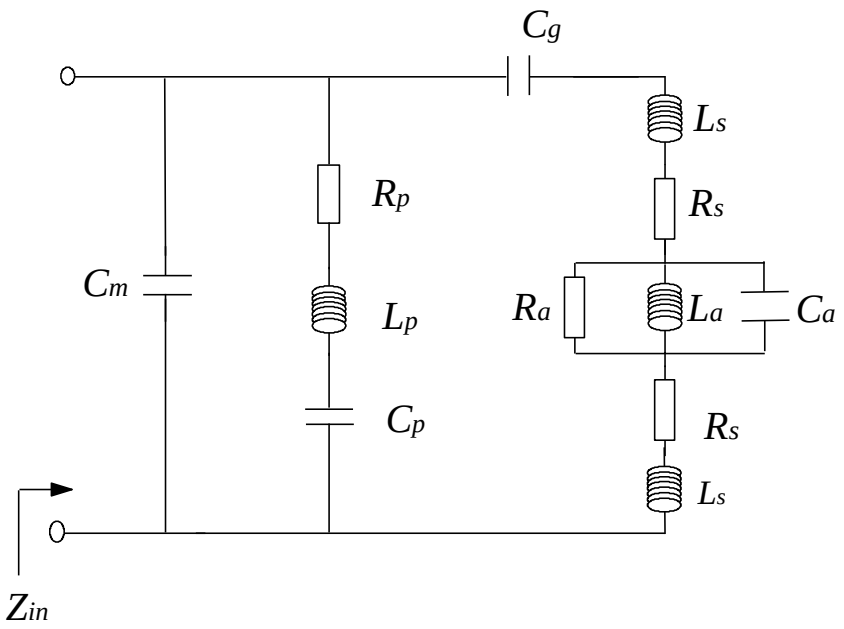

Figure 4.2: Equivalent circuit of the tag antenna.

Table 4.2: The value of the components in the equivalent circuit.

Component	Value	Component	Value
R_a	14.0 kΩ	R_p	0.6 Ω
L_a	13.55 nH	L_p	35.2 nH
C_a	1.89 pF	C_p	0.09 pF
C_m	0.008 Ω	C_g	0.36 nH
R_s	0.1 Ω	L_s	2.2 nH

The equivalent circuit of the tag antenna is depicted in Figure 4.2. With reference to the figure, the capacitance of the gap between the feedlines to place the chip is represented by C_m. The capacitance can be approximated by the formula below.

$$C_m = \varepsilon_o \varepsilon_r k_1 \{\ln[0.25 + (t/b)^2] + (b/t)tan^{-1}(2t/b)\}/(2\pi) \quad , \quad (4.1)$$

where b = 0.15 mm is the width of the gap to place the chip, and ε_r is the permittivity of the polyethylene foam. Then, the pair of coplanar feedlines is modelled by the lumped elements R_p, L_p, and C_p in series. C_g is the capacitance formed in between the radiator patch and the feedline. R_s and L_s are the resistance and inductance of the inductive stubs that connected the patch to the ground plane. Lastly, R_a, L_a, and C_a connected in parallel represent the radiator patch. The capacitance C_a between the patch and the ground can be calculated as

$$C_a = \varepsilon A_T / t \quad , \quad (4.2)$$

where the effective surface area is A_T = 0.6487×10^{-3} m^2. Next, the AC resistance equation can be used to calculate the resistance of the rectangular inductive stub and the formula is given as

$$R_{p,s} = 2[(\rho l_i)/(k_i t_s)][K_C/(1 - e^{-x})] \quad , \quad (4.3)$$

where $x = 2(1 + t_s/k_i)\,\delta/t_s$. Here, the length ($l_i$) and width of the stub (k_i) are all in meter. The values δ = 2.18×10^{-6} m, ρ = 1.678×10^{-8} Ωm, K_c = 1.58, and t_s = 0.000009 m represent the skin depth, resistivity, current crowding factor, and thickness of copper.

$$L_{p,s} = 0.002l_i\{\ln[2l_i/(k_i + t_s)] + 0.50049 + [(k_i + t_s)/3l_i]\} \quad , \quad (4.4)$$

In (Greenhouse, 1974), equation (4.4) is used to calculate the inductance of the stub. In this case, l_i, k_i, and t_s are in centimeters. By using the equations (4.1) and (4.4), C_m, C_a, R_p, L_p, R_s, and L_s are obtained and shown in Table 4.2. The values for R_a, L_a, C_p, and C_g are estimated using the macro model method (Kim and Yeo, 2010). As can be seen in Figure 4.2, after knowing all the elements of the equivalent circuit, the input impedance of the tag antenna can be derived as

$$Z_{in} = \frac{\alpha\beta}{\alpha+\beta} \quad , \quad (4.5)$$

$$\alpha = \frac{A + j\omega R_p C_p}{-\omega^2 R_p C_p C_m + j\omega(C_p + \beta C_m)} \quad , \quad (4.6)$$

$$\beta = \frac{\gamma - \omega^2 R_a L_a C_{g1} - 2\omega^2 \gamma L_s C_{g1} + 2j\omega\gamma R_s C_{g1}}{j\omega\gamma C_{g1}} \quad , \quad (4.7)$$

where $A = 1 - \omega^2 L_p C_p$, and $\gamma = R_a - (\omega^2 R_a L_a C_a - j\omega L_a)$. The simulated, measured, and modelled input impedances are plotted in Figure 4.3. By using equations (4.5) to (4.7), the modelled input impedance can be calculated. From the figure, it can be seen that the simulated and modelled curves have achieved good agreement, indicating that the equivalent circuit is reasonable. The simulated input impedance of the antenna is (32.4 + j131.6) Ω at 923.7 MHz.

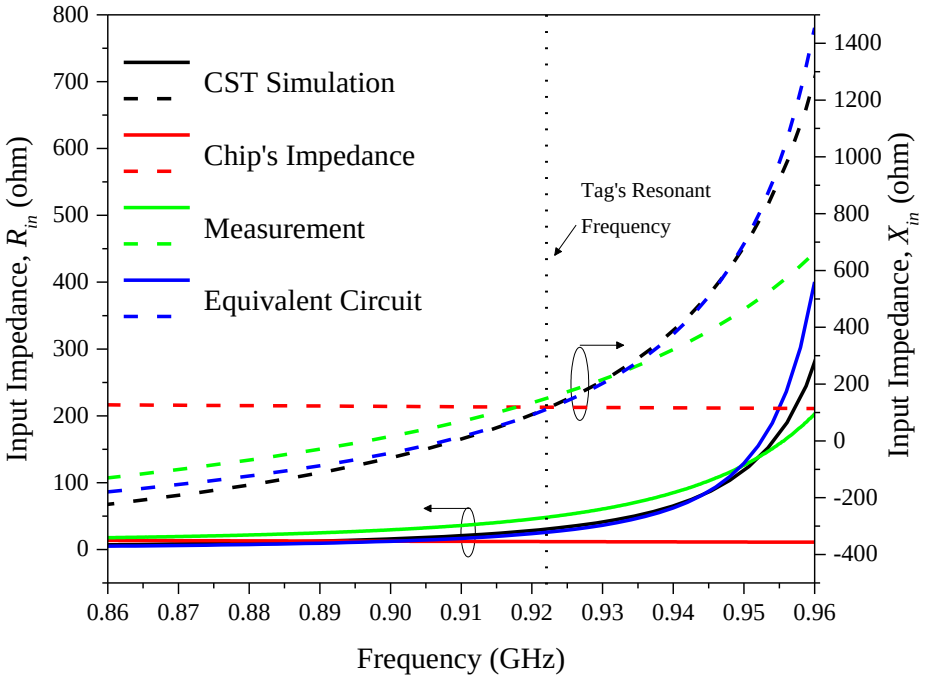

Figure 4.3: Simulated, modelled, and measured input impedances of the proposed tag antenna.

4.3 Frequency, Current, and Impedance Analysis

The effects of the slots are studied using CST simulation. The frequency and current characteristics of the tag antennas with different slots are shown in Figure 4.4. In all the simulations, the tag antennas are placed on a 20 cm × 20 cm metal plate. To start, the tag antenna is simulated without any slots (Structure S0), all of the slots (Slots 1 - 5) are removed to form a new structure. Without inserting the slots, the resonant frequency is found to be 4.78 GHz, not suitable for UHF tag design as it is not located in the UHF frequency band. Later, Slot 5 is inserted diagonally into the new structure to form structure S1, as depicted in Figure 4.4 (a). It is interesting to see in Figure 4.4 (b) that the tag's resonant frequency has lowered down to 972.3 MHz. Next, with reference to Figure 4.4 (a) again, Slot 2 and Slot 4 (with width of g_1 = 1 mm and length of l_3 = 10.6 mm) are included to form the new structure S2. After adding the two slots, the resonant frequency is further reduced to 945.3 MHz, as can be seen in Figure 4.4 (b). Two more slots (Slot 1 and Slot 3) with the same width but different lengths (l_2 = 12.5 mm) are added to the patch in order to further reduce the tag's resonance, as shown in Figure 4.4 (a), for forming the new structure S3. It can be seen (Figure 4.4 (b)) that the resonant frequency has further shifted down to 923.7 MHz. The E- field and surface current distributions for the different structures are simulated and the results are shown in Figure 4.4 (c). As can be seen, the electric field and current paths have increased effectively when more slots are included. This makes the patch to become more inductive, resulting in a lower tag resonant frequency. The

current distribution at the inductive stub is also shown in Figure 4.4 (d). It can be seen from the figure that the currents flow from the patch to the ground plane through the shorting stubs. It is highly inductive due to the high current density, which makes it useful for frequency tuning.

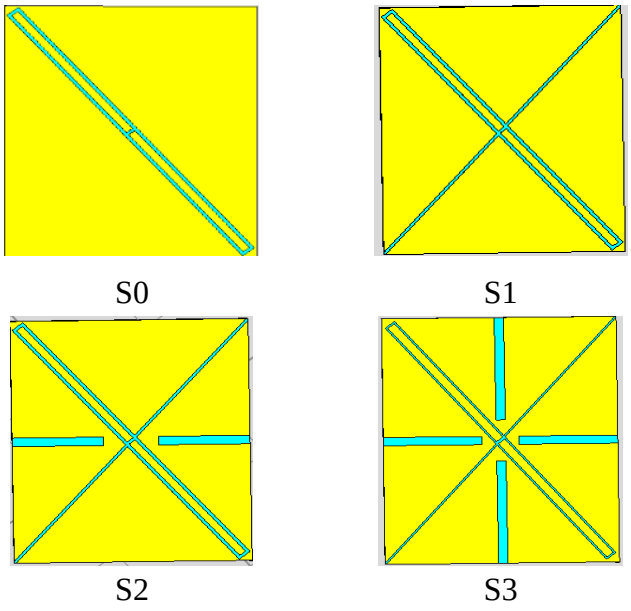

(a)

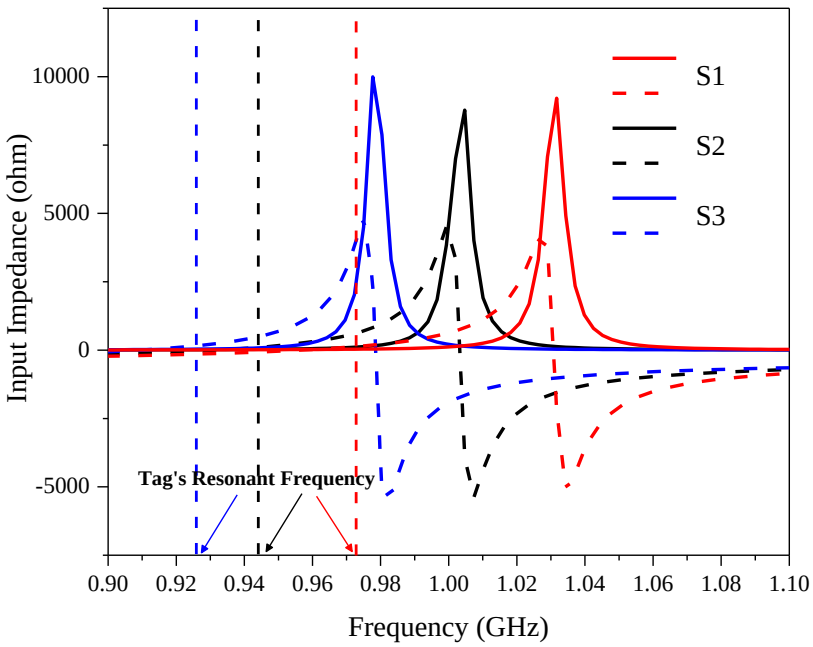

(b)

E-field	Surface current	
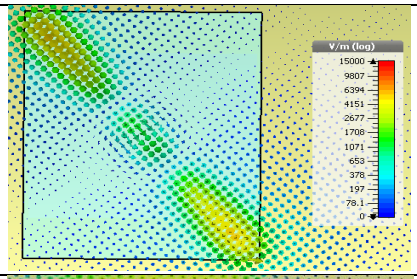	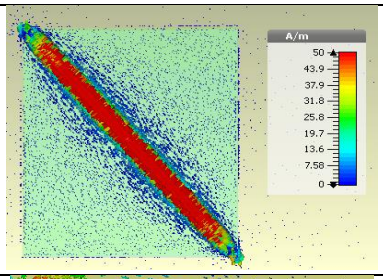	S0
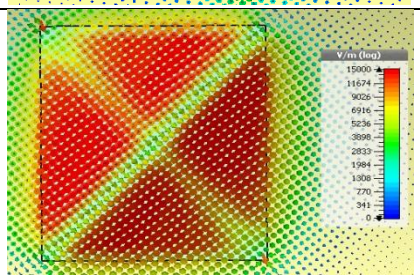	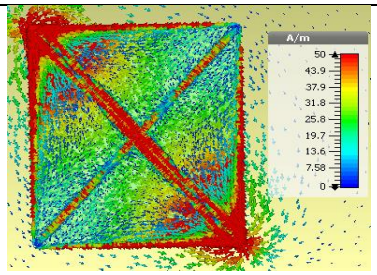	S1
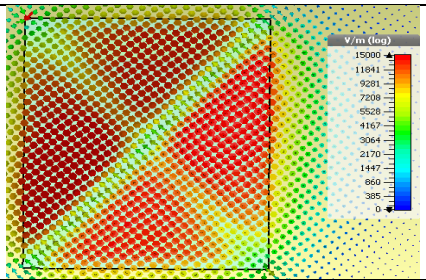	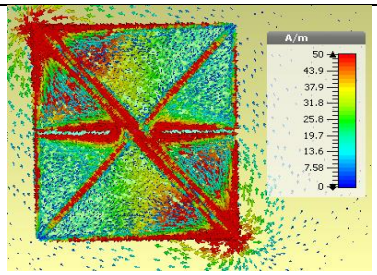	S2
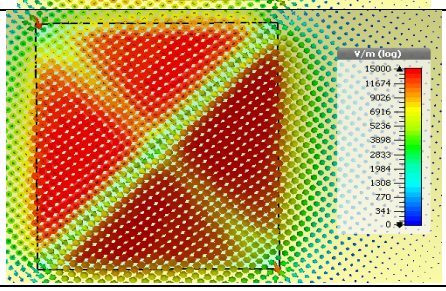	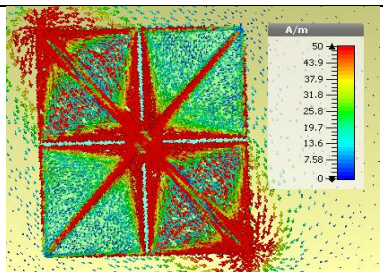	S3

(c)

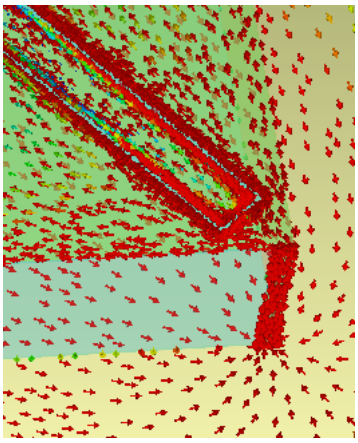

(d)

Figure 4.4: (a) Configurations of tag antennas with different slots. (b) Input impedances for the tag antennas with different slots. (c) Surface current and E-field distributions at their respective resonant frequencies, with all the tag antennas placed on a 20 cm × 20 cm metal plate (d) Surface current distribution on the thin stub.

To understand the impedance characteristics of the proposed tag antenna, the effects of the crucial design parameters are studied. At the beginning, Figure 4.5 shows the effects of altering the stub width (k_0). As can be seen in Figure 4.5 (a), increasing k_0 causes the resistance and reactance to decrease. This is expected as the resistivity and inductivity of the stubs drop when the width is increased. When k_0 is widened from 0.30 mm to 0.50 mm, the resonant frequency increases from 907.5 MHz to 934.5 MHz and the power transmission coefficient increases from 0.7503 to 0.7699, as shown in Figure 4.5 (b). It can be seen from Figure 4.5 (c) that the directivity and radiation efficiency increase when the stubs' width increases.

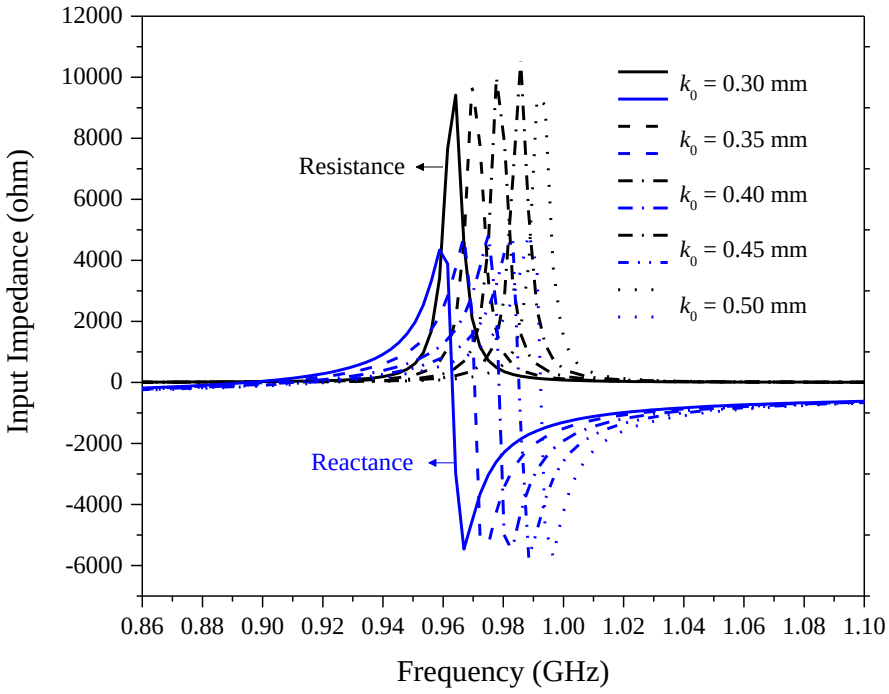
Input Impedance (ohm)
12000
10000
8000
6000
4000
2000
0
-2000
-4000
-6000
Resistance
Reactance
k_0 = 0.30 mm
k_0 = 0.35 mm
k_0 = 0.40 mm
k_0 = 0.45 mm
k_0 = 0.50 mm
0.86 0.88 0.90 0.92 0.94 0.96 0.98 1.00 1.02 1.04 1.06 1.08 1.10
Frequency (GHz)

(a)

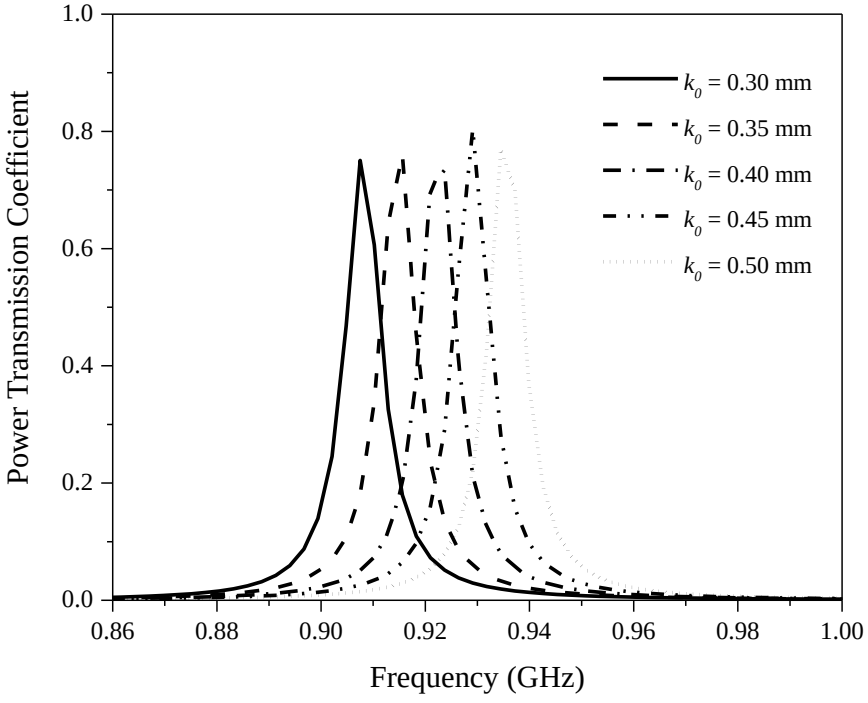
Power Transmission Coefficient
1.0
0.8
0.6
0.4
0.2
0.0
k_0 = 0.30 mm
k_0 = 0.35 mm
k_0 = 0.40 mm
k_0 = 0.45 mm
k_0 = 0.50 mm
0.86 0.88 0.90 0.92 0.94 0.96 0.98 1.00
Frequency (GHz)

(b)

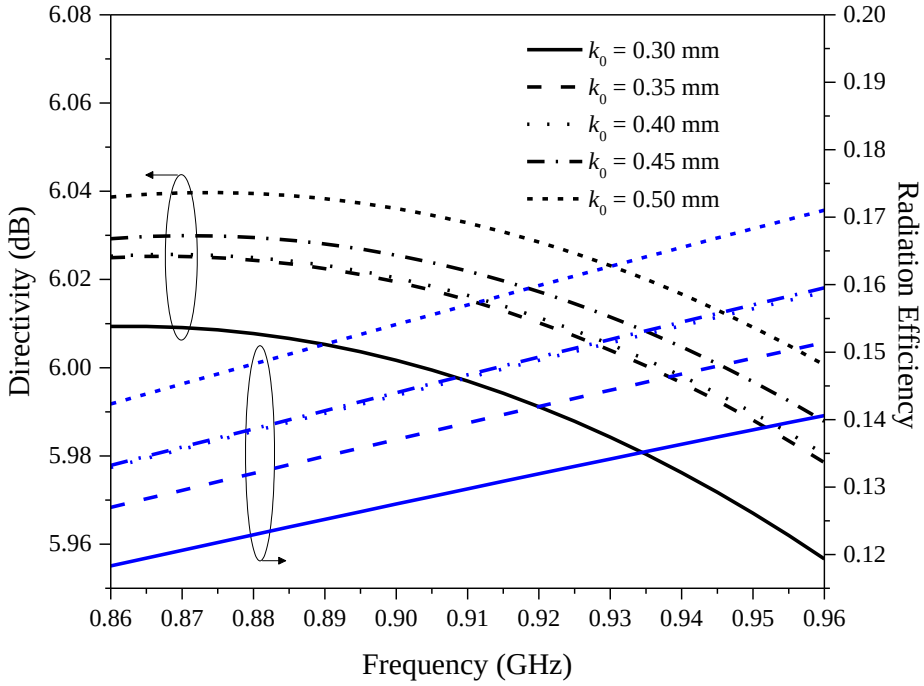

(c)

Figure 4.5: Effects of stub width (k_0) on the (a) resistance and reactance, (b) power transmission coefficient and (c) directivity and radiation efficiency.

Next, the width (g) of the diagonal Slot 5 is studied. With reference to Figure 4.6 (a), it shows that the resonant frequency increases from 883.2 MHz to 950.7 MHz with increasing g. Coarser resolution implies that g can be used to coarse-tune the resonant frequency of the tag antenna. Also observed is that the power transmission coefficient increases from 0.7611 to 0.8286. In this case, the directivity increases with increasing g and the radiation efficiency remains in between 0.14 – 0.15 at 923.7 MHz, as shown in Figure 4.6 (c).

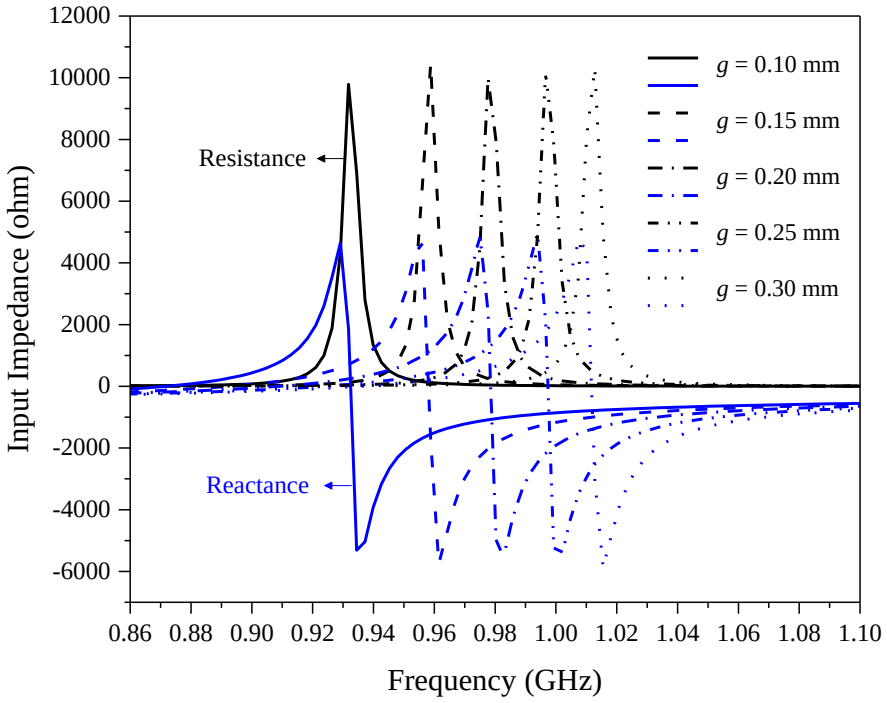
Input Impedance (ohm)
Frequency (GHz)
Resistance
Reactance
g = 0.10 mm
g = 0.15 mm
g = 0.20 mm
g = 0.25 mm
g = 0.30 mm

(a)

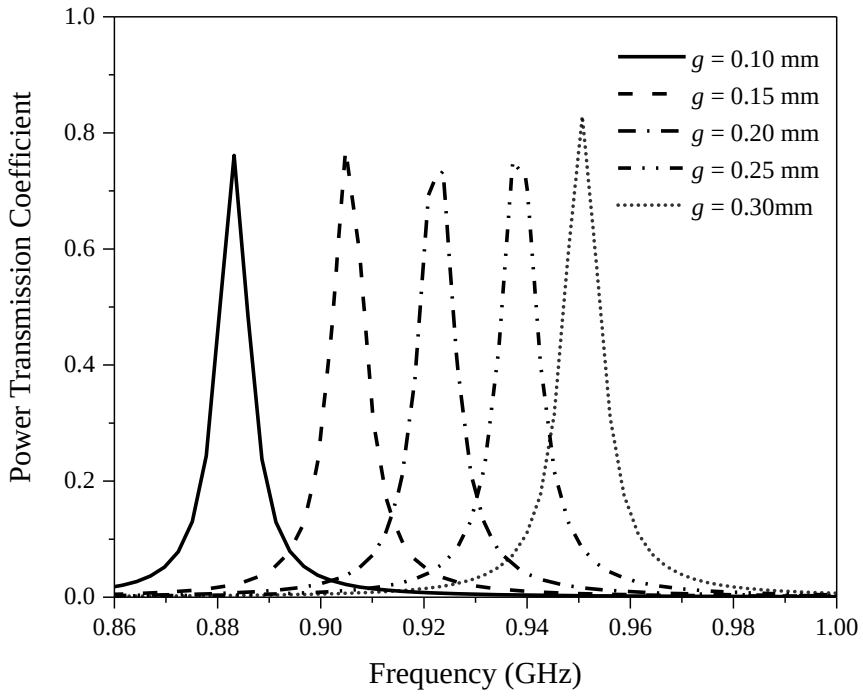
Power Transmission Coefficient
Frequency (GHz)
g = 0.10 mm
g = 0.15 mm
g = 0.20 mm
g = 0.25 mm
g = 0.30mm

(b)

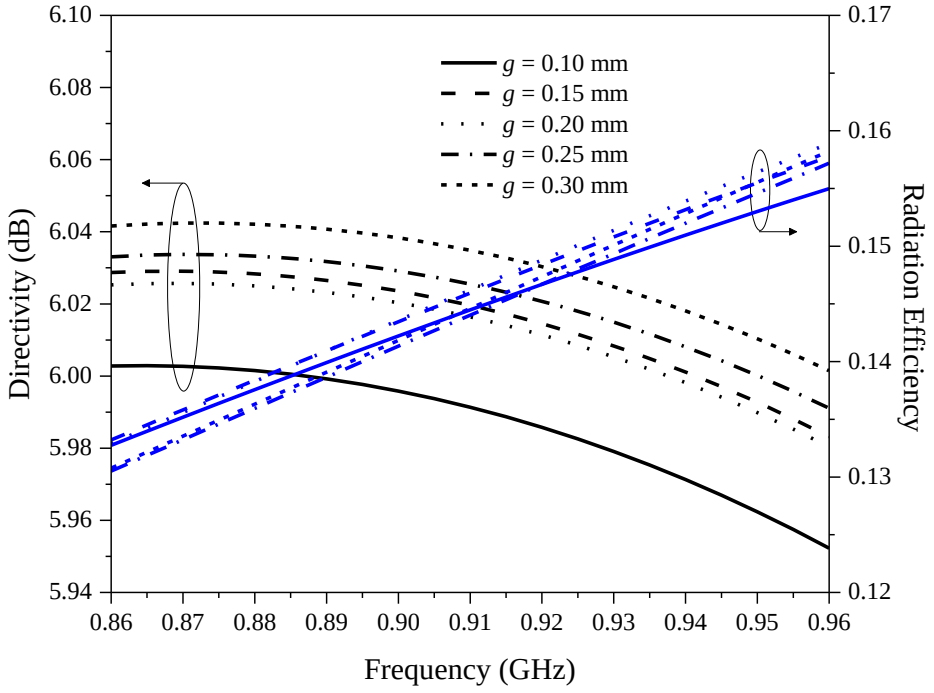

(c)

Figure 4.6: Effects of width (*g*) on the (a) resistance and reactance, (b) power transmission coefficient and (c) directivity and radiation efficiency.

The effects of the slots (1-4) are studied next. With reference to Figure 4.7 (a), widening the width (g_1) of Slots 1-4 increases the resistance and reactance of the tag antenna. When g_1 is changed from 1.8 mm to 1.0 mm, the resonant frequency shifts from 912.9 MHz to 923.7 MHz. However, the power transmission coefficient drops from 0.7729 to 0.7339 when the slots' width is decreased. The directivity falls in the range of 5.99 – 6.02 dB and radiation efficiency maintains around 0.15, as can be seen in Figure 4.7 (c).

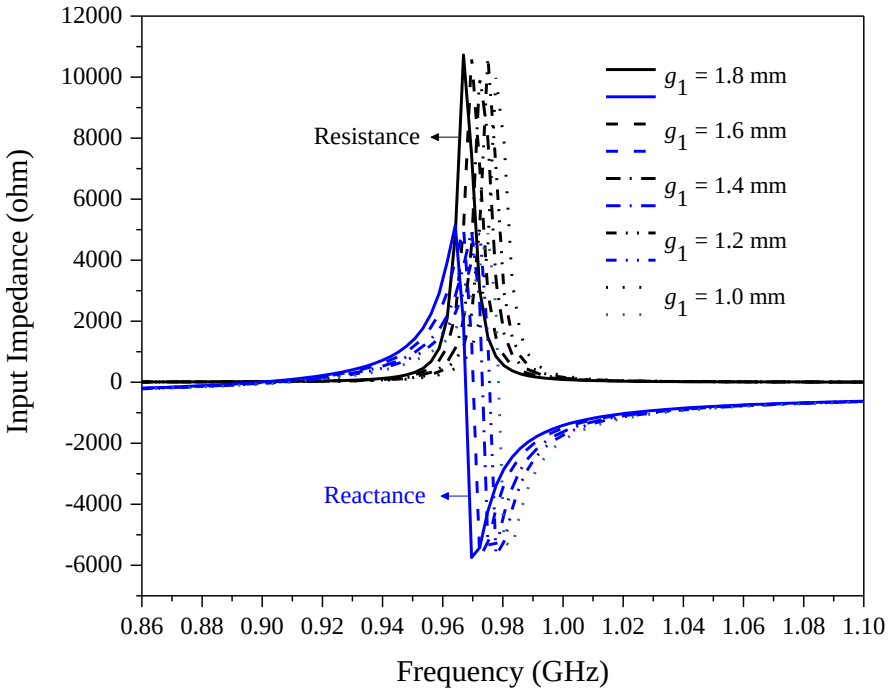
Input Impedance (ohm)
Frequency (GHz)
Resistance
Reactance
g_1 = 1.8 mm
g_1 = 1.6 mm
g_1 = 1.4 mm
g_1 = 1.2 mm
g_1 = 1.0 mm
12000
10000
8000
6000
4000
2000
0
-2000
-4000
-6000
0.86 0.88 0.90 0.92 0.94 0.96 0.98 1.00 1.02 1.04 1.06 1.08 1.10

(a)

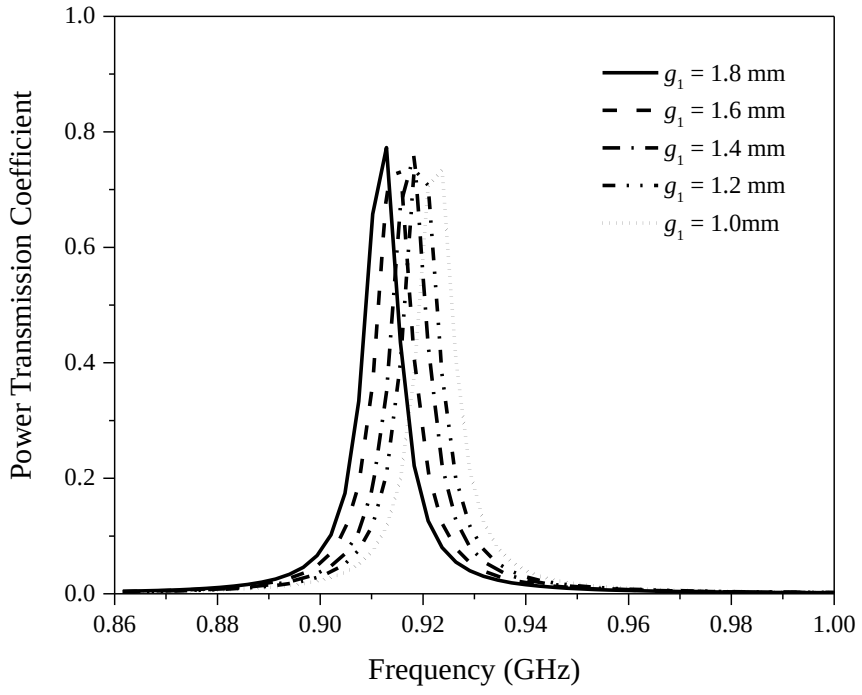
Power Transmission Coefficient
Frequency (GHz)
g_1 = 1.8 mm
g_1 = 1.6 mm
g_1 = 1.4 mm
g_1 = 1.2 mm
g_1 = 1.0mm
1.0
0.8
0.6
0.4
0.2
0.0
0.86 0.88 0.90 0.92 0.94 0.96 0.98 1.00

(b)

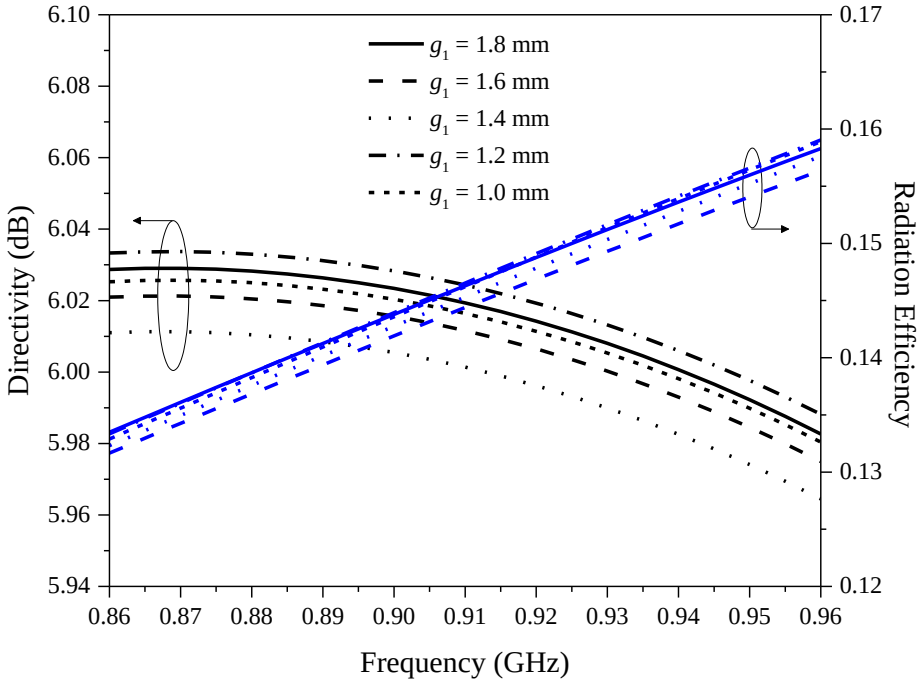

(c)

Figure 4.7: Effects of the slot width (g_1) on the (a) resistance and reactance, (b) power transmission coefficient and (c) directivity and radiation efficiency.

Then, the length (l_2) of Slots 1 and 3 is decreased from 12.6 mm to 8.6 mm. It can be noticed from Figure 4.8 (a) that the resistance and reactance drop slightly with decreasing l_2, causing the resonant frequency to increase. With reference to Figure 4.8 (b), the power transmission coefficient ranges 0.7339 to 0.8016 for different l_2. The directivity remains in the range of 6.01-6.03 dB while the radiation efficiency is not affected much in this parametric study.

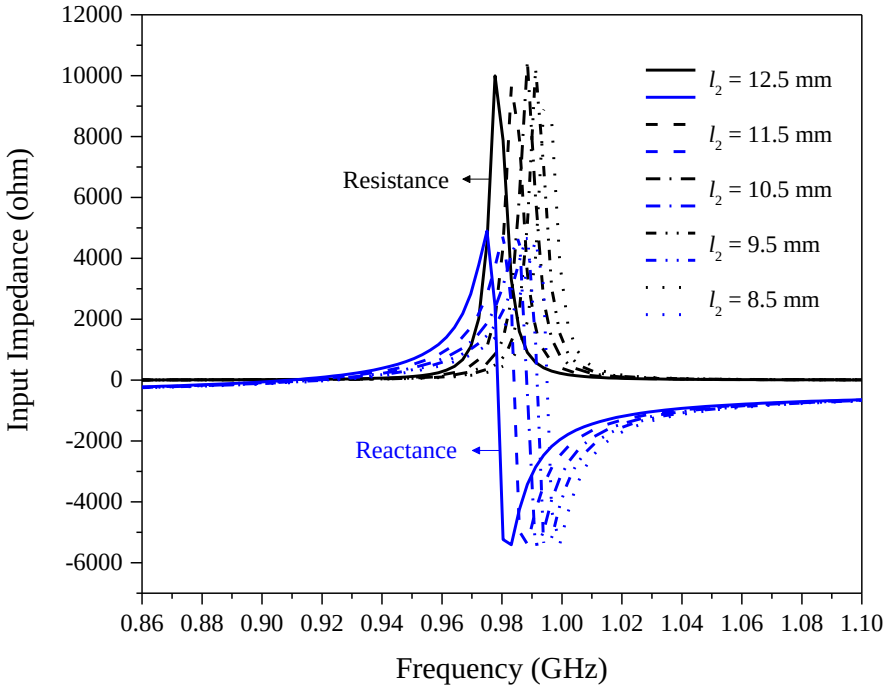
Input Impedance (ohm)
Frequency (GHz)
Resistance
Reactance
l_2 = 12.5 mm
l_2 = 11.5 mm
l_2 = 10.5 mm
l_2 = 9.5 mm
l_2 = 8.5 mm

(a)

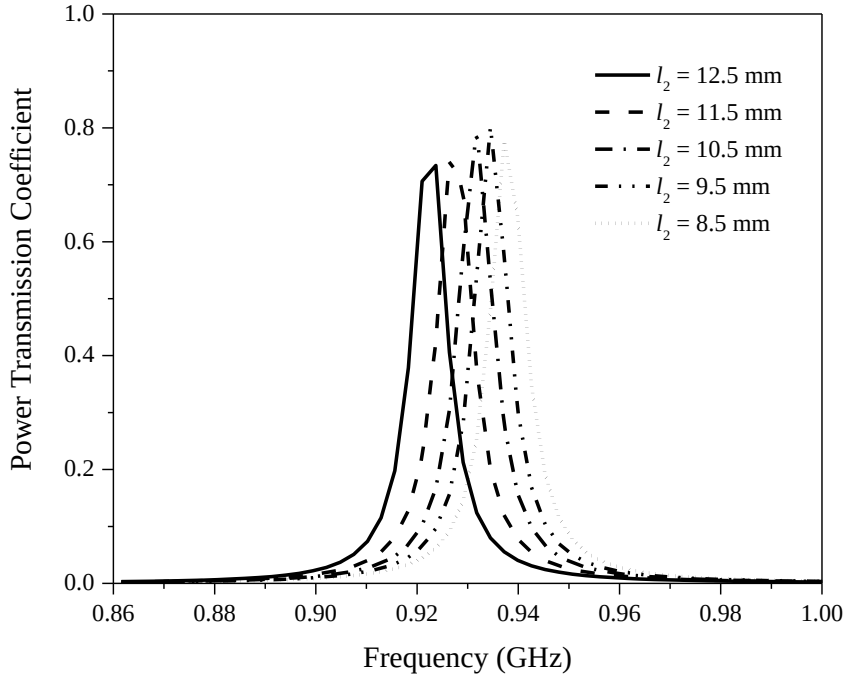
Power Transmission Coefficient
Frequency (GHz)
l_2 = 12.5 mm
l_2 = 11.5 mm
l_2 = 10.5 mm
l_2 = 9.5 mm
l_2 = 8.5 mm

(b)

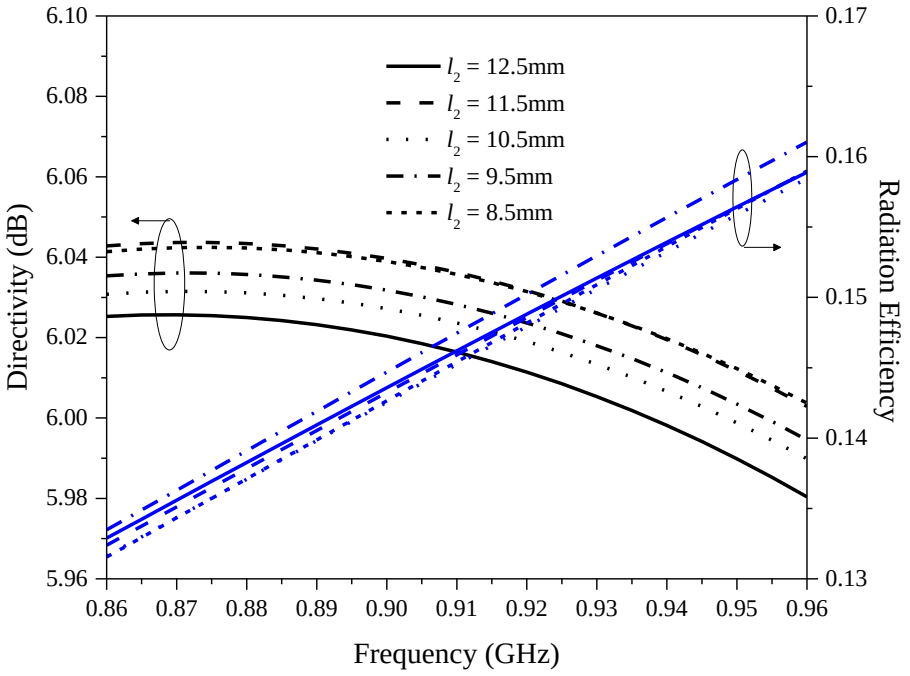

(c)

Figure 4.8: Effects of the length (l_2) of Slots (1 and 3) on the (a) resistance and reactance, (b) power transmission coefficient and (c) directivity and radiation efficiency.

Slots 2 and 4 have the same effects as Slots 1 and 3. It can be observed from Figure 4.9 (a) that shortening the length (l_3) of Slots 2 and 4 causes the resistance and reactance to reduce and the resonant frequency to increase. By referring to Figure 4.9 (b), shortening l_3 from 10.6 mm to 6.6 mm makes the power transmission coefficient to increase from 0.7339 to 0.7513. The directivity varies in the range of 6.01 - 6.02 dB at 923.7 MHz and the radiation efficiency keeps almost the same value for different l_3, as shown in Figure 4.9 (c).

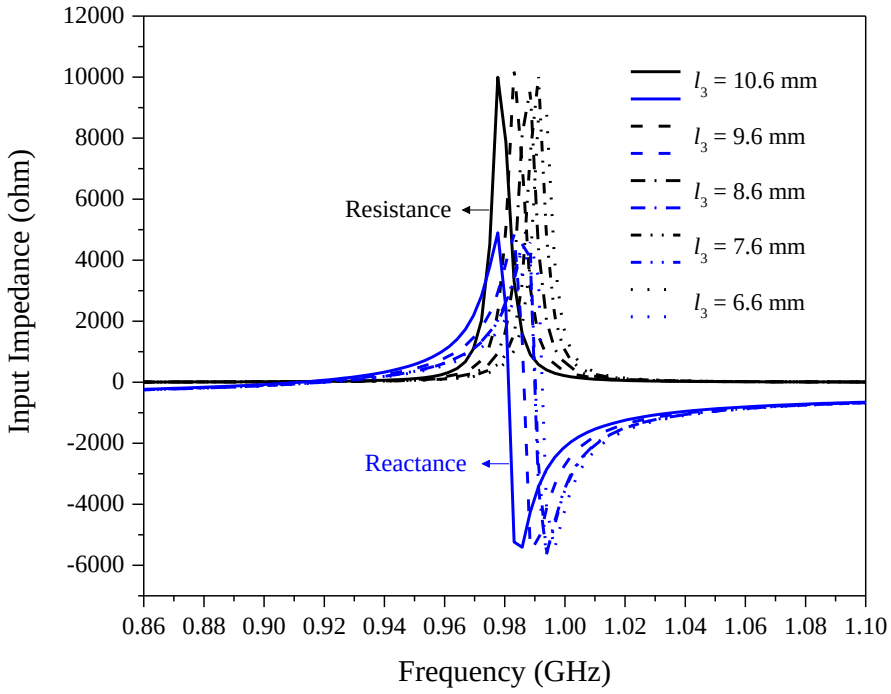
Input Impedance (ohm)
Frequency (GHz)
Resistance
Reactance
l_3 = 10.6 mm
l_3 = 9.6 mm
l_3 = 8.6 mm
l_3 = 7.6 mm
l_3 = 6.6 mm

(a)

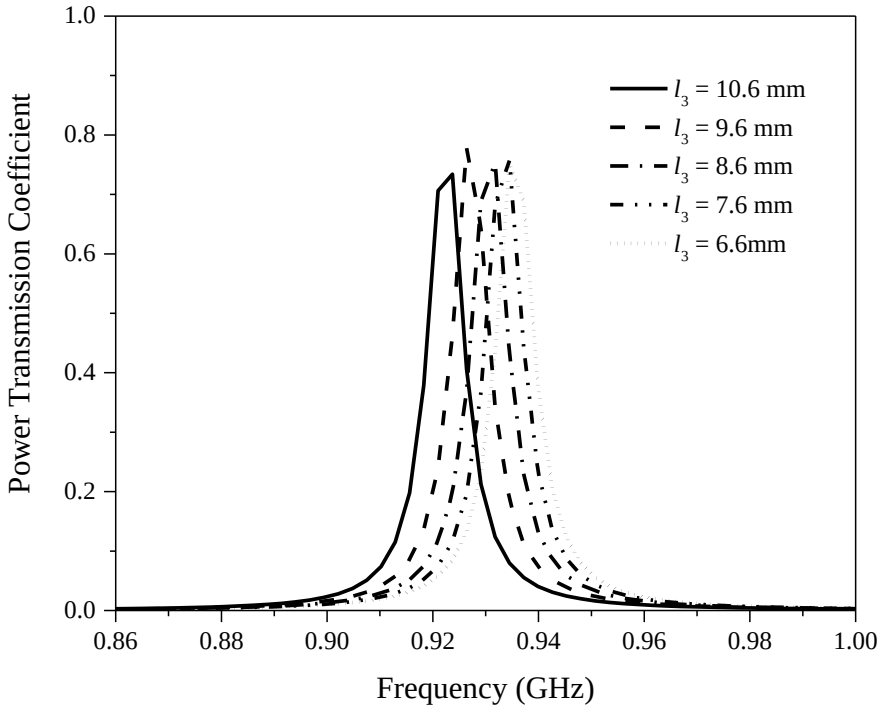
Power Transmission Coefficient
Frequency (GHz)
l_3 = 10.6 mm
l_3 = 9.6 mm
l_3 = 8.6 mm
l_3 = 7.6 mm
l_3 = 6.6mm

(b)

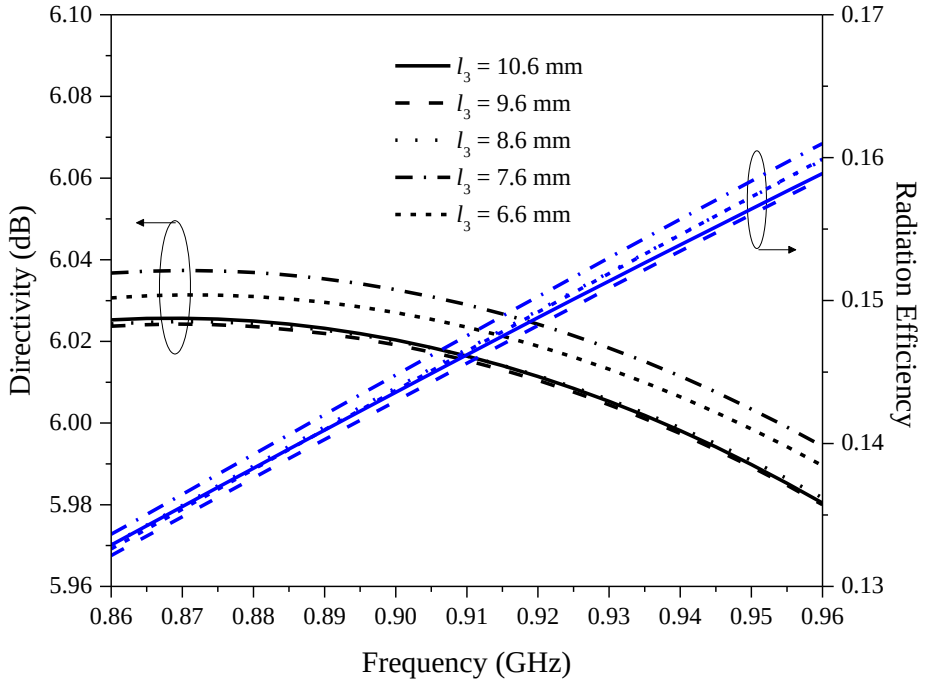

(c)

Figure 4.9: Effects of the length (l_3) of Slots (2 and 4) on the (a) resistance and reactance, (b) power transmission coefficient and (c) directivity and radiation efficiency.

Besides, the resistance and reactance decrease when the length of the feedline (l_1) decreases, as shown in Figure 4.10 (a). This is due to the decrease of the inductance when the feedline length becomes shorter. The power transmission coefficient remains in between the range of 0.7030 – 0.7965 in Figure 4.10 (b). In this case, the directivity and radiation efficiency reduce when the length of the feedline is decreased.

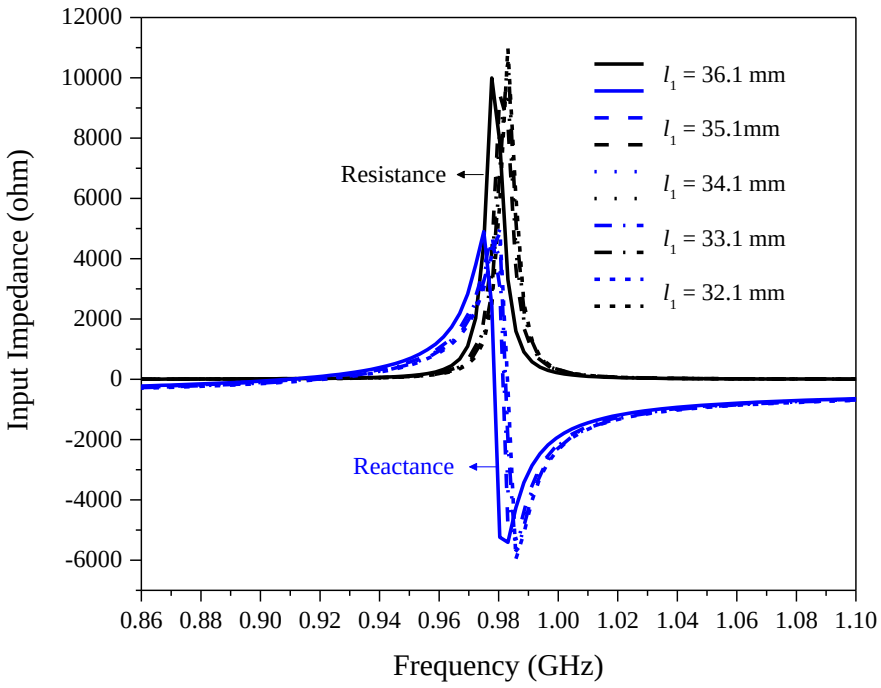
Input Impedance (ohm)
Frequency (GHz)
Resistance
Reactance
l_1 = 36.1 mm
l_1 = 35.1mm
l_1 = 34.1 mm
l_1 = 33.1 mm
l_1 = 32.1 mm

(a)

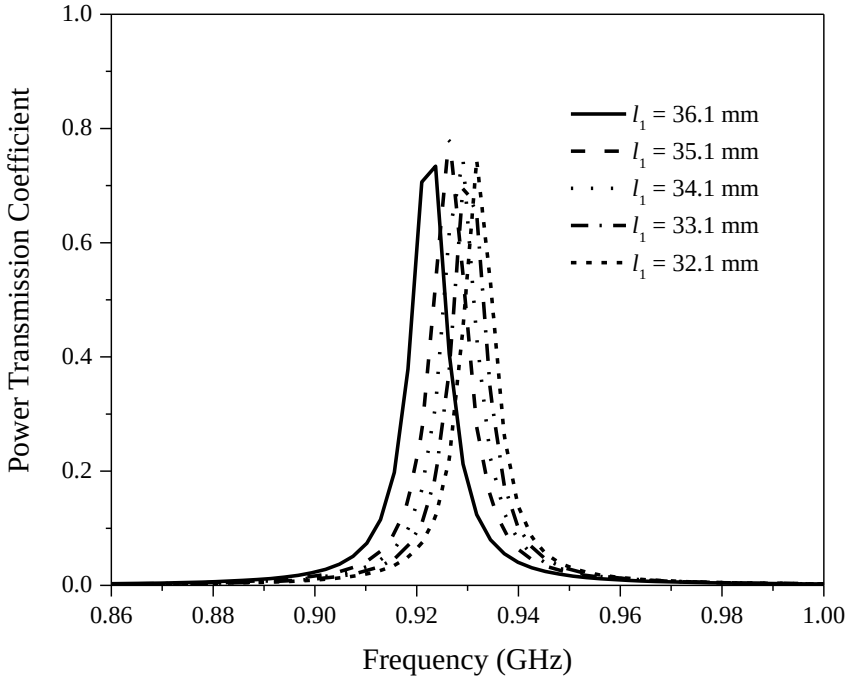
Power Transmission Coefficient
Frequency (GHz)
l_1 = 36.1 mm
l_1 = 35.1 mm
l_1 = 34.1 mm
l_1 = 33.1 mm
l_1 = 32.1 mm

(b)

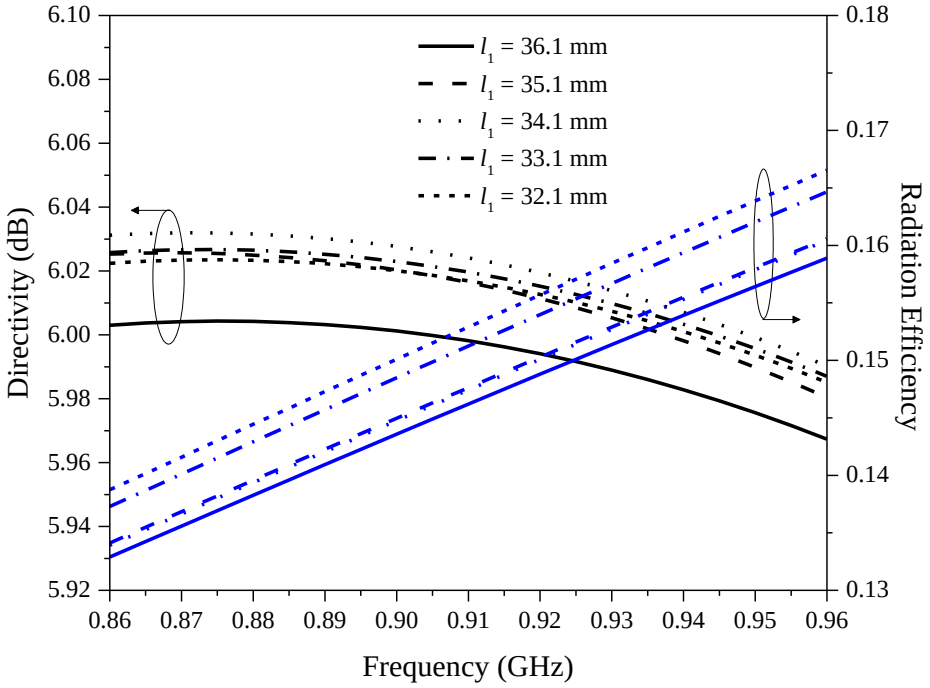

(c)

Figure 4.10: Effects of the length (l_1) of Slot 5 on the (a) resistance and reactance, (b) power transmission coefficient and (c) directivity and radiation efficiency.

The tuning sensitivities of the design parameters are calculated and shown in Table 4.3. It can be concluded that the slot width (g) and stub width (k_0) can be used for adjusting the resonant frequency in large scale to the UHF band at the beginning. This is because changing the two parameters can adjust the resonant frequency in a coarser step. Finally, fine-tuning can be done by using the slots' dimensions (g_1, l_2 and l_3) and the length of the feedline (l_1) to shift the tag's resonant frequency to exactly the desired frequency.

Table 4.3: Tuning sensitivity of the design parameters.

Design Parameter	Tuning Sensitivity, MHz/mm
g	337.5
k_0	135
g_1	13.5
l_2	3.38
l_3	2.7
l_1	2.0

4.4 Results and Discussion

Figure 4.11 shows the experimental setup in the anechoic chamber. As can be seen in the figure, the tag is placed at the center of a piece of 20 cm × 20 cm copper plate, the orientation of the proposed tag antenna is rotated so that its polarization is aligned with that of the reader antenna. By rotating the tag antenna around its own *y*- and *x*- axis, the read patterns in the *xz*- and *yz*- planes can be measured. This makes the definition of the elevation angle (θ) similar to that of the conventional spherical coordinate system. Meanwhile, the *xy*-plane measurement is not the same as the conventional spherical coordinate system. With the reader antenna suspended right above the tag antenna, the *xy*-plane is measured by rotating the tag antenna around its *z*-axis to show the polarization characteristics of the tag antenna in the boresight direction. In other words, the magnitude of ϕ is not the azimuthal quantity of the spherical coordinate.

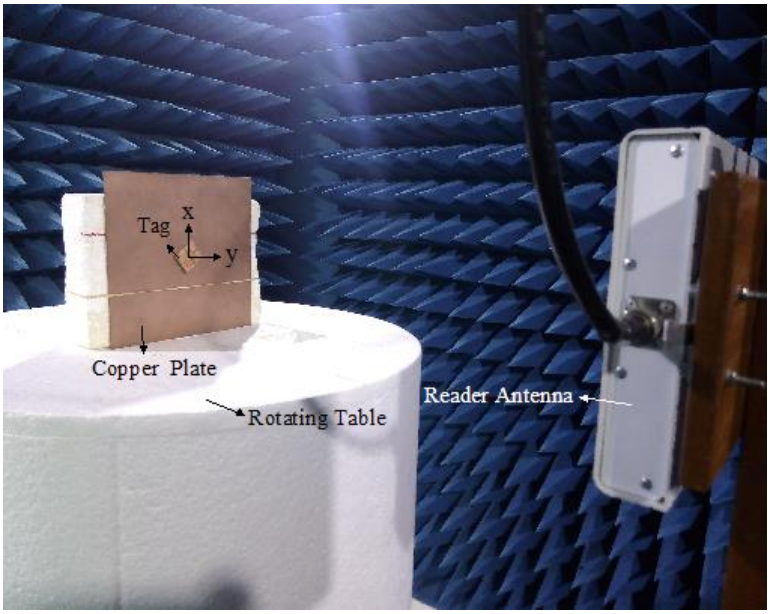

Figure 4.11: Experimental setup in the anechoic chamber.

The measured and simulated realized gains (G_r) plotted in Figure 4.12 are compared and studied. As can be seen in the same figure, the measured realized gain is 2 dBi lower than its simulated counterpart. The measured realized gain is found to be -5.6 dBi at 915 MHz whereas the simulated realized gain is -3.6 dBi at 923.7 MHz. The discrepancy can be caused by various tolerances in the fabrication and experimental processes. The measured tag sensitivity is -14.4 dBm at 915 MHz.

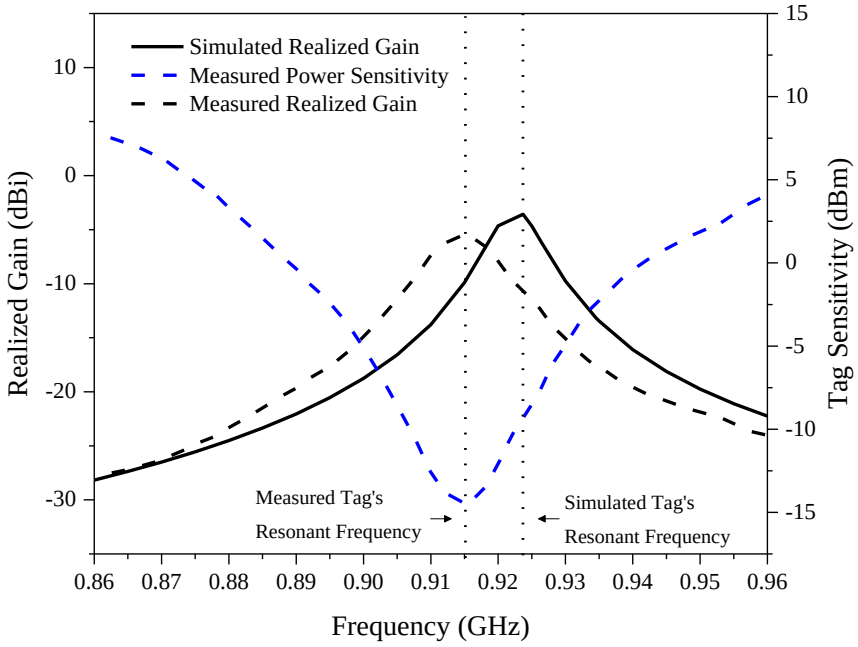

Figure 4.12: Measured and simulated realized gains as well as measured tag sensitivity when the tag antenna is placed on a metal plate of 20 cm × 20 cm.

The results in Figure 4.13 depicts the read distance of the proposed tag antenna in the *xy*-, *xz*-, and *yz*-plane at 915 MHz. With reference to the *xy*-plane, the tag antenna can be read the best in the two directions at the boresight, with a maximum read range of 8.9 m achieved at ϕ =0^o and ϕ =180^o, showing that the tag antenna is linearly polarized. In general, the read distance maintains above 5 m in the angular ranges of (0^o ≤ ϕ ≤ 50^o), (310^o ≤ ϕ ≤ 360^o) and (130^o ≤ ϕ ≤ 240^o). When measuring the *xz*-plane, the measured read distance reaches 8.25 m at θ = 0^o and it goes beyond 5 m in the angular range of (-60^o ≤ θ ≤ 70^o). The maximum read distance of the tag is measured to be 8m at θ =0^o in the *yz*-plane, and the read distance in the entire upper hemisphere (-50^o ≤ θ ≤ 50^o) is able to reach more than 5 m in this plane. The read distance is truncated for (θ ≤ -90^o) and (θ ≥ 90^o) in the *xz* and *yz* planes.

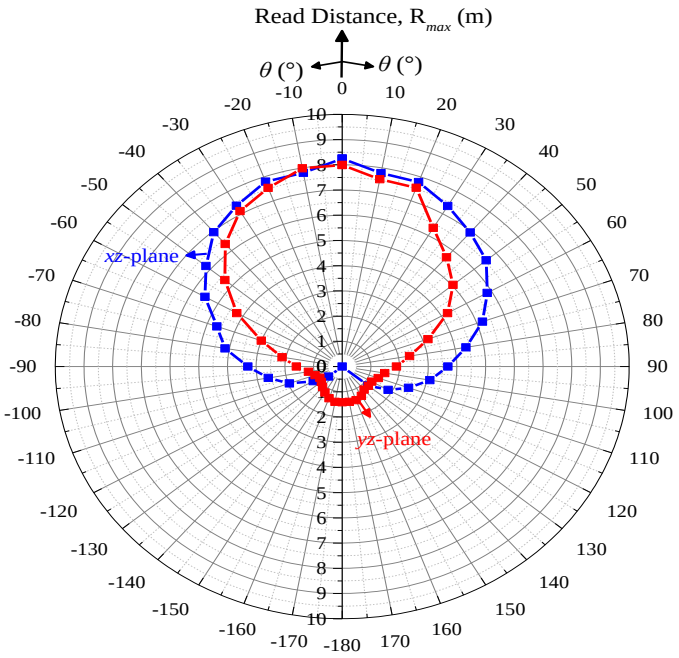

(a)

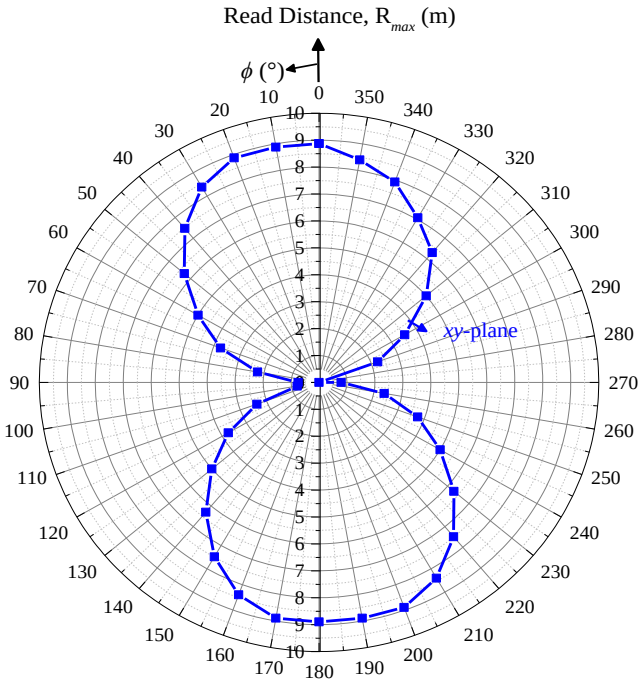

(b)

Figure 4.13: Measured read distances in the (a) *xz*- and *yz*- planes (b) *xy*-plane.

Since the tag antenna is proposed to be placed on metal, the performances of the tag in the boresight ($\theta = 0^{o}$) are measured on metal plates with different sizes. Figure 4.14 shows the measured read distances for different *L* and *W*. With reference to Figure 4.14 (a), the length of the plate *L* is varied while the width *W* is remained constant at 20 cm. In this case, the achievable read distance can be maintained beyond 7 m when *L* is reduced from 24 cm to 8 cm. Referring to Figure 4.14 (b), the read distance decreases to 6.7 m when *W* is shortened from 24cm to 8cm (*L* = 20cm). From the two figures, it can be noticed that the resonant frequency is not affected much by the plate size, it always falls in the range of 910 MHz-920 MHz for all cases.

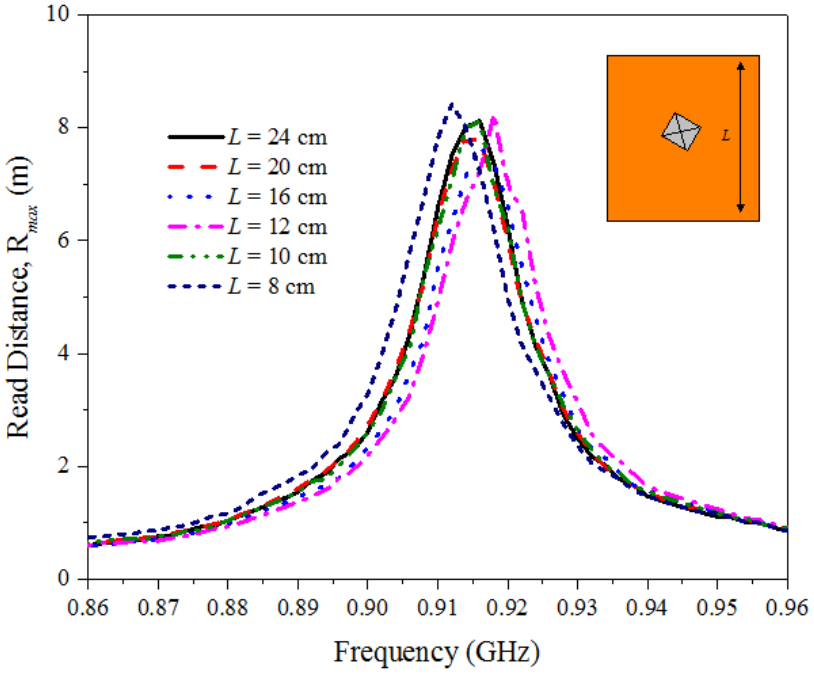

(a)

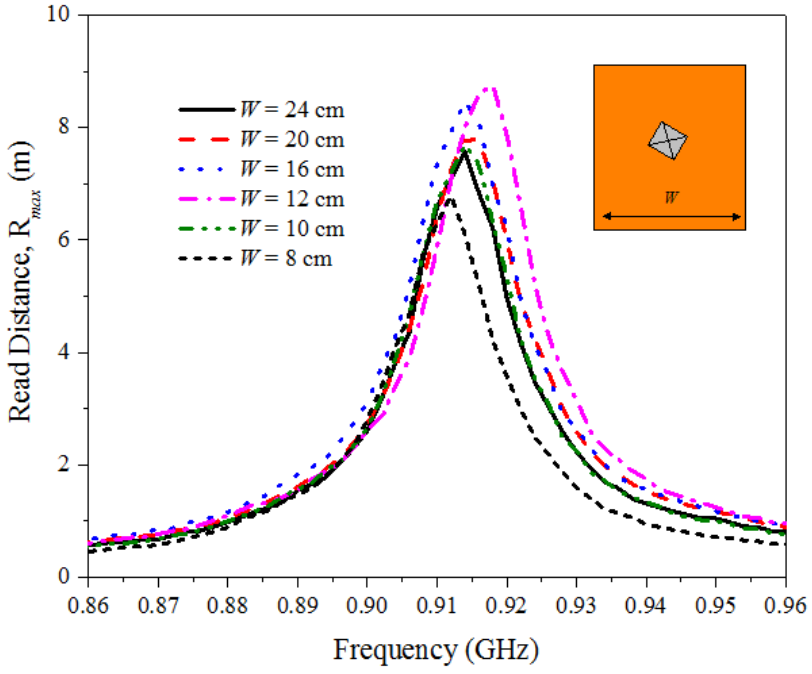

(b)

Figure 4.14: Measured read distances in the boresight (θ = 0°) for different plate sizes when changing (a) *L*, (b) *W*.

Also, the proposed tag antenna is tested on some commercial metallic items in Figure 4.15 (a). All the samples are made of metal but their detailed compositions are not known. . As can be seen in Figure 4.15 (b), the maximum achievable read distance is greater than 5.5 m for all the samples. Most importantly, the resonant frequency is still in the range of 910 MHz – 920 MHz when attached on all the items, showing that the operating frequency is not dependent on the sizes and materials of the backing metal. This is a very desirable feature when designing a metal-mountable tag antenna.

(a)

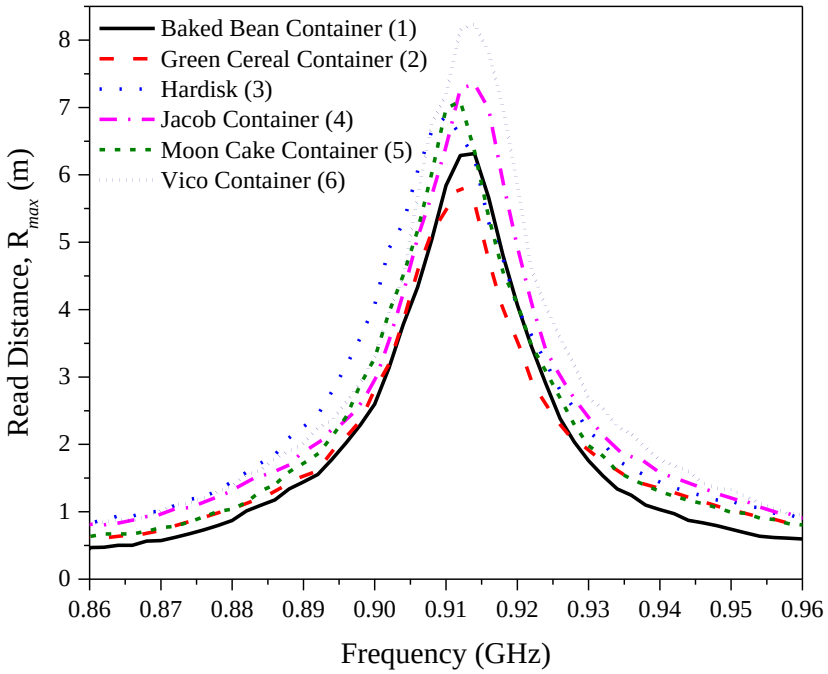

(b)

Figure 4.15: (a) Metallic objects. (b) Read distances in the boresight (θ = 0º) when the tag antenna is placed on different metallic objects.

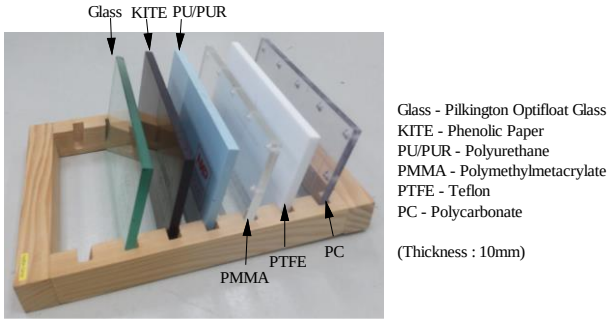

(a)

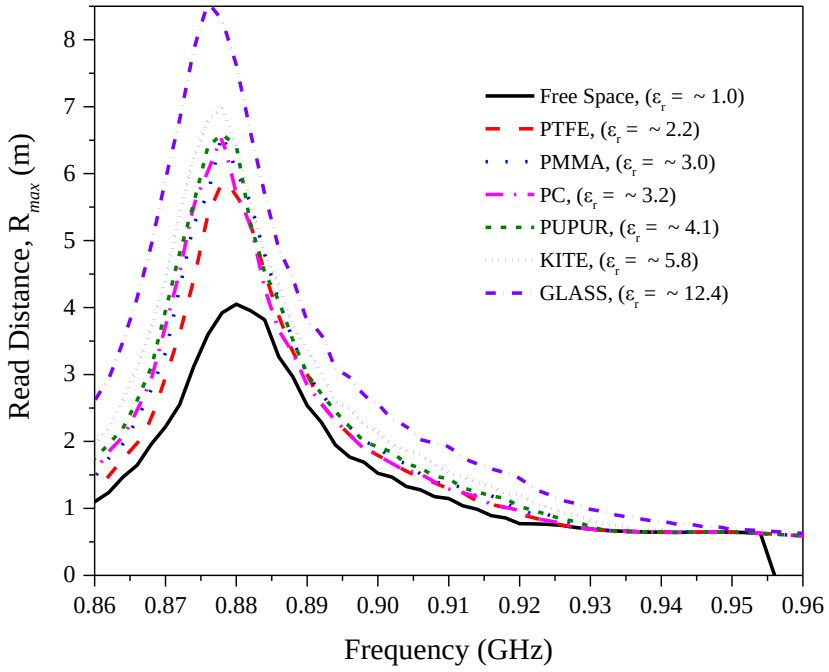

(b)

Figure 4.16: (a) The NXP reference materials. (b) Read distances in the boresight (θ = 0º) when the proposed tag antenna is tested using the NXP reference materials.

Besides metals, the read range of the proposed tag antenna is also tested on dielectric slabs with dielectric constants (ε_r) ranging from 2.2 to 12.4 in the boresight direction. The dimension of the slabs is 24 cm × 12 cm × 1 cm, as shown in Figure 4.16 (a), which are provided by the NXP Semiconductors (AN1629, 2008). It can be seen in Figure 4.16 (b) that the read distances are greater than 6 m for all the dielectric constants (ε_r). Also observed is that the

higher the permittivity, the farther the read distance of the proposed tag antenna. In this case, the operating frequency has moved down to (~ 870 MHz) due to changes in the loading effect of the backing object. This is not a problem as the frequency can always be adjusted by tuning the slots' dimensions of the proposed tag. Referring to the same figure, it is interesting to note that the resonant frequency is pretty much the same for the permittivity range of 2.2 – 12.4. The performance of the tag antenna in free space (ε_r = 1.0) is also evaluated and it is able to achieve ~ 4 m at 880 MHz, as shown in the same figure.

Table 4.4: Comparing the performances of different miniature UHF metal-mountable tag antennas.

	Power	**Flexibility**	**Tag Dimension (mm)**	**Backing Plate Size**	**Max. Read Distance (m)**
This work	4W (EIRP)	Yes	30 × 25 × 3	20 cm × 20 cm	8.9 (on metal) 5 (on dielectrics)
(Zhang and Long, 2014)	4W (EIRP)	No (FR4 substrate + PTFE)	26 × 14 × 2.4	20 cm × 20 cm	5.5 (on metal)
(Soriano and Parrón, 2016)	4W (EIRP)	No (Ceramic, ε_r = 35.95)	14.3× 25 × 3	-	13.3 (on metal)
(Hamani et al., 2017)	4W (EIRP)	No (FR4 substrate)	104 × 31 × 7.6	30 cm × 25 cm	14.6 (on metal)
(Moh, et al., 2018)	4W (EIRP)	Yes	40 × 25 × 3	20 cm × 20 cm	10.7 (on metal) 5 (on dielectrics)

The footprint and performances of the newly proposed tag antenna is compared with other metal-mountable tag antennas, as shown in Table 4.4. Via

holes are employed in the tag antenna (Zhang and Long, 2014; Soriano and Parrón, 2016) for minimizing the antenna size and tuning the impedance matching, which make the fabrication processes difficult. For the tag antenna in (Soriano and Parrón, 2016), it is small in size but a high-permittivity (ε_r) ceramic substrate is used to isolate the antenna from the backing metal surface. The scaling factor of the ceramics is employed for reducing the tag size. However, ceramics needs additional molding and burning processes, which make the tag's costs to become higher. In (Hamani, et al., 2017), the AMC structure was employed for isolating a dipolar tag antenna from the metal surface, with the price of increasing the complexity of the antenna. In order to hold multiple substrates together, screw-holes and spacers are also needed. This makes the fabrication process become much more complicated. Despite its far read distance (Hamani, et al., 2017), the footprint and profile are much higher than ours. Although the coplanar waveguide feeding method was first employed for designing the metal-mountable UHF tag antenna in (Moh, et al., 2018), making it differential is found to be able to reduce the footprint by 25%. For both dielectrics and metal surfaces, the frequency stability of the newly proposed tag is also found to be much better than that in (Moh et al., 2018).

4.5 Conclusion

A differential coplanar feedline has been proposed for designing a miniature metal-mountable UHF RFID tag for the first time. Multiple slots are

incorporated around the edges of the patch for coarse- and fine-tuning the tag's resonant frequency. By adjusting the length and width of the slots, it was found that the tag's resonant frequency can be easily tuned. A pair of inductive stubs has also been introduced for coarse-tuning the operating frequency of the tag antenna. A simple equivalent circuit has been derived to characterize the input impedance of the proposed tag antenna. When attached the tag antenna on a 20 cm × 20 cm metal plate, it is able to reach a maximum read distance of 8.9 m. The tag's resonant frequency is found to be very stable and it is not affected much by the backing metal plate size. Also, the tag antenna can achieve above 4 m when placed on different dielectrics.

CHAPTER 5

SUMMARY AND DISCUSSION

5.1 Summary

In this dissertation, two miniature UHF RFID tags have been proposed for mounting on metal objects. In the first project, the patch antenna is fed by a coplanar feedline and two inductive stubs are employed to connect the patch and the feedline to the ground plane at the back of the tag antenna. The inductive stubs are useful for tuning the performances, such as resonant frequency and the input impedance of the tag. By introducing notches along the stub, the tuning range of the resonant frequency can be significantly extended. When placed on a 20 cm × 20 cm metal surface, the proposed tag can achieve a read distance of greater than 10 m. Besides, the tag is tested on other metallic samples with unknown metal components and different sizes. The read distance can maintain above 5 m for all the cases. Also, the tag can be used on different dielectric materials and the read range is beyond 5 m.

In the second project, a pair of differential fed coplanar waveguides is used to design a metal-mountable tag antenna. Two inductive stubs are connecting the patch to the ground and multiple slots are employed. It is observed that the resonant frequency can be shifted down efficiently when more slots are introduced to the patch. The read range of the proposed tag can

achieve 8.9 m when tested on a 20 cm × 20 cm metal plate. When the tag is tested on different metal objects, the read distances of the tag can be kept beyond 5.5 m. The read distances are also more than 4 m when the tag is attached to various dielectric materials with permittivity values (ε_r) in the range of 1 - 12.4.

To sum up, both of the objectives for this dissertation have been achieved. The first objective is to design a low profile, small size, light weight, high gain and far read range folded-patch RFID tag antenna that is mountable on metal surface. From both of the projects, it can be seen that the sizes of our tags are smaller than others. Light-weight materials such as PET and polyethylene foam have been used to design the tags. High antenna gains and far read ranges have been achieved. The second objective is to investigate the effects of metal object on the performances of the folded-patch RFID tag antennas. Different metallic containers with unknown metal components have been used to test the performances of the tags. From the measurement results, it shows that the tags are functioning well in all cases and the read distances are all going beyond 5 m.

5.2 Limitation and Future Recommendation

From both of the projects, discrepancies are observed between the measurement and simulation results. The measured resonant frequency, input impedance and realized gain are slightly different from the simulation. All

these discrepancies are caused by the fabrication and experimental tolerances. Also, it can be due to component tolerances because active devices usually tend to have a huge manufacturing tolerance. To reduce the discrepancies, the use of printing process as an alternative way to etching in manufacturing of RFID tag antennas can help to minimize the fabrication tolerances as over-etching problems can be avoided by using printing method. Screen printing is always applied in electronic manufacturing. This technique is able to provide a very thin printing by pressing the conductive ink onto the substrate, which can help to reduce the fabrication tolerances (Björninen, et al., 2009). Other than that, polyethylene foam is a poor water resistance material. The performance of the tag will be affected if the foam absorbs water. So, the polyethylene form can be replaced by some water resistance materials such as rubber to prevent degradation in performances.

REFERENCES

Alan Payne, 2016. *The AC Resistance of Rectangular Conductors*, [pdf]. [online]. Available at :< http://g3rbj.co.uk/wp-content/uploads/2016/06/The-ac-Resistance-of-Rectangular-Conductors-Cockcroft2.pdf>.
[Acessed 20 January 2017].

AN1629 UHF RFID Label Antenna Design, [pdf]. [online].Available at :<http://www.nxp.com/documents/application_note/AN162910.pdf>.
[Acessed 2 February 2017].

Babar, A.A., Björninen, T., Bhagavati, V. A., Sydänheimo, L., Kallio, P. and Ukkonen, L., 2012. Small and flexible metal mountable passive UHF RFID tag on high-dielectric polymer-ceramic composite substrate. *IEEE Antennas and Wireless Propagation Letters*, 11, pp. 1319-1322.

Björninen, T., Merilampi, S., Ukkonen, L., Sydänheimo, L., and Ruuskanen, P., 2009. The effect of fabrication method on passive UHF RFID tag performance. *International Journal of Antennas and Propagation*, 2009, pp. 1-8.

Bong, F.L., Lim, E.H. and Lo, F.L., 2017a. Flexible folded-patch antenna with serrated edges for metal mountable UHF RFID tag," *IEEE Transactions on Antennas and Propagation*, 65(2), pp. 873-877.

Bong, F.L., Lim, E.H. and Lo, F.L., 2017b. Compact folded dipole with embedded matching loop for universal tag applications," *IEEE Transactions on Antennas and Propagation*, 65(5), pp. 2173-2181.

Bong, F.L., Lim, E.H., Lo, F.L., 2017c. Miniaturized Dipolar Patch Antenna With Narrow Meandered Slotline for UHF Tag. *IEEE Transactions on Antennas and Propagation*, 65, 4435–4442.

Chen, H. D. and Tsao, Y. H, 2010. Low-profile PIFA array antennas for UHF Band RFID tags mountable on metallic objects. *IEEE Transactions on Antennas and Propagation*, 58(4), pp. 1087-1092.

Chen, S.L., 2009. A miniature RFID tag antenna design for metallic objects application. *IEEE Antennas and Wireless Propagation Letters*, 8, pp. 1043-1045.

Chen, S.L. and Mittra, R., 2010. A long read range RFID tag design for metallic objects. *Proceedings of the Fourth European Conference on Antennas and Propagation, pp 1-3.*

Cho, C., Choo, H. and Park, I., 2008. Design of planar RFID tag antenna for metallic objects. *Electronics Letters*, 44(3), pp. 175–177.

Choi, W. , Son, H. W., Bae, J.H., Choi, G. Y. , Pyo, C. S. and Chae, J. S., 2006. An RFID tag using a planar inverted-F antenna capable of being stuck to metallic objects. *ETRI Journal*, 28, pp. 216-218.

Ding, X., Liu, S., Zhang, K., and Wu, Q., 2014. A broadband anti-metal RFID tag with AMC ground. *3rd Asia-Pacific Conference on Antennas and Propagation*, pp. 647–649.

Dobkin, D.M. and Weigand, S. M., 2005. Environmental effects on RFID tag antennas. *IEEE MIT-S International Microwave Symposium Digest*, pp. 135-138.

Du, J., Wu, C.Y., Zhu, W.J. and Liu, Q., 2011. Ultrathin low cost EBG structure for insulating UHF RFID tag from metal objects. *2011 IEEE International Conference on Signal Processing, Communications and Computing (ICSPCC)*, pp. 1–4.

Emerson & Cuming Microwave Products, 2011. *ECCOSTOCK PP*, [pdf]. Available at: < http://www.eccosorb.com/Collateral/Documents/English-US/PP.pdf > [Acessed 2 January 2018].

Faudzi, N.M., Ali, M.T., Ismail, I., Jumaat, H. and Sukaimi, N.H.M., 2014. Metal mountable UHF-RFID tag antenna with meander feed line and double T-match. *2014 International Symposium on Technology Management and Emerging Technologies*, pp. 33–38.

Fennani, B., Haman, H. and Dahmane, A. O., 2011. RFID overview. *2011 ICM Proceeding*.

Gao, B. and Yuen, M.M.F., 2011. Passive UHF RFID packaging with electromagnetic band gap (EBG) material for metallic objects tracking. *IEEE Transactions on Components, Packaging and Manufacturing Technology*, 1(8), pp. 1140-1146.

Greenhouse, H.M., 1974. Design of planar rectangular microelectronic inductors. *IEEE Transactions on Parts, Hybrids, Packaging*, 10(2), pp. 101-109.

Hamani, A., Yagoub, M.C.E., Vuong, T.P. and Touhami, R., 2017. A Novel Broadband Antenna Design for UHF RFID Tags on Metallic Surface Environments. *IEEE Antennas and Wireless Propagation Letters*, 16, 91–94.

Hamraoui, A. E. , Abdelmounim, E. H. , Zbitou , J. , Bennis , H., Latrach, M., and Errkik, A., 2017. A low cost miniature UHF RFID tag antenna using paper substrate. *International Conference on Wireless Technologies, Embedded and Intelligent Systems (WITS)*, pp. 1–6.

He, Y. and Zhang, H., 2013. A new UHF anti-metal RFID tag antenna design with open-circuited stub feed. *IEEE International Conference on Communication (ICC)*, pp. 5809-5813.

Hirvonen, M., Pursula, P., Jaakkola, K., and Laukkanen, K., 2004. Planar inverted-F antenna for radio frequency identification. *Electronics. Letters*, 40(14), pp. 848–850.

IPJ-W1600 Monza 5 Tag Chip Datasheet, 2016. [online]. Available at: <https://support.impinj.com/hc/en-us/articles/202756948-Monza-5-Tag-Chip-Datasheet> [Acessed 20 May 2017].

IPJ-W1700 Monza R6 tag Chip Datasheet, 2016. [online]. Available at: <https://support.impinj.com/hc/en-us/articles/202765328-Monza-R6-Product-Datasheet> [Acessed 17 August 2017].

Jaakkola, K., 2016. Small on-metal UHF RFID transponder with long read range. *IEEE Transactions on Antennas and Propagation*, 64(11), pp. 4859-4867.

Kim, D. and Yeo, J., 2010. A passive RFID tag antenna installed in a recessed cavity in a metallic platform. *IEEE Transactions on Antennas and Propagation*, 58(12), pp. 3814–3820.

Kim, J.S., Choi, W. and Choi, G.Y., 2008. UHF RFID tag antenna using two PIFAs embedded in metallic objects. *Electronics. Letters*, 44(20), pp. 1181-1182.

Kuo, S.K. and Liao, L.G., 2010. An analytic model for impedance calculation of an RFID metal tag. *IEEE Antennas and Wireless Propagation Letters*, 9, pp. 603-607.

Kwon, H., and Lee, B., 2005. Compact slotted planar inverted-F RFID tag mountable on metallic objects, *Electron. Letters*, 41(24).

Lai, M. Y., Li, L. R., and Tentzeris, M. M., 2010. Low-profile broadband RFID tag antennas mountable on metallic objects. *Proceeding of IEEE International Symposium. Antenna Propag*ation, pp. 1-4.

Li, H., Zhu, J. J., and Yu, Y. F., 2017. Compact single-layer RFID tag antenna tolerant to background materials. *IEEE Access*, 5, pp. 21071-21079.

Lim, E. H. and Leung, K. W., 2012. *Compact multi-functional antennas for wireless systems.* John Wiley & Sons.

Lin, Y. F., Chang, M. J., Chen, H. M., and Lai, B. Y., 2016. Gain enhancement of ground radiation antenna for RFID tag mounted on metallic plane. *IEEE Transactions on Antennas and Propagation*, 64(2), pp. 1193-1200.

Manzari, S., Pettinari, S. and Marrocco, G., 2012. Miniaturised wearable UHF-RFID tag with tuning capability. *Electronics. Letters*, 48(21), pp. 1325-1326.

Ng, W.H., Lim, E.H., Bong, F.L., Chung, B.K., 2018. E-Shaped folded-patch antenna with multiple tuning parameters for on-metal UHF RFID Tag. *IEEE Transactions on Antennas and Propagation*, pp. 1-1.

Nikitin, P.V., Rao, K.V.S. and Lam, S., 2012. UHF RFID Tag Characterization: Overview and State-of-the-Art. *Intermec Technologies Corporation*, pp. 1-6.

Park, I. and Kim, D., 2014. Artificial magnetic conductor loaded long-range passive RFID tag antenna mountable on metallic objects. *Electronics Letters*, 50(5), pp. 335–336.

Partanen, J., 2015. *History of RFID. Retrieved from Rain RFID*, [pdf]. Available at: < http://rainrfid.org/wp-content/uploads/2015/12/History-of-RFID.pdf> [Accessed 12 January 2018].

Petrariu, A., Popa, V., and Chirap, A., 2015. Metal mountable microstrip patch UHF RFID tag antenna. *IEEE International Symposium on Signals, Circuits and Systems (ISSCS)*, pp. 1-14.

Phatarachaisakul, T., Pumpoung, T., and Phongcharoenpanich, C., 2015. Dual-band RFID tag antenna with EBG for glass objects. *Proceeding. IEEE 4th Asia–Pacific Conference Antennas Propag. (APCAP)*, pp. 199-200.

Rao, K.V.S., Nikitin, P.V. and Lam, S.F., 2005. Antenna design for UHF RFID tags: A review and a practical application. *IEEE Transactions on Antennas and Propagation*, 53(12), pp. 3870-3876.

RFID4u, 2018. *Basics-RFID Regulations*. [online] Available at: < https://rfid4u.com/rfid-basics-resources/basics-rfid-regulations/> [Accessed 10 June 2018].

Santiago, A., Costa, J. R., and Fernandes, C. A., 2013. Broadband UHF RFID passive tag antenna for near-body applications. *IEEE Antennas Wireless Propagation Letters*, 12, pp. 136–139.

Shao, S., Burkholder, R. J., and Volakis, J. L., 2014. Design approach for robust UHF RFID tag antennas mounted on a plurality of dielectric surfaces. *IEEE Antennas and Propagation Magazine*, 56(5), pp. 158–166.

Shao, S., Kiourti, A., Burkholder, R. J., and Volakis, J. L., 2015. Broadband textile-based passive UHF RFID tag antenna for elastic material. *IEEE Antennas Wireless Propagation Letters*, 14, pp. 1385–1388.

Sharma, A. and Shrivastava, S.C., 2009. Analysis of resonant frequency & quality factor of Dielectric Resonator at different dielectric constant materials. *2008 International Conference on Recent Advances in Microwave Theory and Applications*, pp. 593-595.

Sim, D.U., Kim, D. H., Choi, J. I. and Choi, H. D., 2007. Design of novel dipole-type tag antennas using electromagnetic bandgap (EBG) surface for passive RFID applications. *2007 IEEE Antennas and Propagation Society International Symposium*, pp. 1333–1336.

Smiley, S., 2014. *UHF RFID Frequency Regulations*. [online] Available at: <https://blog.atlasrfidstore.com/uhf-rfid-frequency-regulations> [Accessed 12 January 2018].

Soriano, S. L., and Parrón, J., 2016. Parallel plate antenna for UHF RFID tags operating over metallic objects. *European Conference on Antennas and Propagation (EuCAP)*, pp. 1–3.

Stockman, H., 1948. Communication by means of reflected power. *Proceedings of the*
IRE, pp. 1196-1204.

Tagformance Measurement System, Manual 5, page 49, copyright@2012, Voyantic, Ltd.

Tashi, Hasan, M.S. and Yu, H., 2016. Design, simulation, prototyping and experimentation of planar micro-strip patch antenna for passive UHF RFID to tag for metallic objects. *2016 IEEE 10th International Conference on Software, Knowledge, Information Management & Applications (SKIMA)* , pp. 243–249.

Ukkonen, L., Sydanheimo, L. and Kivikoski, M., 2004. A novel tag design using inverted-F antenna for radio frequency identification of metallic objects. *2004 IEEE Sarnoff Symposium On Advances in Wired and Wireless Communications*, pp. 91-94.

Understanding the Differences between UHF and HF RFID Technology, 2017. [Online] Available at :< https://www.tersosolutions.com/news/understanding-the-differences-between-uhf-and-hf-rfid-technology/> [Accessed 12 January 2018].

Virtanen, J., Bjorninen, T., Ukkonen, L. and Sydanheimo, L., 2010. Passive UHF inkjet-printed narrow line RFID tags. *IEEE Antennas and Wireless Propagation Letters*, 9, pp. 440-443.

Voyantic Ltd. Voyantic Tagformance Lite. [Online]. Available at :< http://www.voyantic.com/> [Accessed 12 July 2017].

Walton, C. A., 1983. *Portable radio frequency emitting identifier*. California Patent No. 4,384,288.

Wu, G., Ouyang, J., Chen, B., Jin, L. and Long, R., 2016. A small flexible anti-metal RFID tag antenna. *2016 IEEE 5th Asia-Pacific Conference on Antennas and Propagation (APCAP)*, pp. 289–290.

Yang, P. H., Li, Y., Jiang, L., Chew, W.C. and Ye, T.T., 2011. Compact metallic RFID tag antennas with a loop-fed method. *IEEE Transactions on Antennas and Propagation*, 59(12), pp. 4454-4462.

Zhang, J. and Long, Y., 2014. A novel metal mountable electrically small antenna for RFID tag applications with practical guidelines for the antenna design. *IEEE Transactions on Antennas and Propagation*, 62(11), pp. 5820-5828.

Zhang, Y.J., Wang, D. and Tong, M.S., 2017. An adjustable quarter-wavelength meandered dipole antenna with slotted ground for metallically and airily mounted RFID tag. *IEEE Transactions on Antennas and Propagation*, 65(6), pp. 2890-2898.